Genetic analyses of fibronectin functions *in vivo* and *in vitro*

DISSERTATION ZUR ERLANGUNG DES DOKTORGRADES DER NATURWISSENSCHAFTEN (DR. RER. NAT.) DER NATURWISSENSCHAFTLICHEN FAKULTÄT III - BIOLOGIE UND VORKLINISCHE MEDIZIN DER UNIVERSITÄT REGENSBURG

vorgelegt von

Michael Leiß

aus Schlehdorf

Mai 2009

Die vorliegende Arbeit wurde in der Zeit von Mai 2005 bis Mai 2009 unter Anleitung von Herrn Prof. Dr. Fässler am Max-Planck-Institut für Biochemie angefertigt.

Promotionsgesuch eingereicht am:

25. Mai 2009

Tag des Kolloquiums:

26. Oktober 2009

Die Arbeit wurde angeleitet von:

Prof. Dr. med. Reinhard Fässler

Prüfungsausschuss:

Vorsitzender: Prof. Dr. Warth

1. Gutachter: Prof. Dr. Rainer Deutzmann
2. Gutachter: Prof. Dr. med. Reinhard Fässler
3. Prüfer: Prof. Dr. med. Ernst Tamm

Table of contents

Abbreviations

#	number
-	null allele
AdMIDAS	adjacent to MIDAS
AP	alkaline phosphatase
APS	ammonium peroxidisulfate
ALK	activin receptor-like kinase
ATP	adenosine-triphosphate
BCA	bicinchoninic acid
BM	basement membrane
BMP	bone morphogenic protein
bp/kbp	base pairs/1000 base pairs
BSA	bovine serum albumine
Cas	Crk-associated substrate
Cdc42	cell division cycle 42 homologue
cDNA	complementary DNA
cFN	cellular fibronectin
CIB	calcium and integrin binding protein
Col	collagen
CMV	cytomegalovirus
Crk	chicken Tumor Virus 10 regulator of kinase
ctrl.	control samples / animals
D	aspartic acid
DAB	3-3'diaminobenzidine
DAPI	4', 6-Diamidin-2-phenylindol-dihydrochloride
ddH_2O	double-distilled water
DMEM	Dulbecco's Modified Eagle Medium
DMSO	dimethylsulfoxide
DNA	deoxyribonucleic acid

dNTP	deoxynucleotide-triphosphate
DOC	deoxycholate
Dock180	180kDa protein downstream of Crk
DTT	1,4-Dithiothreitol
E	embryonic day / Glutamic acid
ECM	extracellular matrix
EDA	extradomain A
EDB	extradomain B
EDTA	ethylene-diamine-tetraacetic acid
e.g.	for example
EGF	epidermal growth factor
EM	electron microscopy
ES cells	embryonic stem cells
EtOH	ethanol
F-actin	filamentous actin
FA	focal adhesion
FAK	focal adhesion kinase
FC	focal complex
FACS	fluorescence activated cell sorter
FERM	four-point-one, ezrin, radixin, moesin
FGFR	fibroblast growth factor receptor
FITC	fluorescein isothiocyanate
FN	fibronectin
g	gram
GEF	guanine nucleotide exchange factor
GSK-3	glycogen synthase kinase 3
GTP	guanosine triphosphate
h	hour
HCl	hydrochloric acid
H/E	Hematoxylin/Eosin
HEPES	N-(2-hydroxyethyl)-piperazine-N'-2-ethanesulfonic acid

HGF	hepatocyte growth factor
HPLC	high performance liquid chromatography
HRP	horseradish peroxidase
ILK	Integrin-linked kinase
ICAP	Integrin-cytoplasmic domain associated protein
IgG	Immunoglobuline G
JNK	c-Jun N-terminal kinase
kDa	kilo Dalton
LAP	latency associated protein
LB	lysogeny broth
LM111	Laminin111
LTBP	latent TGF-β binding protein
µl	micro litre
M/mM	molar/millimolar
MCS	multiple cloning site
MEF	murine embryonic fibroblast
MeOH	methanol
MIDAS	metal ion-dependent adhesion site
Mg^{2+}/MgCl	Magnesium/Magnesiumchloride
Mn^{2+}	Manganese
mg	milligram
min	minutes
n	number
NaCl	sodium chloride
NaF	sodium fluoride
Na_3VO_4	sodium-orthovanadate
NMR	nuclear magnetic resonance
o/n	overnight
nm	nanometer
OD	optical density
PAK	p21-actovated kinase

PBS	phosphate buffered saline
PCR	polymerase chain reaction
PDGF	platelet derived growth factor
PEST	Proline, Glutamic acid, Serine, Threonine
PFA	paraformaldehyde
pFN	plasma fibronectin
PI3K	phophoinositide 3-kinase
PH	pleckstrin homology
PIP2	phosphatidylinositol (4,5) bisphosphate
PIP3	phosphatidylinositol (3,4,5) trisphosphate
PIX	PAK-interacting exchange factor
PKC	protein kinase C
PLCγ	phospholipase C gamma
pol	polymerase
PSHRN	Pro-Ser-His-Arg-Asn
PSI	plexin, semaphoring and integrin
PVDF	polyvinylidene fluoride
R	Arginine
Rac	Ras-related C3 botulinum substrate
RGD	Arginine-Glycine-Aspartic acid
RNA	ribonucleic acid
RNAi	RNA interference
ROCK	Rho kinase
RPM	rotations per minute
RT	room temperature
RTK	receptor tyrosine kinase
S/Ser	Serine
siRNA	small interfering RNA
shRNA	short hairpin RNA
SDS	sodium dodecyl sulphate
SDS-PAGE	SDS polyacrylamide gel electrophoresis

SFKs	src family kinases
SH	domainsrc-homology domain
SV	simian virus
SyMBS	synergistic metal ion binding site
T/Thr	Threonine
Taq	*Thermophilus aquaticus*
TAE	Tris-acetic acid-EDTA buffer
TBS	Tris-buffered saline
TGF-β	Transforming growth factor β
TE	Tris-EDTA buffer
Tris	Tris (hydroxymethyl) aminomethane
TEMED	N,N,N',N'-Tetramethylethylenediamine
U	Unit
UV	ultra violet
V	Volt
VCAM	vascular adhesion molecule
VEGF	vascular endothelial growth factor
VN	vitronectin
v-region	variable region
VSV-G	vesicular stomatitis viral G protein
w/o	without
wt	wild-type
Y/Tyr	tyrosine

Summary

Fibronectin (FN), a major adhesive glycoprotein ubiquitously present in the extracellular matrix and in blood plasma of vertebrates, is secreted by cells as a disulfide-bonded dimer. FN requires cell surface expressed integrins to assemble into a functional fibrillar network, which in turn orchestrates the assembly of other ECM components to promote cell adhesion, cell migration and a large variety of signaling events.

The most prominent integrin binding site of FN is located in the 10th type-III repeat (FN-III$_{10}$) and consists of an Arg-Gly-Asp (RGD) motif. This motif is considered to be essential for the initiation and assembly of a fibrillar FN matrix through its capability to bind to a variety of different members of the integrin family. Gene ablation studies confirmed that two RGD-dependent FN assembly mechanisms either induced by integrin α5β1 or αv integrins exist *in vivo*, and that each of them can compensate for the absence of the other (Yang, Bader et al. 1999). In order to specifically test how FN-RGD binding integrins compensate for each other during development and FN fibrillogenesis, a mouse strain was generated in which the Asp (D) of the RGD motif was substituted with a Glu (E). This mutation resulted in an integrin-binding-deficient RGE motif. FN-RGE homozygous mice die around embryonic day 10 (E10) of development with shortened posterior trunk, absent tail-bud derived somites and severe defects of the cardiovascular system. All these defects are similar to those observed in α5 integrin-null mice. Surprisingly, the absence of a functional RGD binding site did not abolish assembly of a FN matrix in mutant embryos or on cells derived from mutants. Matrix assembly assays and solid-phase binding assays performed in this study reveal that αvβ3 integrin assembles FN-RGE by binding to an *iso*DGR-motif in FN-I$_5$, which is generated by the non-enzymatic rearrangement of Asn (N) into *iso*-Asp (*iso*D). This study unravelled a novel motif for integrin binding and fibril formation in FN whose activity is controlled by amino acid modification.

The dimerization of FN is facilitated by two cysteines at the C-terminus which are forming a pair of disulfide-interchain bonds. Fibronectin dimerization has been shown to be essential for the assembly of a fibrillar FN matrix network *in vitro*. To directly test the function of the dimerization *in vivo*, a mouse strain was generated that is exclusively expressing a monomeric form of FN by exchanging the two cysteines (C) against two serines (S). This study shows that FN-monomer homozygous mice die around E11.0, displaying severe cardiovascular defects and a growth arrest commencing around E9.0 – E9.5. Interestingly, these defects are similar to those observed in mouse models with compromised TGF-β signaling. Moreover, monomeric FN was assembled into a FN matrix in mutant embryos. Matrix assembly assays and biochemical analyses revealed that FN-monomer is also assembled *in vitro*, but fails to orchestrate assembly of other ECM proteins such as LTBP-1 leading to an impaired targeting of latent TGF-β to the

ECM. This in turn leads to altered TGF-β signaling underlying the cardiovascular defects. This study demonstrates that dimeric FN is not required for FN fibril assembly *in vivo*, but is essential for sequestration and activation of TGF-β and normal FN fibrillogenesis *in vitro*.

1 Introduction

1.1 The extracellular matrix (ECM)

The extracellular matrix (ECM) is a heterogeneous meshwork of fibrillar and non-fibrillar components. The ECM plays crucial roles in development, tissue homeostasis and disease by providing a structural scaffold for cell adhesion and migration, by acting as a repository to store various growth factors and control their bioavailability, and by regulating numerous cell functions through activating multiple signaling pathways at cell adhesion sites. The ECM fibrillar network is a highly dynamic structure that is subjected to constant reorganization mediated by cells and tissue motion.

The major constituents of the ECM are different proteoglycans, glycosaminoglycans and glycoproteins. The most abundant glycosaminoglycan in the ECM is hyaluronan, which is a carbohydrate polymer (Laurent and Fraser 1992). Proteoglycans such as perlecan, aggrecan, biglycan and decorin are highly glycosylated proteins that support cell adhesion and bind various growth factors (Timpl 1993; Iozzo 1998).

A major fraction of the ECM is composed of glycoproteins, such as collagens, laminins, fibrillins and fibronectin, which serve as substrates for different adhesion molecules including integrins (Humphries, Travis et al. 2004; Dallas, Chen et al. 2006). A comprehensive introduction of all constituents of the ECM would be far beyond the scope of this introduction. Therefore, only a selection of the most important ECM glycoproteins will be briefly introduced within this section.

The more than 30 members of the collagen-family represent the major proteinaceous component of the ECM in most organs. The triple-helical proteins provide a scaffold for the organization of cells in a given tissue. Collagens can be roughly divided into two classes; the fibril forming collagens (Col I, II, III, V and XI) and the more heterogeneous class of non-fibrillar collagens, including the typical basement membrane collagens IV, Col VIII and Col X. Some collagens are almost ubiquitously expressed, while others are found only in distinct tissues, such as for example, Col X in cartilage (Aumailley and Krieg 1996; Kadler, Hill et al. 2008).

The fibrillin-family of ECM proteins including fibrillin-1, -2, -3 and the latent transforming growth factor binding proteins (LTBPs) 1 trough 4, form microfibrils and regulate growth factor activity. Fibrillins are found in various connective tissues in association with elastin with which they form the so-called elastic fibers (Kielty, Sherratt et al. 2005).

The heterotrimeric laminins are abundant glycoproteins in basement membranes. Laminins polymerize into sheet-like supramolecular structures which interact with the collagen network via entactin or perlecan and with receptors on the cell surface such as

integrins and dystroglycans. Mammals possess at least 15 different laminin isoforms, two of which have been reported to be essential for development (Laminin-1 and -10), whereas the other laminins play tissue and cell-type specific roles required for specialized organ functions (Miner and Yurchenco 2004).

Fibronectin is an abundant constituent of the ECM. FN exhibits multiple sites that interact with integrins, other cell surface receptors and ECM components. As one of the earliest ECM components to be assembled, it is thought to act as an orchestrator for the assembly of multiple ECM proteins (Schwarzbauer and Sechler 1999; Pankov and Yamada 2002). Since FN is in the focus of this study, it will be introduced in more detail in one of the following sections (see 1.3).

Importantly, these ECM components are all secreted by cells as non-functional building units, which are assembled into functional supramolecular structures in a highly regulated manner (Larsen, Artym et al. 2006; Vakonakis and Campbell 2007). Integrin cell surface receptors play a key-role in many of these assembly processes and are therefore introduced in the following chapter.

1.2 The integrin cell surface receptor family

1.2.1 Integrins

Integrins represent a family of cell adhesion receptors that are ubiquitously expressed in all metazoan tissues. The heterodimeric cell surface receptors recognize numerous ligands, among which are ECM-molecules, cell-surface receptors and soluble proteins, such as latency-associated protein (LAP) or the milk fat globule-EGF factor 8 (MFGE8). Integrins exhibit large extracellular domains, transmembrane domains and cytoplasmic domains, which connect to the actin-cytoskeleton via numerous cytoplasmic adaptor proteins. Thus, integrins link the cytoskeleton with the ECM, which facilitates bi-directional signaling across the cell membrane and enables cells to mechanically and chemically integrate with their extracellular environment. This is important for executing integrin functions such as cell adhesion, migration, survival, gene expression and differentiation (Sheppard 2000; van der Flier and Sonnenberg 2001; Hynes 2002; Legate, Wickstrom et al. 2009).

1.2.2 The integrin family and ligands

Integrins are heterodimeric proteins, consisting of α and β transmembrane type I protein subunits, which are non-covalently linked to each other. The number of different integrin subunits encoded in the genome correlates with the complexity of the organism. Mammals express 18α and 8β subunits which can form 24 known combinations of different heterodimers. Splicing of some subunits increases the diversity (van der Flier and Sonnenberg 2001). The ligand-specificity of each heterodimer is determined by the types of α and β subunits associated with each other (Hynes 2002). While some integrins exhibit a stringent ligand-specificity, others are promiscuous. In general,

integrins can be assigned to distinct subgroups regarding their ligand recognition specificity (see Fig 1.1); the RGD-binding integrins, which recognize ECM molecules containing RGD motifs such as FN, vitronectin (VN), thrombospondin, osteopontin and tenascin; the laminin-binding integrins; the collagen binding; integrins which recognize the LDV motif present in FN, in vascular cell adhesion molecule-1 (VCAM-1) and Mucosal addressin cell adhesion molecule-1 (MAdCAM-1); and integrins expressed on cells of the haematopoietic system, which mediate cell-cell interactions by binding counter-receptors of the IgG-superfamily (Humphries, Byron et al. 2006; Legate, Wickstrom et al. 2009).

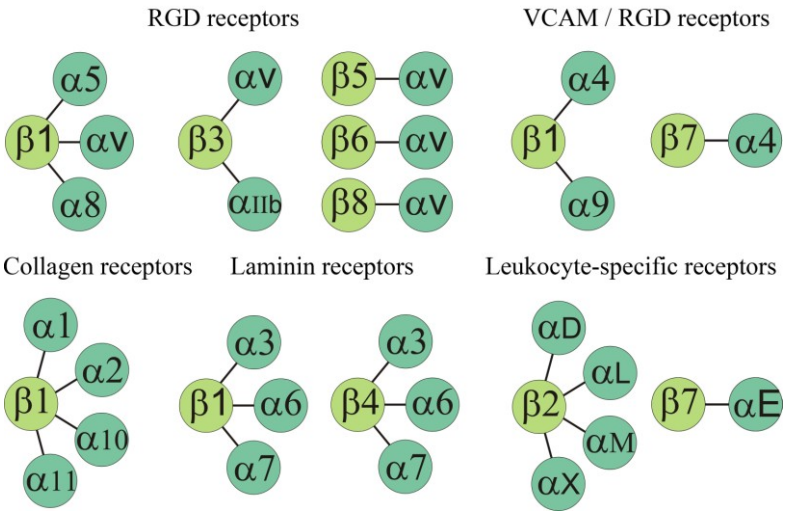

Fig 1.1. ***Mammalian integrin heterodimers****. Integrins can be classified in subgroups regarding their ligand specificity. RGD receptor integrins recognize the RGD motif, which is present in FN and vitronectin (VN). FN is also recognized by another subgroup of integrins (α4β1, α4β7 and α9β1) that are additionally capable to interact with VCAM-1 (vascular cell adhesion molecule). Two further integrin subgroups mediate interactions with ECM proteins of the collagen- and laminin-family. A group of leukocyte-specific integrins mediates cell-cell adhesions in the haematopoietic system to Ig-superfamily counter receptors. (Based on Hynes, 2002).*

1.2.3 Integrins structure

Integrins are approximately 28 nm long. Their α and β subunits have a size of 150-180 kDa and ~100 kDa, respectively. The large extracellular domain of each subunit is linked to the cytoplasmic tail via a single α-transmembrane helix. A hallmark of almost all integrin subunits is their rather short cytoplasmic tail, which is made up of only about 10-70 amino acids. The β4 subunit is an exception with a much larger cytoplasmic tail composed of 1072 amino acids (Wegener and Campbell 2008). Both integrin subunits consist of modules. The ectodomain of α subunits consists of a N-terminal β-propeller domain, an Ig-like domain (thigh) and two β sandwich domains (calf-1 & -2). The ectodomain of β subunits comprises a N-terminal β I domain followed by a Ig-like domain ("Hybrid"), a PSI (plexin, semaphorin and integrin)

domain, four tandem repeats of epidermal growth factor-like (EGF-like) domains and a β-tail domain (Zhu, Luo et al. 2008) (See fig. 1.2). Structural data of integrin ectodomains indicate that both subunits assemble into a "head on two tails"-like structure. The β-propeller of the α subunit, together with the β I and Hybrid domain of the β subunit form the headpiece, which contains the ligand binding pocket. An important structural property required for ligand binding are the metal ion coordinating sites located in the β I domain, which consist of an Mg^{2+}/Mn^{2+} binding site (Metal ion-dependent adhesion site, MIDAS) and two flanking Ca^{2+} (synergistic metal ion binding site, SyMBS and adjacent to MIDAS, AdMIDAS site) binding sites (Hynes 2002; Wegener and Campbell 2008).

It is widely recognized that integrins can switch between two conformational states; a bent, closed conformation which characterizes inactive integrins with low ligand affinity, and an extended, open conformation representing active integrins with high ligand affinity (Xiong, Stehle et al. 2001; Takagi, Petre et al. 2002; Zhu, Luo et al. 2008). The bent conformation is achieved by bending of the ectoplasmic "tails" between the thigh and calf-1 domain of the α subunit and bending of the β integrin subunit between the I-EGF domains 1 & 2. In order to obtain the active conformation, the ectoplasmic tails need to switch to an extended conformation. The extension is believed to be initiated by separation of the cytoplasmic and transmembrane domains upon binding of proteins to β integrin cytoplasmic domains. This model of long range conformational changes is referred to as "switchblade" model (see Fig 1.2). However, it is still disputed whether integrins can adopt different bent conformations which are also capable to bind ligands with varying affinities ("deadbolt" model) (Carman and Springer 2003; Arnaout, Mahalingam et al. 2005).

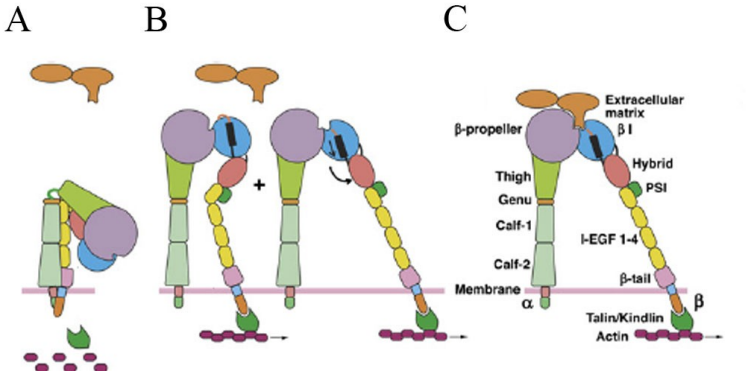

Fig 1.2. ***The "switchblade" model of integrin activation****. **A**. Integrin in the bent conformation with low affinity for the ligand. **B**. Binding of cytoplasmic proteins to the β subunit leads to separation of the cytoplasmic tails (opening) and extension of the ectodomains. The binding pocket in the headpiece is now accessible for the ligand. **C**. Ligand-bound integrin in the extended, active conformation. (modified from Zhu et al., 2008).*

1.2.4 Regulation of integrin activation and "inside-out" signaling

Integrin activation is a process that requires tight regulation, since many cellular processes, such as for example platelet aggregation in response to injury, are fundamentally dependent on localized and accurately timed integrin activation (Bennett 2005). Integrins cytoplasmic tails are small compared to the extracellular domains and are devoid of enzymatic activity but have been shown to play a central role in integrin functions. Numerous studies demonstrated that integrin activation and integrin mediated signal transduction is facilitated by direct interactions between intracellular proteins and conserved motifs in integrins cytoplasmic tails (Calderwood 2004; Legate and Fassler 2009). Hydrophobic interactions and a proposed salt-bridge formed between the Asp residue in the β-tail HDRK motif and the Arg residue in the α-tail GFFKR motif result in a close association of both subunits in integrins inactive state. Upon intracellular stimuli, specific FERM-domain containing proteins, such as talin and kindlin, bind to conserved motifs in β integrins cytoplasmic tail, which leads to disruption of the weak tail-tail interactions and integrin activation (Vinogradova, Velyvis et al. 2002; Wegener, Partridge et al. 2007; Moser, Nieswandt et al. 2008; Wegener and Campbell 2008). Besides talin and kindlin, several other proteins have been reported to activate integrins by direct interaction with the cytoplasmic tail, such as cytohesin I, calcium and integrin binding protein (CIB) and β3 endotoxin (Travis, Humphries et al. 2003; Legate and Fassler 2009). The regulation of integrin activity through interaction with intracellular proteins is referred to as "inside-out" signaling.

Up to now, more than 20 different proteins have been shown to directly interact with integrins cytoplasmic tails, most of which bind to the β subunit. These include actin-binding proteins (e.g. Talin, α-actinin, Myosin), kinases (FAK), adaptor proteins (i.e. kindlin, paxillin, ILK), transcriptional co-activators (JAB1), transmembrane proteins (CD98) and guanine nucleotide exchange factors (Cytohesin-1, -3) (Liu, Calderwood et al. 2000). The diversity of this group of interaction partners highlights the complexity of integrin signaling, which is far from being fully understood and can not be exhaustively introduced here. Instead, the reader is referred to some outstanding reviews about integrin signaling (Schwartz and Ginsberg 2002; Guo and Giancotti 2004; Legate and Fassler 2009; Moser, Legate et al. 2009).

1.2.5 Integrin-actin interaction at cell adhesion sites

One of the major functions of cytoplasmic integrin binding proteins is to facilitate the linkage of integrins to the actin cytoskeleton. The actin binding protein talin is known to play a pivotal role for this interaction, since it is not only required for integrin activation, but also provides a direct physical link between integrins and actin (Tanentzapf, Martin-Bermudo et al. 2006; Zhang, Jiang et al. 2008). Upon integrin binding, talin recruits and activates phosphoinositol-phosphate kinase type I gamma (PIPkγ) which catalyses the local production of phosphatidylinositol (4,5) bisphosphate (PIP2). At sites of cell adhesions, PIP2 serves two functions: Firstly, it enhances the

interaction of talin with integrins β subunit. Secondly it recruits other PIP2 binding proteins, such as vinculin, to integrin cell adhesion sites. The talin binding protein vinculin strengthens the indirect integrin-actin interaction in various ways: It probably acts as a cross-linker of the talin-actin interaction (owing to its capability to bind to both proteins), and enhances talins capability to cluster integrins (Giancotti and Tarone 2003; Gallant, Michael et al. 2005; Humphries, Wang et al. 2007). Moreover, vinculin undergoes a conformational change upon PIP2 binding which leads to its increased affinity for actin, resulting in enhanced recruitment of F-actin to sites of integrin mediated cell adhesion (see Fig 1.3). This process provides an example, how tight integrin-actin interactions are established. The total number of interactions increases gradually, starting out with only few ECM-bound integrins clustered in so called nascent adhesions (Choi, Vicente-Manzanares et al. 2008). These unstable adhesion structures may increase in size, as more and more ECM-bound integrins cluster, and mature into larger multiprotein adhesion structures with gradually increasing size and complexity, such as dot-shaped focal complexes (FCs), focal adhesions (FAs) and, finally, streak-like fibrillar- (Geiger, Bershadsky et al. 2001) and 3D-matrix adhesions (Cukierman, Pankov et al. 2001). Particularly the larger, more advanced structures such as FAs and fibrillar adhesions mediate the interaction of integrins with thick F-actin bundles called stress fibers in a highly dynamic fashion (Zamir and Geiger 2001). The creation of a tight integrin mediated ECM-cytoskeleton linkage finally paves the way for further cytoskeletal rearrangements which facilitate the transmission of cytoskeletal pulling- and traction-forces required for cell migration and cell shape modulations during differentiation and proliferation.

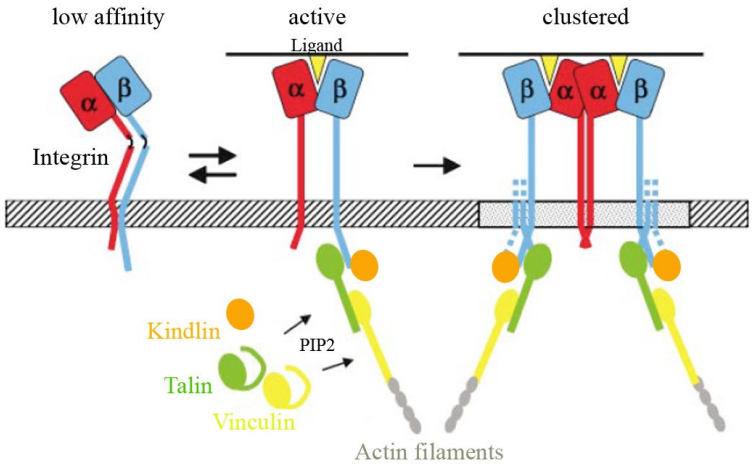

Fig 1.3. ***Indirect integrin – F-actin interconnection via talin and vinculin****. Binding of talin and kindlin to the cytoplasmic tail of the β integrin subunit is necessary to synergistically induce integrin activation through tail separation. Active integrin binds to extracellular ligands on the ectoplasmic face and recruits PIPkγ to the cytoplasmic face. Local PIP2 production by PIPkγ attracts PIP2 binding vinculin. The PIP2-bound vinculin is capable to interact with talin and facilitates the recruitment of F-actin. (Modified from Giancotti and Tarone, 2003).*

1.2.6 Integrins role in FN assembly

The assembly of elongated FN fibrils is a cell dependent process termed FN fibrillogenesis. This process requires a dynamic, directional integrin movement to stretch integrin-bound fibronectin on the cell surface, and is found to coincide with the assembly of streak-like adhesion structures called fibrillar adhesions. These elongated structures are characterized by a high content of FN binding α5β1 integrins and tensin, and typically lack other integrins, paxillin, vinculin and tyrosine-phosphorylated proteins (Zamir, Katz et al. 2000). Fibrillar adhesions are considered to be emerging from FAs; upon FN binding, α5β1 integrins are pulled out from sites of FAs and move towards the cell center to form fibrillar adhesions, in which integrin-bound FN fibrils are aligned with F-actin and multiple signaling molecules (Pankov, Cukierman et al. 2000; Zamir, Katz et al. 2000; Ohashi, Kiehart et al. 2002).

The traction forces required for fibrillar adhesion assembly are generated by myosin II-dependent contraction of the F-actin cytoskeleton, which is linked to integrins via the actin and integrin-binding protein tensin (Lo, Weisberg et al. 1994). Translocation of FN-bound integrin facilitates the mechanical stretching of the FN molecule (see Fig 1.4), resulting in the exposure of cryptic self assembly sites which results in FN self assembly (Yamada, Pankov et al. 2003).

Interestingly, loss of α5β1 integrin in cells and ablation of the α5 integrin gene in mice revealed, that FN can still be assembled by the remaining FN binding integrins, most notably the αv integrin subfamily (Yang, Rayburn et al. 1993; Wu, Keivens et al. 1995; Wennerberg, Lohikangas et al. 1996). However, FN fibrils produced by αv-class integrins appear short and thick and often resemble the shape and dynamics of αv integrin containing FAs that may be attributed to the inability of these integrins to move out from FAs (Wennerberg, Lohikangas et al. 1996; Wu, Hughes et al. 1996). The crucial role of α5 and αv integrins for FN assembly have been confirmed by a double knock out of both genes, which ablates FN fibril formation (Yang, Bader et al. 1999). An interesting but still unanswered question is whether αv mediated thick and short FN fibrils co-exist with the fine and thin α5-mediated FN fibrillar meshwork *in vivo*. The co-existence of different types of FN fibrils would provide tissues with qualitatively different FN matrices and different functional properties.

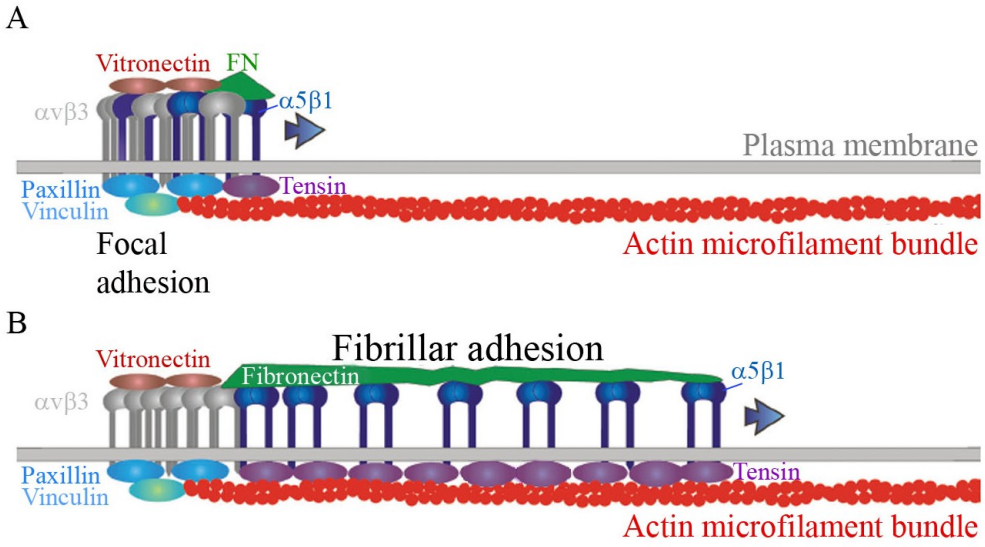

Fig 1.4. ***Integrin translocation facilitating FN fibrillogenesis****.* ***A****. Cells use focal adhesions as anchors. Strong adhesion is mediated e.g. to Vitronectin (VN) using αvβ3 integrin. Intracellular contractility leads to directional movement of FN-bound α5β1 integrin along actin-filaments from FAs towards the cell center. As a result, FN is stretched.* ***B****. Stretching of the FN molecule leads to unfolding of cryptic self-assembly sites, resulting in the assembly of a linear FN fibril. This process requires intracellular actomyosin contractility and the cytoskeletal protein tensin. Note that the translocation of integrins during formation of fibrillar adhesions is restricted to α5β1 integrins. (Modified from Yamada et al., 2003).*

1.2.7 "Outside-in" signaling

Integrin activation through "inside-out" signaling increases the affinity of individual integrins for their ECM ligands. However, strong cell-ECM interactions foremost require increased avidity which is only achieved through clustering of several hundred integrins at sites of adhesion, so that individual weak interactions add up to a tightly bound cell adhesive site. Dense clustering of ECM-bound active integrin induces the recruitment of cytoplamic tail binding proteins to adhesion sites which in turn initiate numerous intracellular signaling cascades in a process that has been termed "outside-in" signaling (see Fig 1.5). These regulate the activity of signaling proteins, including members of the Rho GTPase family, focal adhesion kinase (FAK), extracellular regulated kinase (ERK), cyclic AMP (cAMP) dependent kinase, protein kinase C (PKC), tyrosine phosphatases as well as phosphate inositol metabolism (Lee and Juliano 2004). As a result of all these complex signal transduction processes, a large signaling hub is assembled at sites of cell adhesion which affects cell cycle progression, differentiation, cell shape, survival and cell migration (Lee and Juliano 2004).

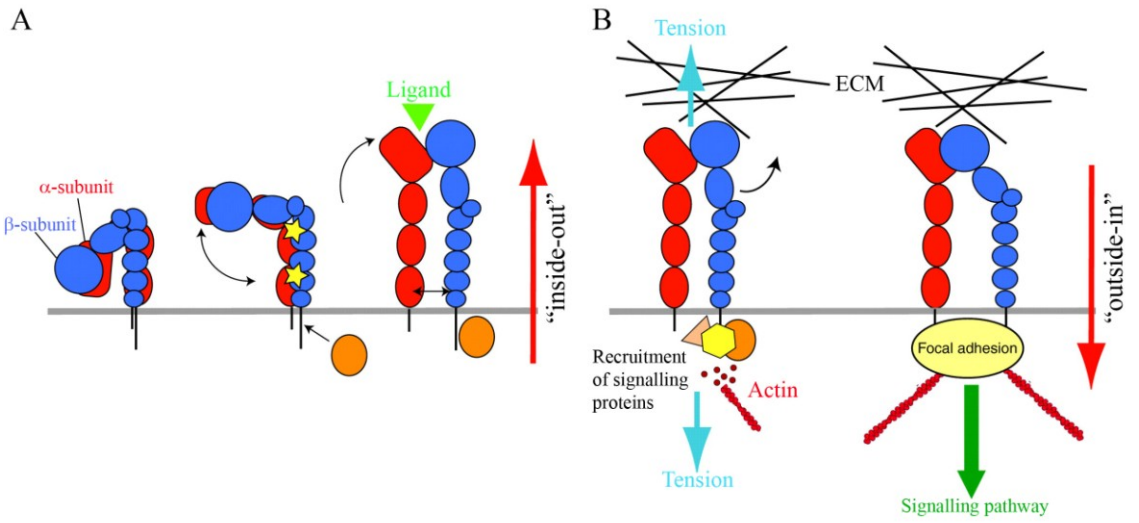

Fig 1.5. ***Bi-directional integrin mediated signaling****.* ***A****. Regulation of integrin activity by intracellular proteins, termed "inside-out" signaling. Note that the inactive integrin is bent with both subunits associated, while the active integrin exhibits an extended conformation with separated subunits ("switchblade" model).* ***B****. ECM bound active integrins recruit complex intracellular signaling platforms to adhesion sites, resulting in "outside-in" signaling. (Modified from Askari et al., 2009).*

One of the earliest events in integrin mediated "outside-in" signaling is the activation of Src family kinases (SFKs), tyrosine phosphatases and focal adhesion kinase (FAK). FAK acts as a central scaffold and activator for multiple signaling proteins in integrin- and receptor tyrosine kinase (RTK) dependent signaling. It is composed of an N-terminal FERM-homology domain which facilitates integrin binding, a central kinase domain and a C-terminal FA targeting domain. Once recruited to nascent focal adhesions or focal adhesions (FAs), FAK is activated in response to integrin ligation by autophosphorylation on tyrosine residue Y397, which creates a docking site for a number of SH2 domain containing proteins including PI-3-kinase, PLCγ and SFK family members, including Src and Fyn (Schaller 2001). FAK recruits SFK family members to sites of cell adhesion and positions them in close proximity to their target-effectors which in turn become activated and mediate numerous signaling events (Sieg, Hauck et al. 2000). FAK-Src interaction, for instance, stabilizes active Src, which then fully activates FAK by phosphorylation of five other sites on FAK (Schlaepfer and Hunter 1996). Active SFK-FAK complexes trigger, amongst others, the Ras-MEK-MAPK pathways, resulting in activation of ERK1/2, c-JUN kinase (JNK) and p38 MAPK which affect the regulation of cell proliferation, cell growth and differentiation (Giancotti and Ruoslahti 1999; Miranti and Brugge 2002). Activation of FAK also leads to the recruitment of PI-3-kinase to FAs, leading to activation of downstream effectors such as Akt and Gsk3β which regulate cell differentiation and survival. Other sites on FAK, such as the C-terminal Proline rich sequence, can serve as binding sites for SH3 domain containing proteins such as p130Cas and GRAF. Once p130Cas becomes phosphorylated by the FAK-Src complex, it is capable to recruit further adaptor proteins

such as Crk and Nck. Crk recruitment by active p130Cas initiates the engagement of the adaptor protein ELMO and the guanine exchange factor (GEF) Dock180, leading to activation of the small GTPase Rac1, which promotes Arp2/3 mediated F-actin polymerization (Schaller 2001; Chodniewicz and Klemke 2004). Alternatively, the small Rho GTPases Rac1 and Cdc42 can be regulated through the PIX/GIT pathway, both of which get targeted to FAK associated paxillin (Hoefen and Berk 2006). The latter signaling pathways exemplify that integrins do not only act as important signaling receptors and cell anchorage proteins, but also mediate – along with growth factor receptor signaling - a number of cytoskeletal remodelling processes via regulation of small Rho GTPases. These include master regulators of cell-migration and cell-contractility such as RhoA, Rac1 and Cdc42 (see Fig 1.6) (Price, Leng et al. 1998; Ren, Kiosses et al. 1999).

To date, more than 156 molecules have been found to form intracellular integrin signaling complexes (Zaidel-Bar, Itzkovitz et al. 2007). This enormous number of signaling proteins recruited to sites of cell adhesion reflects the vast complexity of possible signaling events, which might be even higher when cell-type specific expression or different isoforms of the signaling molecules are taken into account.

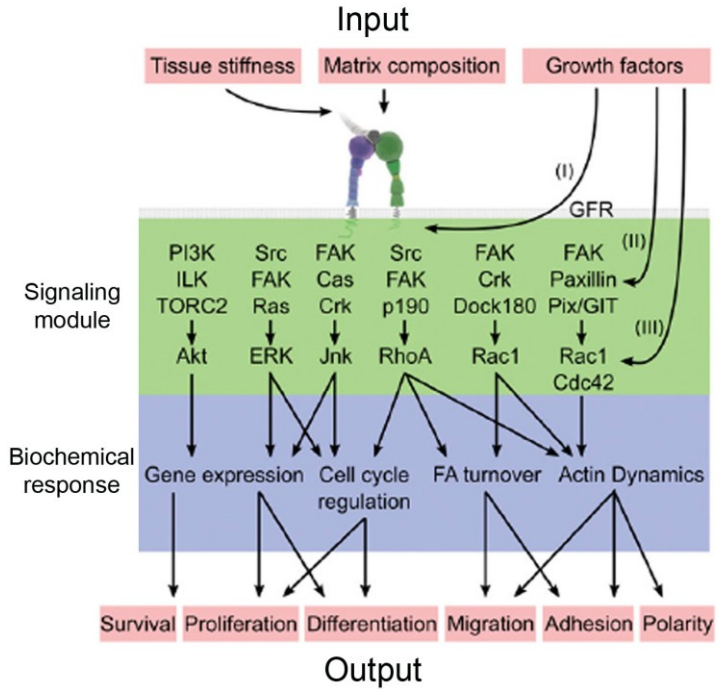

Fig 1.6. ***Examples of integrin "outside-in" signaling pathways****. Combined integrin and growth-factor receptor signaling regulates a huge repertoire of signaling pathways which allows the cell to respond to extracellular cues. (Modified from Legate et al., 2009).*

Integrins can also regulate the responses to other cell-surface receptors and vice versa. A dense network of crosstalks between multiple signaling pathways downstream of integrins and other cell-surface receptors provides a multilevel coordinated control of

cell responses to the extracellular environment. Coordinated signaling through α5β1 integrin and the heparin proteoglycan cell surface receptor syndecan-4 in response to FN binding, for instance, has been reported to promote the assembly of FAs and actin-stressfibers in a Rho dependent manner (Saoncella, Echtermeyer et al. 1999). The crosstalk between integrins and receptor protein tyrosine kinases (RTKs), which bind to cytokines and soluble growth factors, is yet another extensively studied field of coordinated integrin-cell surface receptor signaling. Prominent examples are represented by the integrin dependent transactivation of epithelial growth factor receptor (EGFR), platelet derived growth factor receptor (PDGFR), vascular endothelial growth factor receptor (VEGFR) (Sundberg and Rubin 1996; Soldi, Mitola et al. 1999) which in turn are capable to amplify integrin signals. This applies for instance to the ERK/Shc pathway, which is triggered in response to combined signals from integrins and integrin activated EGF receptors (Moro, Venturino et al. 1998). Another type of integrated co-signaling of RTKs and integrins is characterized by integrin induced clustering of RTKs which has been demonstrated for EGFR, PDGFR and FGFR (Plopper, McNamee et al. 1995; Miyamoto, Teramoto et al. 1996; Sundberg and Rubin 1996), which is initiated by active integrins organizing signaling platforms, which can be subsequently shared with clustered RTKs for combined signal propagation. All these examples only represent a small selection of possible crosstalks between integrin and RTK triggered signaling pathways. For detailed information about the RTK-integrin cross-talk, the reader may be referred to the following review: (Giancotti and Tarone 2003).

1.2.8 Integrins role in development

The analysis of genetically engineered mice provides a powerful tool to study integrin function during development. Up to now, all β subunits and all but two α subunits (αD, αX), have been knocked out in mice. The ablation of integrin genes leads to various phenotypes, ranging from apparently normal mice to early embryonic lethality (see Fig 1.7).

Integrin	phenotype	Reference
β1	peri-implantation lethality by E5.5; defective BM assembly	Meyer and Fässler, 1995
β2	V / F; impaired inflammatory response, leukocytosis	Scharffetter-Kochanek, 1998
β3	V / F; no platelet aggregation; osteosclerosis	Hodivala-Dilke, 1999
β4	perinatal lethal; severe skin blistering	van der Neut, 1996
β5	V / F; no obvious defects	Huang et al., 2000
β6	V / F; inflammation in skin and airways	Huang et al., 1996
β7	V / F; no formation of Peyer's patches	Wagner et al., 1996
β8	lethal at E10.5, placental defects or perinatal lethal	Zhu et al., 2002
α1	V / F; reduced tumor vascularization	Gardner et al., 1996
α2	V / F; delayed platelet aggregation	Holtkotter et al., 2002
α3	perinatal lethal; renal tube defects; mild skin blistering defect	Kreidberg et al., 1996
α4	lethal at E11-14 due to heart and extraembryonic tissue defects	Yang et al., 1995
α5	lethal at E10-11; mesodermal defects; no formation of posterior somites	Yang et al., 1993
α6	perinatal lethal; severe skin blistering	Georges-Labouesse et al., 1996
α7	V / F; muscular dystrophy	Mayer et al., 1997
α8	perinatal lethal; no or defective kidney formation	Muller et al., 1997
α9	perinatal lethal; lymphatic duct defect	Huang et al., 2000
α10	V / F; mild skeletal defects	Bengtsson et al., 2005
α11	V / F; dwarfism; increased mortality due to impaired tooth development	Popova et al., 2007
αv	lethal at E10.5, placental defects or perinatal lethal	Bader et al., 1998
αIIb	V / F; no platelet aggregation	Tronik-Le Roux, 2000
αE	V / F; reduced number of lymphocytes	Schon et al., 1999
αL	V / F; impaired leukocyte recruitment	Schmits et al., 1996
αM	V / F; impaired phagocytosis and apoptosis of neutrophils	Coxon et al., 1996

Fig 1.7. ***Integrin knock out phenotypes****. The diversity of different phenotypes emphasizes the important functions of integrins in development as well as in maintaining tissue integrity. V/F, viable / fertile; (Modified from Bouvard et al., 2001).*

Targeted inactivation of genes encoding for the α5 integrin results in a severe phenotype with embryonic lethality around E10-11. Pronounced defects in the posterior trunk and the yolk sac vasculature demonstrate the essential role of α5β1 integrin in mesoderm function, formation or migration. Interestingly, α5-null mice progress much further than FN-null mice, suggesting a compensatory role for other FN-binding integrins in FN activation and fibril assembly (Yang, Rayburn et al. 1993). Indeed, mice carrying deletions of both the α5 and the αv integrin gene exhibit an even more severe phenotype than FN-null mice and display a severly compromised FN matrix assembly, which proved that αv integrins facilitate FN assembly in absence of α5β1 (Yang, Bader et al. 1999).

The development of conditional, tissue-specific knock out techniques helps to overcome the problem of recessive embryonic lethality of most integrin-null mice (α4, α5, α8, αv) and facilitates the analysis of integrins role for adhesion and signaling processes in a tissue specific manner. Integrins are still object of extensive studies, particularly since integrin mutations seem to be involved in the progression of various diseases.

1.3 Fibronectin (FN)

1.3.1 Fibronectin - Structure and distribution

FN is a widely distributed high-molecular weight ECM glycoprotein of about 250 kDa, which can be found in connective tissue matrices, basal laminae and plasma of vertebrates (Kornblihtt, Pesce et al. 1996). It is one of the earliest ECM proteins to be assembled and regulates numerous processes including cell attachment, migration, survival, proliferation, differentiation (Ffrench-Constant and Hynes 1988; Smith, Symes

et al. 1990). FN is a modular organized protein that consists of an array of type I, II and III domains which are later found also in a wide range of other vertebrate proteins (see Fig 1.8). The type I and II domains contain two intra-chain disulfide bridges, while type III domains lack disulfide bonds. Type I domains contain highly conserved aromatic amino acid residues and disulfide bridges building a hydrophobic core which is enclosed by stacked β-sheets (Baron, Norman et al. 1990). The type II domains are made up of two anti-parallel β-sheets that are linked via the disulfide bridges in a perpendicular orientation to each other (Constantine, Brew et al. 1992). FN's type III domain structure has been extensively studied by means of nuclear magnetic resonance spectrometry (NMR) and X-ray crystallography. These data demonstrate that type III domains are composed of seven β-strands that form a sandwich of two anti-parallel β-sheets which are connected to each other through flexible loops (Dickinson, Veerapandian et al. 1994).

The FN molecule is characterized by several specific features: It is secreted as a disulfide-bonded dimer, and the dimerization seems to be required to assemble FN into a fibrillar matrix (see Fig 1.8) (Schwarzbauer 1991; Leiss, Beckmann et al. 2008).

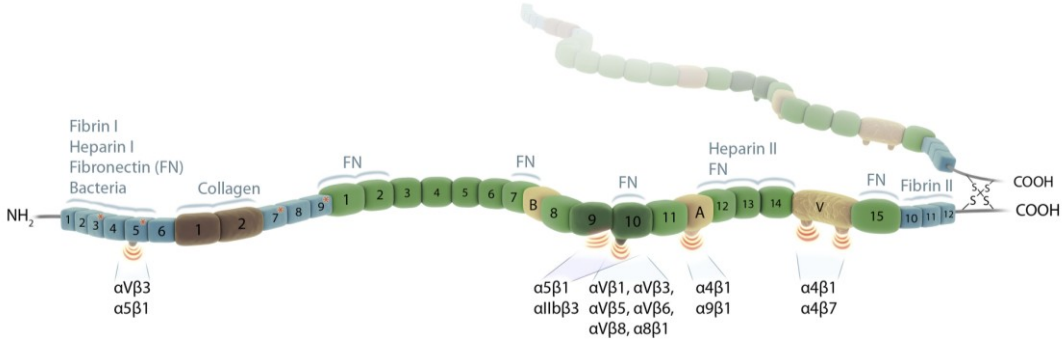

Fig 1.8. ***Schematic depiction of the modular structure of fibronectin****. FN consists of three different modules (type I, blue; type II, brown; type III, green). The alternatively spliced extradomains B, A, and the variable region (v) are shown in ochre. The dimer forms via two disulfide-bonds at the C-terminus. Integrin binding sites, as well as binding domains for FN, collagen, fibrin, heparin and bacteria are indicated. Note that the α5β1 as well as the αIIbβ3 integrins require the synergy region in domain III_9 to bind to the RGD motif located in domain III_{10}. (Modified from Leiss et al.)*

Furthermore, the FN gene can be alternatively spliced allowing the expression of up to 20 monomeric isoforms in man and up to 12 in mouse which may result in an even larger variety of FN dimers (Pankov and Yamada 2002). Finally, FN exists in two forms; cellular FN (cFN), which is present in tissues where it is assembled into a fibrillar matrix, and hepatocyte produced plasma FN (pFN), which is secreted at high concentrations (300 µg/ml in man) into the blood where it remains in a non-fibrillar, soluble form (Pankov and Yamada 2002) and is implicated in blood clotting, skin wound healing, atherosclerosis and liver fibrosis (Kornblihtt, Pesce et al. 1996).

1.3.2 FN assembly – a cell mediated process

The existence of fibrillar cFN and soluble pFN largely results from the fact that the assembly of the FN fibrils is a cell-driven process, in which integrin cell-surface receptors play a central role. Integrins shift between a low affinity (also called inactive) and a high affinity (active) conformation (Luo, Carman et al. 2007). In tissues, cells express activated integrins that immediately bind cFN. In blood, haematopoietic cells express their integrins in an inactive conformation, which prevents cells from binding pFN and assembling fibrils. As soon as the blood cell integrins, however, shift into the high affinity conformation, for example when platelets are activated in response to a vascular injury, pFN is bound and assembled into fibrils, which in the case of platelets are required for thrombus stability (Ni, Yuen et al. 2003; Cho and Mosher 2006). A recent report showed that pFN can also diffuse into tissues where it is incorporated into the fibrillar matrix (Moretti, Chauhan et al. 2007).

The assembly of a FN matrix is a complex process involving interactions between various self assembly sites along the length of the molecule, which facilitate the elongation and stabilization of the fibrils. During assembly, FN is initially organized into arrays of fine, cell-associated fibrils, which accumulate and become gradually converted into a dense network of detergent-insoluble fibrils. The differential solubility of the FN matrix in the detergent deoxycholate (DOC) underlies the principle for its biochemical fractionation (Wierzbicka-Patynowski, Mao et al. 2004). The mechanisms of FN self-assembly and fiber organization are still poorly understood but are probably determined by intermolecular interactions involving several FN domains simultaneously. Up to now at least six FN self-binding sites have been identified. The site located in the first five type I modules ($I_{1\text{-}5}$) of the N-terminus is considered to be the most important one, since fragments containing these N-terminal domains can completely inhibit FN-fibrillogenesis without affecting FN-integrin interactions (Wierzbicka-Patynowski and Schwarzbauer 2003; Mao and Schwarzbauer 2005). A further self assembly site is made up of domains $III_{1\text{-}2}$ and seems to promote FN assembly through the interaction between III_1 and C-terminal modules, which in turn unmasks additional FN assembly sites (Xu, Bae et al. 2009). There is a number of conflicting reports about other regions along the FN molecule implicated in FN self-binding. For a review, the reader may be referred to (Mao and Schwarzbauer 2005).

1.3.3 Fibronectins cell binding motifs

FN fibrils provide structural support for cell adhesion at the same time as the adhesion receptors, most notably integrins, transduce signals that promote actin dynamics, cell migration, cell proliferation and apoptosis (Larsen, Artym et al. 2006; Vakonakis and Campbell 2007). Cell adhesion to FN is mainly dependent on the RGD motif located in the 10^{th} type III domain (III_{10}) (see Fig 1.8 and Fig 1.9). This RGD motif is bound by α5β1 integrin (Pierschbacher and Ruoslahti 1984), all members of the αv subfamily, α8β1, α9β1 and the platelet specific αIIbβ3 integrin (see Fig 1.8) (Hynes 2002; Liao,

Gotwals et al. 2002). Among FN binding integrins, however, α5β1 integrin is considered of major importance for the formation of an elaborate meshwork of FN fibrils.

α5β1 integrins require a second FN-binding site in addition to RGD, called synergy region, to obtain maximum binding affinity. This binding site comprises the PSHRN minimal sequence and is located in the ninth type III module (III_9) adjacent to the RGD motif (see Fig 1.8 and 1.9); (Nagai, Yamakawa et al. 1991; Bowditch, Hariharan et al. 1994; Aota and Yamada 1997; Chada, Mather et al. 2006). A combination of electron microscopy and surface plasmon resonance analyses demonstrated that the synergy region is not in contact with the α5β1 integrin bound to FN, and propose an indirect function of the synergy region for the high affinity binding of α5β1 to FN by optimally exposing the flexible RGD motif, or by inducing long range electrostatic steering (Baron, Main et al. 1992; Takagi, Strokovich et al. 2003). More recently it was reported that the α5 integrin subunit engages FN's synergy site in response to increased cytoskeletal forces tensioning the α5β1-FN bond. This study proposes a "catch-bond" model in which FN-bound integrin α5β1 is capable to switch between two states of activation; an active state, facilitating binding to RGD, and a tensed active state, which results in simultaneous binding of synergy region and RGD motif. The additional interaction strengthens integrin-ECM interactions and switches on specific integrin mediated signaling pathways in a force-dependent manner (Friedland, Lee et al. 2009). Mutations in the synergy region reduce α5β1 integrin-mediated FN matrix assembly (Sechler, Corbett et al. 1997), which could result from a shift from α5β1 to αv integrin engagement, as the latter does not require the synergy region for optimal FN binding.

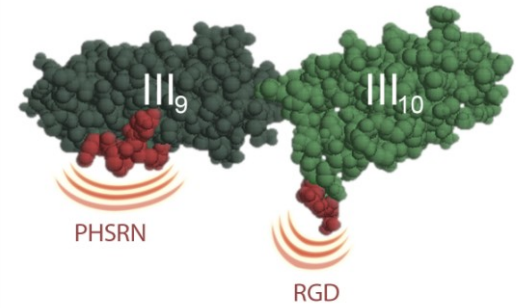

Fig 1.9. ***Schematic representation of FN domain pair type $III_{9\text{-}10}$.*** *The RGD motif extends in a loop-like structure from domain III_{10}. The synergy region, encoded by the minimal sequence PHSRN, is located in domain III_9, adjacent to the RGD motif (Modified from Leiss et al., 2008).*

Some integrin interaction sites within the FN meshwork can be regulated by alternative splicing. One alternatively spliced domain is the variable-region (v-region), which can give rise to five different splice variants in man. Rodents possess two variants of the v-region, named V120 and V95 according to their molecular weight (Schwarzbauer 1991). cFN harbours a v-region in both subunits, while pFN contains only one subunit with a v-region. Biosynthetic analyses of intracellular FN dimer formation revealed, that at least one v-region is essential for formation and secretion of native FN dimers

(Schwarzbauer, Spencer et al. 1989). The v-region, particularly the V120 isoform, can associate with two non-RGD-binding integrins, α4β1 and α4β7, both of which bind the minimal sequences LDV and REDV (Wayner, Garcia-Pardo et al. 1989; Guan and Hynes 1990). Recruitment of FN by α4β1 is able to induce FN assembly *in vitro*, which is independent of the interaction of α5β1 with the RGD-motif (Sechler, Cumiskey et al. 2000). It is unclear, however, whether α4β1-mediated FN fibrillogenesis is relevant *in vivo*. The alternatively spliced extra domain A (EDA) and extra domain B (EDB) are both exclusively present in cFN (see Fig 1.8), and the EDGIHEL sequence of the EDA is thought to facilitate binding to α4β1 and α9β1 integrins (Liao, Gotwals et al. 2002; Shinde, Bystroff et al. 2008). While the *in vivo* role of the integrin binding site in EDA has not been determined yet, ablation of either the entire EDA or EDB allows normal development, while ablation of both extradomains (EDA and EDB) results in early embryonic lethality with multiple cardiovascular defects (Fukuda, Yoshida et al. 2002; Muro, Chauhan et al. 2003; Astrof, Crowley et al. 2007). Since deposition of FN fibrils in mutant mice constitutively lacking the EDA domain was not affected, it is likely that the integrin binding site in EDA is not essential for assembling a FN matrix.

In addition to the previously mentioned integrin binding sites, FN also exhibits two heparin binding domains that mapped to the first five type I domains ($I_{1\text{-}5}$) and the three type III domains preceding the v-region ($III_{13\text{-}15}$) (see Fig 1.8) (Pankov and Yamada 2002). Both domains facilitate the binding of non-integrin cell surface receptors, most notably members of the syndecan family. Although it has been shown that syndecan-2 and syndecan-4 promote FN assembly (Klass, Couchman et al. 2000; Woods, Longley et al. 2000; Morgan, Humphries et al. 2007) via distinct mechanisms, it has not been examined whether the interaction of syndecans with FN by itself is sufficient to induce FN fibril formation.

1.3.4 Fibronectin - a “master organizer” of ECM biogenesis

The functional properties of the FN fibrillar matrix are diverse and represent a prime example of how ECM protein assembly functions. FN fibrils possess binding sites for multiple ECM components (Fig 1.1), which are used to orchestrate the assembly of several other ECM proteins. Up to now, the presence of extracellular FN fibrils has been shown to be essential for the assembly of fibrillins (Kinsey, Williamson et al. 2008; Sabatier, Chen et al. 2009), collagen I, III and thrombospondin-1 (McDonald, Kelley et al. 1982; Sottile and Hocking 2002; Velling, Risteli et al. 2002; Li, Van Den Diepstraten et al. 2003), fibulin-1 (Godyna, Mann et al. 1995) and fibrinogen (Pereira, Rybarczyk et al. 2002). Moreover, it has been reported that a continuous assembly and supply of FN is a prerequisite for continued assembly and matrix stability of collagen I, thrombospondin-1 and fibrillin-1 (Sottile and Hocking 2002; Dallas, Sivakumar et al. 2005).

1.3.5 TGF-β

Deposition into the ECM is a major mechanism known to regulate bioavailability and activity of growth factors. Within the ECM, growth factors can be either stored in an inactive state, or activated to carry out critical functions *in situ* during tissue morphogenesis and repair. The activity of numerous growth factors, including fibroblast growth factor (FGF), vascular endothelial growth factor (VEGF), bone morphogenic protein (BMP) and transforming growth factor β (TGF-β) is regulated through their association with the ECM (Flaumenhaft and Rifkin 1992; Taipale and Keski-Oja 1997; Gregory, Ono et al. 2005). A well characterized example of how ECM regulates growth factor activity is transforming growth factor β1 (TGF-β1), a prototypic member of a large family of secreted cytokines that plays a crucial role in multiple processes during development, including vascular development, hematopoiesis and ECM production, and in the maintenance of tissue homeostasis in adult life (for a review, see (ten Dijke and Arthur 2007). Most cells secrete TGF-β as an inactive complex containing the TGF-β precursor, the so called latency-associated protein (LAP) linked to various latent TGF-β binding proteins (LTBPs) (see Fig 1.10; (Dallas, Miyazono et al. 1995)). LTBPs are members of the fibrillin superfamily and are well established as extracellular key-regulators of TGF-β actions reviewed in (Hyytiainen, Penttinen et al. 2004). They facilitate the secretion of latent TGF-β from cells and target the growth factor to the ECM. Finally, they provide mechanisms to activate TGF-β from ECM associated latent complexes either through proteolytic cleavage or via a αvβ6 integrin dependent mechanism (Annes, Rifkin et al. 2002; Dallas, Sivakumar et al. 2005; Fontana, Chen et al. 2005). Recent studies have shown that the continuous assembly of LTBP-1, similarly to fibrillin-1, is critically dependent on the continual presence of a fibrillar FN matrix, highlighting the fact that FN does not only act as an orchestrator for assembly of multiple ECM proteins, but also modulates growth factor signaling events by regulation of the growth factors bioavailability.

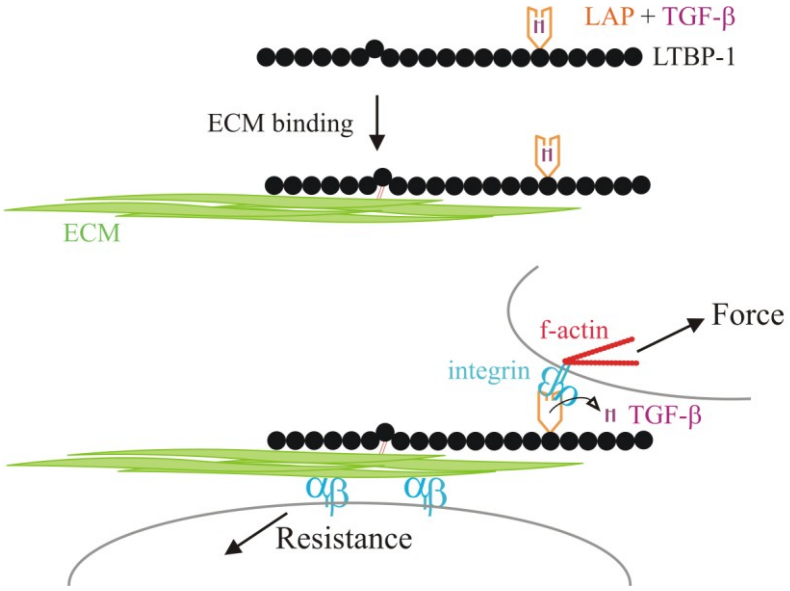

Fig 1.10. ***Integrin-mediated activation of ECM anchored latent TGF-β****. Latent TGF-β is comprised of TGF-β (magenta), latency associated protein (LAP, orange) and latent TGF-β binding protein (LTBP, black). Once latent TGF-β is fixed to the ECM, integrin αvβ6 on an adjacent cell may bind to LAP and transmit an actomyosin generated retractile force which releases biologically active TGF-β (Based on Annes et al., 2002).*

TGF-β superfamily members utilize a variety of type I and II Ser/Thr kinase cell surface receptors. The vast majority of cell-types express the activin receptor like kinase-5 type I receptor (ALK5) and TGF-β type II receptors (TGF-βRII). One of the best characterized mechanisms of TGF-β initiated signal transduction is mediated via ALK-mediated phosphorylation of Smad effector proteins. They can be grouped in three classes based on their functions; the receptor-activated Smads (R-Smad 1, 2, 3, 5 and 8), the common mediator Smad (Co-Smad 4) and inhibitory (I-) Smads 6 and 7. ALK5, for instance, mediates the activation of the R-Smads 2 and 3, whereas the endothelial specific ALK1 mediates the activation of the R-Smads 1 and 5. Upon activation, R-Smads are capable to associate with Co-Smads resulting in the formation of a heteromeric complex that accumulates in the nucleus and triggers gene transcription (see Fig 1.11) (reviewed in (Rahimi and Leof 2007; ten Dijke and Arthur 2007)).

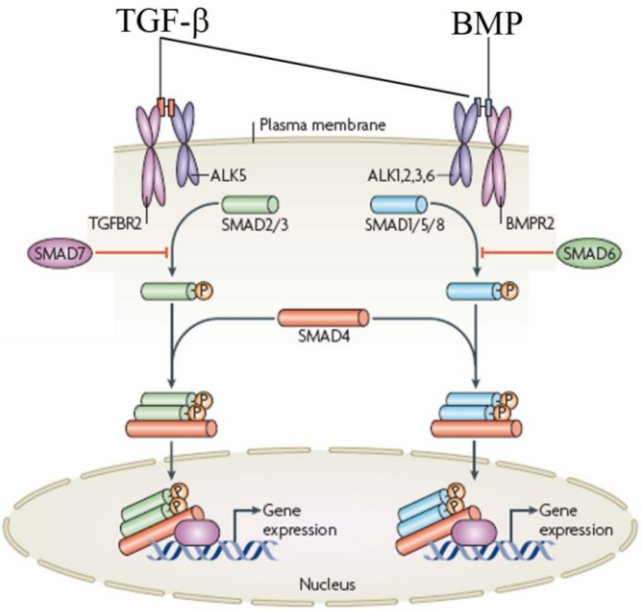

Fig 1.11. ***Canonical pathway of TGF-β induced Smad activation****. In most cells, TGF-β signals via TGF-βRII and ALK5, resulting in activation of R-Smad 2 and 3 mediator proteins. Endothelial cells additionally express the ALK1 receptor, which activates R-Smad 1 and 5 in response to TGF-β binding. Activated R-Smads associate with Smad 4, translocate in the nucleus, where they regulate the expression of target genes (Modified from ten Dijke et al., 2007).*

Genetic ablation of TGF-β pathway components impressively underscored the importance of TGF-β signaling for proper yolk sac angiogenesis and hematopoiesis during embryonic development (Goumans, Liu et al. 2009).

1.3.6 FNs role in development

The expression of FN in mice sets in at the blastocyst stage where it is involved in parietal endoderm migration and trophoblast outgrowth during implantation (Armant, Kaplan et al. 1986). Later in gastrulation, FN expression is mainly localized to the ectodermal-mesodermal interface, where it may promote the migration of mesodermal cells (Smith, Symes et al. 1990). Experiments utilizing anti-FN antibodies injected into embryos during gastrulation inhibited lateral migration of mesodermal cells and the migration of ectoderm derivatives such as neural crest cells (Lallier, Artinger et al. 1990). In addition, FN has been reported to promote the migration of primordial germ cells; it is implicated in heart development, somitogenesis and vasculogenesis (Linask and Lash 1986; Risau 1991; Icardo, Nakamura et al. 1992). The initiation of epithelial branching, a process taking place during the development of organs including salivary gland, lung and kidney has also been shown to depend on FN as an inducer of cleft formation (Sakai, Larsen et al. 2003).

Targeted inactivation of the FN gene in mice leads to early embryonic lethality around E8.5 due to severe defects in the development of the mesoderm and mesoderm-derived

structures. Very early occurring developmental processes, such as implantation and initiation of gastrulation, which is accompanied by extensive mesodermal movement, proceed normally in FN-null embryos. Until E7.5, mutant homozygous embryos appear largely normal with respect to their number of germlayers and the morphology of extraembryonic membranes. Abnormalities are first visible by E8.0 and are manifested in a shortened anterior-posterior axis, a deficient head and trunk mesoderm, a disorganized notochord and a complete absence of somites (see Fig 1.12). Additionally, the ectoderm of FN-null embryos at this stage shows multiple bends and distortions, whereas allantois and yolk sac including red blood islands appear to be normal compared to wild-type controls. By E8.5, the shortened anterior-posterior axis is even more pronounced between mutants and wild-type littermates at this stage. The head-folds have arrested development and appear distorted. Some FN-null embryos exhibit a kinked neural tube and only a fraction possesses a primitive heart bulge, while none of the mutant embryos has initiated turning. In contrast to the 8-12 somite pairs present in wild-type control embryos at this stage, FN-null embryos lack somites (George, Georges-Labouesse et al. 1993; Georges-Labouesse, George et al. 1996). In summary, the observed defects are proving the essential requirement of FN for normal development and in particular for the development of mesoderm-derived tissues.

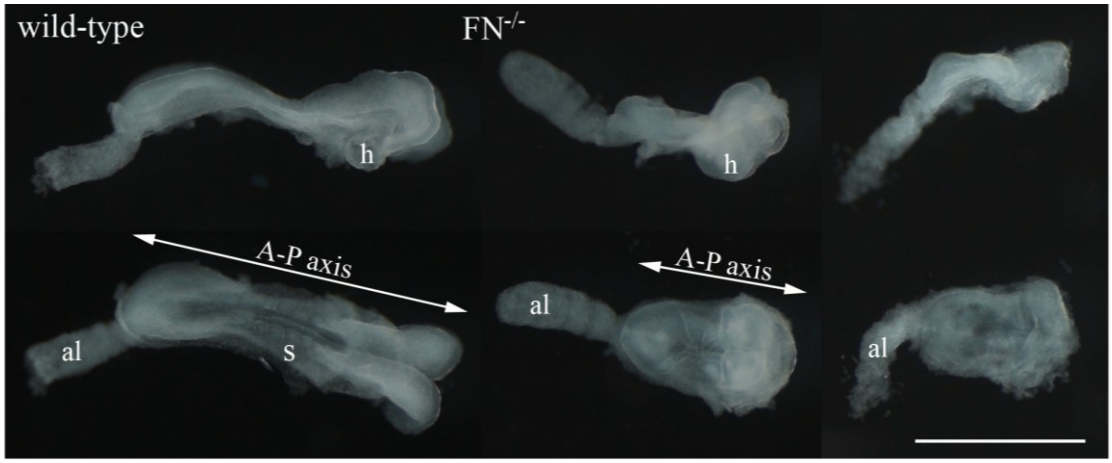

Fig. 1.12. ***Whole mount images of wild-type and FN-null- embryos****. Side (top) and dorsal view (bottom) of E8.0 embryos. FN-null embryos exhibit a notably shortened anterior-posterior axis (A-P axis) as compared to the wild-type littermate. Note that all mutants lack somites and that some of the FN$^{-/-}$ embryos lack a primitive heart (right). al, allantois; h, heart; s, somite; Scale bar: 500 µm.*

1.3.6.1 FNs role in somitogenesis

Somites are mesoderm-derived structures, which are formed transiently during vertebrate development and give rise to the prospective skeletal muscles, dermis and vertebra in the adult organism. Somites are budding off as regular shaped segments in a head-to-tail manner from the anterior end of the presomitic mesoderm (PSM), which is located paraxially to the neural tube demarcating the A-P axis of the embryonic midline

(see Fig 1.13). In terms of their position, somites can be divided into anterior and posterior groups, each of which exhibits individual gene regulation and growth rate. The mechanism of pre-patterning and formation of epithelialized somite-blocks with defined boundaries is dependent on a plethora of temporally exactly defined signaling events, which are mainly represented by a cyclic signaling network involving the Notch, fibroblast growth factor (FGF), Wnt, and retinoic acid pathways (reviewed in (Pourquie 2001; Chong and Jiang 2005; Gridley 2006; Aulehla and Pourquie 2008)). A crucial role for FN-integrin signaling in somite formation has been suggested by the observation, that FN-deficient mouse embryos completely lack somites, whereas mice lacking the FN receptor integrin α5β1 develop only anterior somites and completely lack posterior somites (George, Georges-Labouesse et al. 1993; Yang, Rayburn et al. 1993). Targeted inactivation of the *fibronectin1* and *α5 integrin* genes in zebrafish revealed that the FN-α5 integrin interaction is indeed indispensable for somite epithelialization and the maintenance of intersomitic boundaries of the anterior somites (Julich, Geisler et al. 2005; Koshida, Kishimoto et al. 2005). The restriction of the observed defects to the anterior somites is probably due to a functional redundancy of FN binding integrins exclusively expressed in the caudal located presomitic mesoderm of the zebrafish. Despite the converse orientation of somites groups affected by integrin α5β1-FN signaling in zebrafish and mice, somitogenesis provides a telling example on how FN-integrin interactions affect the mesodermal development.

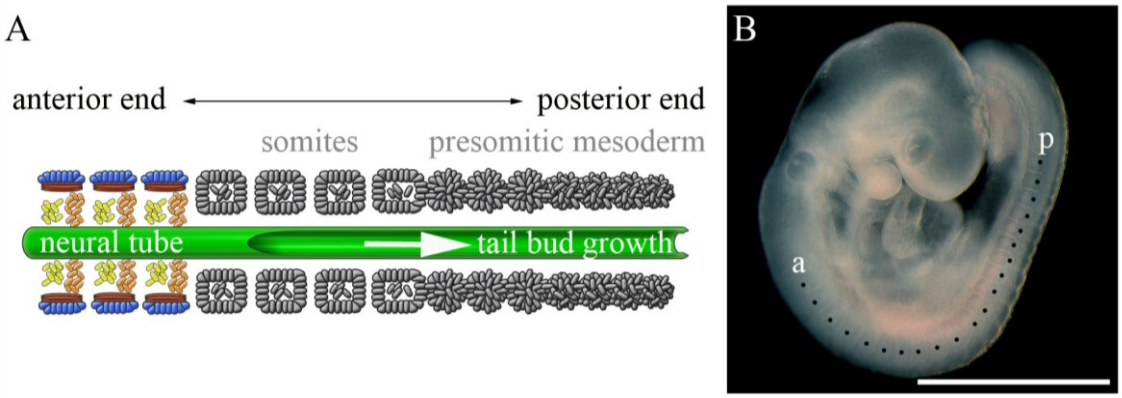

Fig 1.13. ***Formation of somites from the presomitic mesoderm (PSM)****.* ***A****. Pairs of somite blocks bud off simultaneously from the anterior end of the presomitic mesoderm on both sides of the neural tube. Anterior somites differentiate, giving rise to dermatome, myotome and sclerotome (depicted in blue, red and orange).* ***B****. Side view of an E9.5 embryo. Note the somite blocks marked with black dots along the A-P axis. a, anterior somite; p, posterior somite; Scale bar: 500 µm*

1.3.6.2 FNs role in neovessel formation

The cardiovascular system is the first organ to develop and to become functional during embryogenesis. A characteristic trait of FN-null embryos is the severely impaired development of the cardiovascular system.

The first step in neo-vascularization is the formation of the so called primitive vascular plexus by *in situ* differentiation of mesodermally derived angioblasts - vascular endothelial cell precursors that have not yet formed a lumen (see Fig 1.14). This process, termed vasculogenesis, is largely dependent on vascular endothelial growth factor (VEGF) and fibroblast growth factor (FGF), and results in the generation of primitive blood vessels, which basically consist of endothelial-lined capillaries. Once the primitive vascular plexus has formed, more endothelial cells are generated in a second step, which leads to formation of new capillaries. These can be either formed by sprouting or splitting (intus-susception) of pre-existing capillaries, in a process termed angiogenesis (see Fig 1.14). During angiogenesis, some capillaries are further remodelled into larger vessels and recruit several layers of smooth-muscle cells to the vessel walls in a platelet derived growth factor (PDGF)-dependent manner. While vasculogenesis is restricted to early developmental stages, angiogenesis starts during development and lasts throughout post-natal life (Flamme, Frolich et al. 1997; Pepper 1997; Risau 1997).

Studies of mutant mice revealed that endothelial, ECM-bound integrins trigger numerous signaling pathways crucial for vasculogenesis and angiogenesis. Both processes of neovessel formation seem to require the interaction of fibrillar FN with its integrin receptors α5β1 and αvβ3 (Zhou, Rowe et al. 2008) for a review, see (Stromblad and Cheresh 1996). This finding may also explain the severe vascular phenotype observed in FN-null embryos. Similarly, TGF-β was shown to be essential for these neo-vessel formation processes, since mice with compromised TGF-β signaling exhibit severe vascular defects, characterized by a stalled angiogenesis in yolk sacs (see Fig 1.13; for a review, see (ten Dijke and Arthur 2007).

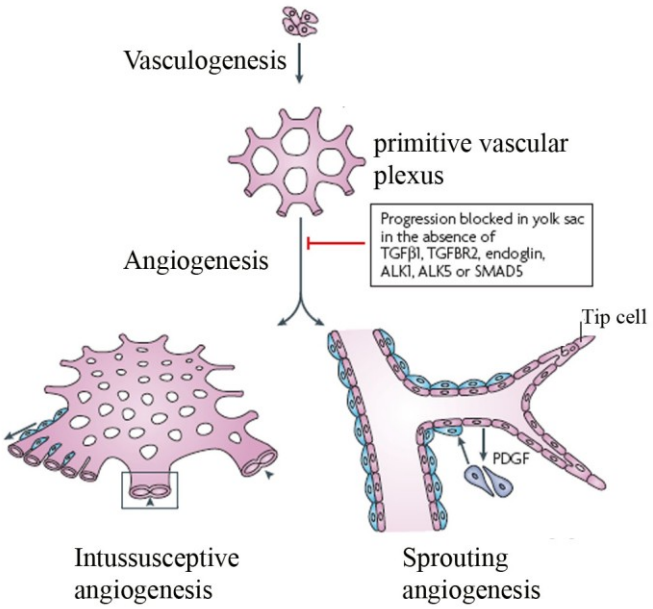

Fig 1.14. ***Processes of neovessel formation****. Endothelial progenitor cells (angioblasts) differentiate to endothelial cells that form the primitive vascular plexus in a process called*

vasculogenesis. Angiogenesis leads to formation of new vessels from pre-existing capillaries in two different ways: Either through sprouting of capillaries or through splitting of a capillary resulting in formation of two capillaries. Growth factors including VEGF, TGF-β, FGF and PDGF, as well as integrin interactions with a fibrillar FN matrix, in which the endothelial cells are embedded, are required for these processes (Modified from ten Dijke et al., 2007).

1.4 Aims of the projects

Part I

It is thought that FN assembly is induced by α5β1 integrin binding to the RGD motif located in FN's 10th type III domain along with the synergy motif located in the adjacent 9th type III domain. Additional RGD binding integrins, including αvβ3 and αIIbβ3 can partially substitute for α5β1 integrin in FN matrix assembly. Gene ablation studies in mice confirmed that these two RGD dependent FN matrix assembly mechanisms induced by either α5β1 or αv integrins exist *in vivo* and that each of them can compensate for the absence of the other. To test how FN binding receptors compensate for each other during development and FN fibril formation, it would be necessary to generate double, triple or even higher order combinations of FN cell-surface receptor knock out mice. However, the necessary intercross combinations can not be performed since most integrin-null mice are recessive lethal (α4, α5, αv, α8). Moreover, FN cell-surface receptors, including integrins and syndecans, interact with multiple ECM components and vice versa, which would further complicate the interpretation of the phenotypes. In order to specifically test the role of FN-RGD binding integrins *in vivo*, a mouse strain was generated in which the aspartic acid residue (D) of FN's RGD motif was exchanged against glutamate (E), resulting in a complete inactivation of this motif for cell adhesion. One goal was to investigate the consequences of this knock in mutation *in vivo* with a particular emphasis on the development of the mesoderm and mesoderm-derived structures. A second goal was to characterize the effects of the FN-RGE mutation on FN matrix assembly *in vivo* and *in vitro*.

Part II

FN is a dimeric glycoprotein, and several studies reported that the dimerization is essential for the assembly of a fibrillar FN matrix. All these studies were performed *in vitro* and with truncated FN polypeptides. In order to test this function with full length FN *in vivo*, a genetically modified mouse strain was generated which exclusively expresses a monomeric form of FN. The second goal of this study was to investigate the consequences resulting from this mutation on the physiological and molecular level.

2 Materials and Methods

2.1 Common chemicals

Unless further specified, all chemicals used in this study were purchased from: Sigma Aldrich (Munich, Germany), Riedel de Haen (Seelze, Germany), Carl Roth GmbH (Karlsruhe, Germany), Merck (Darmstadt, Germany), Serva (Heidelberg, Germany) and Roche Diagnostics GmbH (Mannheim, Germany).

2.2 Animals

All mouse strains used in this study were maintained and bred in the animal facility of the Max-Planck-Institute of Biochemistry (Martinsried, Germany). The strains were backcrossed to C57BL6 for at least 7 generations. 3-4 weeks after birth, the pups were weaned, separated according to gender and marked with ear tags. For genotyping, tail-tip biopsies were taken and immediately subjected to DNA isolation (2.8.1.1). For matings, female mice of at least 6 weeks of age, and male mice older than 9 weeks were used. All experiments were carried out according to the German Animal Protection Law.

2.2.1 Breeding scheme

In order to generate mice homozygous for the FN knockin mutations, heterozygous mice were intercrossed overnight. Successful mating was indicated by a female vaginal plug whose presence marks the day 0.5 of gestation (also: 0.5 dpc or E0.5). Embryos were harvested and dissected at indicated days of gestation.

2.2.2 Dissection of mouse embryos

Both mutations in FN analysed in this study represented a recessive embryonic lethal trait. Therefore it was necessary to analyse mouse embryos at defined post-implantation stages. In order to dissect embryos, the pregnant mother was euthanized and laid supine on a Styrofoam pad. Subsequently, the animal was fixed on the pad with needles and soaked with 70% ethanol to reduce the risk of contaminating the dissection. Using surgical scissors, a lateral incision along the midline was made to expose the abdominal cavity. The female reproductive organs, two uterine horns, the oviduct and the ovaries, are located at the dorsal region of the body cavity. The uterine horns containing the embryos were grasped below the oviducts and were removed by cutting them free along the mesometrium. Dissected uteri were transferred into ice-cold PBS and each embryo was separated by cutting between implantation sites along the uterine horn. All further dissection steps were performed under a stereomicroscope (2.9.5) using watchmaker's

forceps. At each embryo, the muscle layer lining the decidual tissue was removed and the embryo was carefully shelled out of the decidua. Finally, the yolk sac and amnion were removed and little pieces of the yolk sac were collected for genotyping (2.8.1.2). Dependent on the further histological application, the bare embryo was either stored in ice-cold PBS or fixed overnight at 4°C in the appropriate fixative.

10 x PBS: 80 g NaCl, 14.4 g Na_2HPO_4, 2.4 g KH_2PO_4, 2 g KCl filled up to 1 l with ddH_2O and adjusted to pH 7.4 with HCl

2.3 Histological analysis of Fibronectin (FN) knockin mice

2.3.1 Material Histology

Embedding machine: Shandon, HistoCentre 2

Microtomes: Microm, Vacutome HM5000M, HM355S

Cryomold: Sakura, Tissue-Tek, #4566

Cryomatrix: Thermo Scientific, Shandon Cryomatrix™, #6769006

Microscope slides: Thermo Scientific, Menzel-Gläser Superfrost®Plus, #J1800AMNZ

Entellan mounting medium: Merck, #1.07960

Meyers hemalaun: Merck, #1.09249

Eosin G: Merck, #1.09844

2.3.2 Histological methods

The performance of a significant histological analysis strongly depends on the best possible conservation of the specimen's morphology and its biological activity. Both properties of the specimen are negatively affected by fixation and embedding, which are crucial steps in the histological workflow. Therefore it is necessary to choose the most suitable from a variety of fixation and embedding protocols for each particular experiment. Paraformaldehyde (PFA) and alcohols (ethanol, methanol) are among the most widely used fixatives. PFA – and alcohol to a lesser extent - preserves the morphology very well but may compromise the biological activity of the specimen. In contrast, unfixed tissue is prone to morphological disaggregation, but features a maximum of biological activity. If a histological assay is rather unsusceptible for PFA treatment, PFA fixation and paraffin embedding is the method of choice. Paraffin embedding preserves the morphology of the specimen very well and allows cutting of thin sections of around 6 µm thickness (2.3.2.1). Freezing of the specimen in cryomatrix was the second embedding method used in this study (2.3.2.2). This procedure does not require fixation and thus optimally maintains the biological activity, but results in a limited conservation of the morphology.

PFA fixing solution: 3.7% PFA in PBS, boiled briefly and cooled on ice

2.3.2.1 Preparation of Paraffine sections

Pregnant mice were sacrificed at selected days of gestation, embryos were dissected (2.2.2) and fixed in freshly prepared, ice-cold paraformaldehyde (3.7% PFA in PBS) overnight at 4°C. Next day, the embryos were washed with ice-cold PBS and then dehydrated by sequential incubation in ethanol solutions with ascending concentrations (70%, 80%, 90%, 95% and 100%) for 1 h each. Subsequently, the embryos were incubated in fresh xylene for 2 x 10 min and then transferred in 5 ml of melted paraffin–wax for 2 h at 65°C. The paraffin was changed further two times, followed by 2 h incubation at 65°C each time. Next, the embryos were embedded in a paraffin block using an embedding machine and were then stored at 4°C until cutting. For cutting, the paraffin block was mounted in a microtome and cut into 6 µm thick sections. During the process, the quality of each section was routinely checked under a light microscope (2.9.4). Finally, sections were air-dried overnight at 37°C and subsequently stored at 4°C.

2.3.2.2 Preparation of Cryo-sections

Embryos were sequentially incubated in sucrose solutions with ascending concentrations (0.5%, 1%, 2%, 5%, 10%, 20% sucrose in PBS) for 1 h each step. Subsequently, the embryos were orientated on the bottom of a small tissue tek plastic container under a stereomicroscope (2.9.5) and all residual liquids were carefully removed using the tip of a facial tissue. Next, the embryos were covered with Cryomatrix^{TM} and subsequently frozen by placing the whole container on a copper plate situated on dry-ice. Frozen blocks were stored at - 80°C until cutting. For cutting, the tissue tek container was removed, the frozen block mounted on a cryo–microtome and cut into 8 µm sections at a maintained temperature of –17°C. The sections were transferred to glass microscope slides and dried for ~ 20 min at RT before they were stored at -80°C.

2.3.2.3 Hematoxylin/Eosin (H&E) staining of sections

H&E staining is a commonly used histological technique to demonstrate the morphology of a broad variety of different tissue structures. Haematoxylins major oxidation product Hematein stains basophilic molecules, such as DNA, RNA and acidic proteins in blue, whereas Eosin stains cytoplasmic components and connective tissues in pink. In order to perform an H&E stain, paraffin sections were de-paraffinised for 2 x 5 min in xylene. Afterwards, sections were re-hydrated in 100%, 95%, 90%, 80% and 70% ethanol for 2 min each. Next, the slides were stained for 1 min in a Hematoxylin solution, followed by a washing step in tap water. After the Hematoxylin stain was completed, the slides were stained for 1 min in Eosin solution. The staining was again terminated by a washing step in tap water. In order to allow the final mounting step of the slides, the sections had to be dehydrated by subjecting the slides to ethanol and xylene in the reverse order as mentioned above. Finally, slides were mounted with Entellan and stored at 4°C.

2.4 Immunological Methods

2.4.1 Material Immunological Analysis

Antibody	Company	Cat. No.	species	dilutions				special treatments
				IF	IHC	WB	FACS / MACS	
α4 integrin-PE	BD	557420	rat	-	-	-	1:200	
α5 integrin-PE	PharMingen	557447	rat	1:50	-	-	1:200	
α6 integrin-PE	PharMingen	555736	rat	-	-	-	1:200	
αv integrin-PE	BD	551187	rat	-	-	-	1:200	
β1 integrin-PE	BioLegend	102207	rat	-	-	-	1:200	
β3 integrin-PE	eBioscience	12-1106	rat	-	-	-	1:200	
cCasp 3	Cell signaling	#9661	rabbit	-	1:200	-	-	boil sections 15 min in 10 mM Citrate pH 6.0
Endomucin	Santa Cruz	sc-53941	rat	1:300	1:300	1:500	-	
pERK1/2	Cell signaling	#4376	rabbit	-	-	1:1000	-	WB: block and incubate in 5% BSA/PBS
ERK1/2	Cell signaling	#9102	rabbit	-	-	1:1000	-	WB: o/N at 4°C in 5% BSA/PBS
FAK	Abcam	ab71563	rabbit	-	-	1:1000	-	WB: block and incubate in 5% BSA/PBS
pY397FAK	Biosource	#44-624G	rabbit	-	-	1:1000	-	WB: o/N at 4°C in 5% BSA/PBS
FN	Chemicon	Ab 2033	rabbit	1:400	1:400	1:20000	-	
FN	M. Humphries	-	chicken	1:300	1:300	-	-	
GAPDH	Calbiochem	CB 1001	mouse	-	-	1:25000	-	
Lamin A	Cell signaling	#2032	rabbit	-	-	1:1000	-	
LTBP-1	C. Heldin	-	rabbit	1:300	-	1:20000	-	
Pecam (CD 31)	PharMingen	01951D	rat	1:300	1:200	-	-	
phalloidin Alexa 488	Invitrogen	A12379	-	1:400	-	-	-	
phalloidin Alexa 647	Invitrogen	A22287	-	1:400	-	-	-	
pHiston3	Upstate	16-189	rabbit	-	1:100	-	-	treat sections 30 min in 2 M HCl at 60°C
pSmad2/3	Santa Cruz	sc-11769-R	rabbit	-	-	1:1000	-	WB: o/N at 4°C in 5% BSA/PBS
Smad2/3	Santa Cruz	sc-8332	rabbit	-	-	1:1000	-	
Smad4	Epitomics	#1676-1	rabbit	-	-	1:5000	-	
tubulin	Chemicon	Mab1864	rat	-	-	1:10000	-	
sec. antibodies								
anti-mouse HRP	BioRad	170-6516	goat	-	-	1:20000	-	
anti-rabbit HRP	BioRad	170-6515	goat	-	-	1:20000	-	

anti-rat HRP	Jackson	712/035/150	donkey	-	-	1:20000	-	
streptavidin-HRP	Vector Lab.	SA-5004	-	-	-	-	-	1:1000 in solid-phase binding assay
anti- rabbit Alexa 488	Invitrogen	A11008	goat	1:400	1:300	-	-	
anti-rabbit Alexa 547	Invitrogen	A11010	goat	1:400	1:300	-	-	
anti-rabbit Alexa 647	Invitrogen	A21244	goat	1:400	1:300	-	-	
anti-chicken Cy3	Jackson	703-165-155	donkey	1:400	1:300	-	-	
anti-rat Alexa 488	Invitrogen	A11008	goat	1:400	1:300	-	-	
anti-rat Alexa 647	Invitrogen	A21247	goat	1:400	1:300	-	-	

Were indicated, a 5 min staining with 4', 6-Diamidino-2-phenylindole (DAPI, 1:10000 in PBS) was made prior to the final steps of washing and mounting in order to visualize the nuclei.

LabTek chamber slide: Nunc, #177402

Pap pen: Kisker-Biotech, #MKP-1

Elvanol: 12 g Mowiol 4 – 88 (Roth, #0713) dissolved in 30 ml 87% glycerol, 60 ml Tris-HCl pH 8.5 and 30 ml H_2O

DAPI: Sigma, Biochemica, #32670

2.4.2 Immunohistochemistry (IHC)

2.4.2.1 Preparation of sections for IHC

Prior to staining, paraffin sections were de-paraffinized and re-hydrated as mentioned above (2.3.2.3). Cryo–sections were thawed at RT for 10 min and subsequently rinsed two times for 1 min each in ddH_2O to remove all remnants of cryo–matrix. After short rinsing with PBS, each specimen was circled with a hydrophobic barrier pen (Pap pen) in order to minimize the required volume of staining solutions.

2.4.2.2 Immunofluorescence staining of sections

For detection of intracellular proteins, prepared (2.3.2.3) sections were permeabilized with 0.1% Triton X-100 in PBS for 10 min at RT prior to blocking in blocking buffer (3% BSA in PBS) for 1 h at RT. After blocking, overnight incubation of the sections with the indicated primary antibodies (diluted in blocking buffer) was performed at 4°C in a humidified chamber. Next day, slides were washed 3 x 10 min in PBS and subsequently incubated with the appropriate secondary antibodies (diluted in blocking buffer) for 2 h at RT in the dark. After three final washes with PBS (10 min each, in the dark), the sections were mounted with Elvanol (2.4.1).

2.4.2.3 3, 3'-Diaminobenzidine (DAB) staining of sections

3, 3'-Diaminobenzidine is a substrate for peroxidase that forms a brown precipitate when it reacts with this enzyme. Based on this reaction, epitopes bound by peroxidase-conjugated antibodies can be specifically stained by application of DAB. Since endogenous peroxidases are prevalent in most tissues, it is necessary to block the activity of those enzymes by a H_2O_2 treatment prior to the DAB staining procedure. In order to perform a DAB staining on sections, slides were prepared as mentioned above (2.3.2.3) and subsequently incubated for 10 min in a 0.3% H_2O_2 / methanol solution to block endogenous peroxidases. After a 5 min wash in PBS, the sections were blocked in blocking buffer (5% goat serum in PBS-T) for 1 h at RT. Subsequently the indicated primary antibody (diluted in blocking buffer) was added for overnight incubation at 4°C in a humidified chamber. Next day, the slides were washed 3 x 10 min with PBS-T prior to incubation with the appropriate peroxidase-conjugated secondary antibody (diluted in blocking buffer) for 1 h at RT. Consecutively, 3 x 10 min washes with PBS were performed and DAB solution containing 0.03% H_2O_2 was added to start the staining-reaction. After a satisfactory staining intensity was reached (takes ~ 1–2 min), the reaction was stopped by extensive washes with tap water. Finally, a Hematoxylin counter-stain (2.3.2.3) was performed (~ 30 sec) to improve the contrast of the specimen, before the slides were subjected to dehydration and mounting with Entellan (2.3.1).

PBS-T: 0.1% Tween-20 in PBS

DAB solution: 0.3 mg DAB in 0.5 M Tris-HCl pH7.6

2.4.3 Whole mount staining of embryos

2.4.3.1 Whole mount immunofluorescence staining

Staged embryos (2.2.2) were dissected in PBS and fixed overnight at 4°C in Dent's fixative. Next day, embryos were sequentially re-hydrated in methanol / PBS-T solutions with decreasing methanol contents (75%, 50%, 25% methanol) for 1 h each. Subsequently, re-hydrated embryos were blocked 2 x 1 h in blocking buffer (5% goat serum in PBS-T) before the primary antibodies (diluted in blocking buffer) were added for overnight incubation at 4°C. Embryos were washed extensively for 5–8 h in TBS-T, and subsequently incubated with the appropriate secondary antibodies (diluted in 5% BSA / TBS-T) overnight at 4°C in the dark. Finally, after extensive washes in TBS-T (5–8 h, in the dark at RT), the embryos were carefully mounted in Elvanol (2.4.1).

Dent's fixative: 20% DMSO in methanol

TBS: 150 mM NaCl in 50 mM Tris-HCl pH 7.5

TBS-T: 0.1% Tween-20 in TBS

2.4.3.2 Whole mount DAB staining

Staged embryos (2.2.2) were dissected in PBS and fixed overnight at 4°C in Dent's fixative. In order to block endogenous peroxidases, the embryos were transferred to a methanol / DMSO / 30% H_2O_2 (4:1:1) solution for 5 h at RT. Next, re-hydration was performed as mentioned previously (2.4.3.1) and the embryos were subsequently transferred to a PBS-MT blocking solution for 2 x 1 h at RT. After blocking, the primary antibody (diluted in PBS-MT) was applied for overnight incubation at 4°C. The embryos were washed for 2 x 1 h at 4°C and 3 x 1 h at RT in PBS-MT before an overnight incubation at 4°C with the appropriate secondary antibody (diluted in PBS-MT) was performed. In order to achieve a low background signal, the embryos were subjected to extensive washes: 2 x 1 h in PBS-MT at 4°C, 3 x 1 h in PBS-MT at RT and 20 min in PBS-BT at RT. Subsequently, embryos were incubated in a defined volume of DAB solution (2.4.2.3) for 30 min at RT. To develop the DAB precipitate, H_2O_2 was added to a final concentration of 0.03% and the staining-reaction was monitored under a stereomicroscope (2.9.5) until the stained structures became visible (duration: ~ 10 min). As soon as the desired staining intensity was reached, the reaction was stopped by repeated washes with PBS. To further optimize the imaging results, the embryos were cleared. To achieve clearance, the embryos were dehydrated (inverse procedure as mentioned in (2.4.3.1)) and subsequently transferred into a glass vial containing the clearance solution (1:2 mixture of benzyl alcohol and benzyl benzoate). Cleared embryos were stored at 4°C.

PBS-MT: 2% skim milk powder and 0.1% Triton X-100 in PBS

PBS-BT: 0.2% BSA and 0.1% Triton X-100 in PBS

2.4.4 Immunostaining of adherent cells

All immunostainings of adherent cells were performed on pre-coated LabTek chamber slides. Coating was performed overnight at 4°C with proteins and protein-concentrations indicated. Next day, slides were washed once with PBS and 1 - 8 x 10^4 cells - dependent on the type of assay performed - were seeded into one well (final volume: 400 µl medium). After indicated times of culture in a cell incubator, cells were washed once with PBS and fixed with freshly prepared, ice–cold PFA (2.3.2) for 10 min at RT. Subsequently, slides were washed in PBS and incubated for 1 h in blocking solution. After blocking, the indicated primary antibodies (diluted in blocking buffer) were added and incubated for 2 h at RT. Next, 3 x 10 min washing steps with PBS were performed, followed by incubation with the appropriate secondary antibodies (diluted in blocking buffer) for 1 h at RT. Finally, slides were washed three times 10 min each in PBS and mounted in Elvanol (2.4.1).

2.4.5 Flow cytometry (FACS)

Flow cytometry is a widely used fluorescence-based technique that allows the discrimination of different cell populations in a heterogeneous cell suspension. Before a

FACS run is performed, cell-surface proteins are either directly or indirectly labelled with antibodies conjugated to different fluorochromes (e.g. FITC, PE or Cy5). During the FACS run, the labelled cell suspension is sucked up into a capillary and subjected to a liquid flow that only allows single cells to pass a cuvette. There, a laser excites the fluorochromes linked to the cell and the emitted fluorescence and scattered light of each individual cell is measured simultaneously. The so-called forward scatter signal (FSC) provides information about the cell size, whereas the side scatter signal (SSC) is proportional to the granularity of the cells. The light-signals are detected by a photomultiplier, are integrated and online displayed in a cumulative curve diagram.

2.4.5.1 FACS of surface antigens

In order to determine the expression level of integrins on the cell-surface, FACS analysis was performed: 5 x 10^5 – 1 x 10^6 cells were pelleted and re-suspended in 200 µl FACS buffer and transferred into a U-bottom well of a 96 well plate. Next, cells were spun down (5 min at 4°C, 1500 RPM) and the pellet was subsequently re-suspended in 50 µl of the primary antibody solution (Antibody in FACS buffer). The cell suspension was left on ice in the dark for 30 min. After a washing step with 150 µl FACS buffer, cells with un-conjugated primary antibodies were incubated (15 min, on ice, in the dark) with 50 µl of secondary antibody solution; whereas cells with fluorochrome coupled primary antibodies were simultaneously incubated in FACS buffer w/o antibodies. After a final washing step, cells were re-suspended in 200 µl FACS buffer and transferred to FACS tubes. Until measurement, all samples were kept on ice in the dark. Shortly before application on the flow cytometer, dead cells in the cell suspension were stained with propidium-iodine. Therefore, a propidium-iodine solution (1 mg/ml, working concentration 1:400) was mixed with the cells in order to allow distinction between living and dead cells. The obtained data was processed using CellQuest™ software.

Flow cytometer: Becton Dickinson, FACSCalibur

FACS tubes: Alpha Laboratories, #QS845

FACS buffer: 2% FBS and 2 mM EDTA in PBS, sterile filtered

Propidium-iodine: Roth GmbH, #CN74.1

2.5 Cell culture methods

2.5.1 Material cell culture

5, 10, 25 ml pipettes: Corning, Costar Stripette, #4487, #4488, #4489

Multi-well plates (Corning): 96 well: #3799, 24 well: #3524, 6 well: #3046

15, 50 ml tubes: Corning, CentriStar, #430791, #430829

Cryogenic vial: Corning, #430489

60, 100 mm dishes: Falcon, Easy Grip, #353004, #353003

140 mm dish: NUNC, #168381

Cell growth media: Gibco, DMEM (#31966-021), DMEM/F-12 (#31331), AIM-V Medium (#12055), RPMI 1640 (#31870)

Non-essential amino acids (NEAA): Gibco, MEM NEAA x 10, #11140

Foetal bovine serum (heat inactivated: 15 min at 65°C): Gibco, #10270-106

Trypsin: Gibco, Trypsin / EDTA (x 10), #15400-054

P/S: PAA, Penicillin / Streptomycin (x 100), #P11-010

Endothelial cell growth supplement: Sigma, #E2759

Heparin: Sigma, #H1027

Fibronectin: Calbiochem, bovine plasma, #341631

Vitronectin: BD, human, #354238

Laminin 111: gift from Prof. Dr. Rainer Deutzmann, University of Regensburg, Germany

2.5.2 Isolation and culture of primary embryonic fibroblasts

Fibroblasts were isolated from E9.5 staged embryos. Each embryo was dissected in PBS (2.2.2) and shortly after transferred in 50 µl of 0.5 x Trypsin / EDTA solution. Release of fibroblasts from the tissue was achieved by up and down pipetting, followed by a 3 min digestion step in the Trypsin solution. Finally, the digest was mixed with 1.5 ml growth medium and was transferred into a 24 well cell culture dish. Primary fibroblasts were maintained in growth medium in a humidified atmosphere (5% CO_2, 95% H_2O) at 37°C.

Growth medium: DMEM supplemented with 10% FBS and 1 x P/S

2.5.3 Immortalization and cloning of primary embryonic fibroblasts

The large T antigen of the simian virus 40 (SV40) is capable to immortalize primary cells in culture through binding and stabilization of the tumor-suppressor p53 (O'Reilly 1986). Large T is a valuable tool to immortalize primary cells, since its expression does not result in major changes of the cell-morphology and anchorage dependent cell-growth. In this study, primary embryonic fibroblasts were immortalized by retroviral transduction of SV40 large T antigen. Therefore, a cell line producing a retrovirus containing the large T gene and a resistance cassette to neomycin (Brown, McCormack et al. 1986) was cultured in growth medium until the cells reached ~ 80% confluency. At this stage, the medium was exchanged against fresh growth medium and cells were further incubated for 16 h to maximize the virus-titer in the medium. Next day, the virus containing medium was spun down (3 min at 900 RPM) and sterile filtered (0.45 µm

filter pore-size) to remove residual cells. Shortly after, primary cells (2.5.2) were covered with a thin layer of the obtained virus-soup and incubated for 1 h at 37°C (5% CO_2, 95% H_2O). The infection was repeated 2 more times after 8 and 24 h, respectively. Infected cells harbouring the large T antigen could be isolated by virtue of resistance to 0.5 mg / ml neomycin during ~ 5 days of selection. In order to isolate single clones, the resistant cell population was trypsinized (2.5.4.1) and low cell numbers (~ 200–500) were plated on a 100 mm cell culture dish. 1-2 weeks later, single colonies could be visualized under the microscope. Single colonies were scratched - and sucked off using a pipette and re-plated in a 24 well in 1 ml growth medium. Once cells reached confluency, they were trypsinzed and 50% were frozen down (2.5.4.3), while the rest was further expanded.

2.5.4 Cell culture of immortalized mouse cell lines

2.5.4.1 Passaging of cells

Prior to trypsinization, layers of adherent cells were washed once with 1xPBS. To achieve detachment of the cells form the culture dish, the cell layer was subsequently incubated for 2-3 min at 37°C with a 1x Trypsin – EDTA solution. To stop the trypsin treatment, detached cells were re-suspended in fresh cell growth medium and spun down for 3 min at 900 RPM. The cell pellet was re-suspended in fresh medium and cells were seeded with the desired density on a new culture dish.

2.5.4.2 Culture of fibroblast cell lines in serum-replacement medium

Foetal bovine serum (FBS) is a widely used supplement in most cell growth media and contains large amounts of fibronectin (FN). Given that assays with self-produced FN critically depend on the absence of serum-derived FN, it was necessary to perform all *in vitro* experiments in the present study with fibroblasts grown in serum replacement medium. In order to adapt the cell metabolism to serum replacement medium, the serum content in the growth media was reduced with each passage (10% - 5% - 2% - 1% - 0.5% - 0.1% - 0%) by diluting DMEM (supplemented with 10% FBS and P/S) with serum replacement medium.

Serum replacement medium: AIM-V, DMEM, RPMI, NEAA (47.5: 47.5: 5: 1)

2.5.4.3 Cryo-preservation of mouse cell lines

For long-term storage, cells were trypsinized as mentioned in (2.5.4.1). After centrifugation (3 min at 900 RPM), the cell pellet was re-suspended in ice cold freezing medium. Aliquots of the cell suspension were filled into cryogenic vials and frozen at -80°C. For prolonged storage, cryo-cultures were stored in liquid nitrogen at -196°C.

Freezing medium: FBS : DMEM : DMSO (5 : 4 : 1)

2.5.4.4 Thawing of cryo-preserved cells

Cryo-cultures were thawed at 37°C. Immediately after the freezing medium had thawed, the cells were added to pre-warmed growth medium (~ 10 times the volume of the freezing medium) and centrifuged for 3 min at 900 RPM. The cell pellet was re-suspended in growth medium and cells were plated on culture dishes of appropriate size.

2.6 Cell biological assays

All assays were performed with cells cultured in serum replacement medium or EC growth medium supplemented with 0.1% FN-stripped FBS (2.5.1).

2.6.1 Fibronectin fibrillogenesis assay

To analyze the assembly of FN matrix by fibroblast cell lines, 8 x 10^4 cells in serum replacement medium were seeded on pre-coated LabTek chamber slides. Cells were typically incubated for 16 h up to 5 days at 37°C (5% CO_2 and 95% H_2O). Coating substrates and incubation times are indicated in the respective experiment. At the end of the incubation time, the medium was removed and cells were subjected to immunostaining (2.4.4) with the indicated antibodies.

2.6.1.1 FN fibrillogenesis inhibitor assay

Analysis of FN matrix assembly was performed a described previously (2.6.1). Apart from that, cells were incubated for 2 h before inhibitory peptides and proteins were added with indicated concentrations. Subsequently, cells were incubated for additional 14 h until they were subjected to immunostaining (2.4.4) with the indicated antibodies.

cycloRGDfV: biomol, #AM-100

cycloRADfV: biomol, #AM-101

cyclicRGD-2C, cyclicRGE-2C, cyclicNGR-2C, linRGD, linRGE: gift from Prof. Dr. H. Kessler, Technical University Munich

2.7 Biochemical methods

2.7.1 Material Biochemistry

Protease inhibitor cocktail: Roche, Complete Mini / EDTA free, #12740900

Phosphatase inhibitor cocktails 1 & 2: Sigma, #P2850, #P5726

N-Ethylmaleimide (NEM): Sigma, #E3876

Microtip Sonifier: Branson, #B-12

Precision Plus Protein™ Caleidoscope™ Standards: BioRad, #161-0375

2.7.2 Preparation of protein lysates

2.7.2.1 Preparation of total protein lysates from adherent cells

The adherent cells were once washed with ice-cold PBS prior to addition of the appropriate amount of cell lysis buffer. Cell lysis was allowed to occur within 10 min incubation time on ice. Thereafter, cells were scraped off the dish using a cell scraper and transferred into a microcentrifuge tube. Cell lysates were briefly sonified on ice (1 sec at intensity 4) using a microtip and were subsequently spun down at 15000 x g for 1 min at 4°C. Next, the protein concentration of the supernatant was determined using a BCA protein assay kit (2.7.5.1). After protein concentrations had been adjusted, lysates were either snap-frozen in liquid N_2 and stored at -80°C, or directly processed to perform SDS-PAGE (2.7.6).

2.7.2.2 Preparation of total protein lysates from mouse embryonic tissue

Embryos were dissected in PBS (2.2.2) and tissue was subsequently transferred into 50–100 µl of the appropriate lysis buffer. The embryonic tissue was mechanically disintegrated by pipetting up and down and by sonification (1 sec, intensity 4, on ice) using a microtip sonifier. Lysates were briefly spun down (30 sec at 15000 x g, 4°C) and the protein concentration of the supernatant was determined using a BCA protein assay kit (2.7.5.1). Further processing of the lysates was performed as indicated for each experiment.

Cell lysis buffer (RIPA): 150 mM NaCl, 1 mM EDTA, 1% Na-deoxycholate, 0.1% SDS, 1% Triton X-100, 10 mM NaF, 1 mM Na_3VO_4 in 50 mM Tris-HCl pH 7.8, protease inhibitor cocktail 1 tablet / 10 ml

4 x SDS sample buffer (SDS-SB): 16 ml 20% SDS, 0.32 ml 0.5 M EDTA, 16 ml 87% glycerol, 0.001% bromphenol blue in 50 mM Tris-HCl pH 6.8 (optional: 4% mercaptoethanol)

2.7.2.3 Nuclear fractionation of lysates from adherent cells

Proteins that trans-locate into the nucleus upon activation are involved in a vast number of signaling events. In order to assess the intracellular distribution of signaling proteins, nuclear fractionation is an applicable preparative method to separate a cell lysate into its nuclear- and cytosolic-fraction. The fractionation was performed after 1.5 x 10^5 cells had been cultured in a 100 mm cell culture dish for 3 and 6 days, respectively. Cells were harvested and subjected to nuclear fractionation using a NE-PER® Nuclear and Cytoplasmic Extraction Kit according to the manufacturer's instructions. Protein concentrations of obtained fractions were determined (2.7.5.1) and adjusted. Samples were snap-frozen in liquid N_2 and stored at -80°C until SDS-PAGE (2.7.6) was performed.

NE-PER® Nuclear and Cytoplasmic Extraction Reagents: Pierce, #78833

2.7.3 Deoxycholate extraction of soluble and insoluble FN matrix fractions

Increasing fibronectin depositions on cells lead to an enhanced complexity of the fiber-network. As a consequence, the network becomes gradually insoluble in the detergent deoxycholate (DOC) (Hynes and Destree 1977; Keski-Oja, Mosher et al. 1977). The method of DOC extraction facilitates the separation of DOC soluble- and insoluble FN matrix fractions. In order to compare the DOC solubility properties of mutated FN and wild-type FN, extractions of DOC-soluble and DOC-insoluble fractions were performed.

2.7.3.1 Deoxycholate extraction of FN matrix fractions from adherent cells

1.5 x 10^5 cells were grown in a 100 mm cell culture dish for 4 – 6 days. The cell layer was washed twice with ice-cold PBS prior to addition of 300 µl DOC lysis buffer. Lysis was performed on ice for 10 min. Thereafter, cells were scraped off the dish using a cell scraper and the lysate was passed several times through a 26G syringe-needle. Subsequently, the lysate was centrifuged at 20000 x g for 10 min at 4°C. The supernatant (DOC soluble fraction) was carefully removed and collected, while the pellet (DOC insoluble fraction) was washed twice in 500 µl ice-cold PBS. Finally, the pellet was re-suspended in 100 µl PBS and briefly sonified (2 sec, intensity 3, on ice). The protein concentrations of both samples were determined using a BCA protein assay kit (2.7.5.1). After protein concentrations had been adjusted, lysates were either snap-frozen in liquid N_2 and stored at -80°C, or directly processed to perform SDS-PAGE under non-reducing conditions (2.7.6).

DOC lysis buffer: 2% DOC, 2 mM EDTA, 2 mM N-Ethylmaleimide in 20 mM Tris-HCl pH 7.8

2.7.3.2 Deoxycholate extraction of FN matrix fractions from embryos

Staged embryos (E9.5) were dissected in PBS (2.2.2). 3–4 embryos of the same genotype were transferred into 200 µl DOC lysis buffer and mechanically disintegrated by pipetting up and down and by sonification (2-3 sec, intensity 4, on ice) using a microtip sonifier. Subsequently, the embryo lysate was centrifuged at 20000 x g for 10 min at 4°C. The supernatant (DOC-soluble fraction) was carefully removed and collected, while the pellet (DOC-insoluble fraction) was washed in 500 µl ice-cold PBS. The pellet was finally re-suspended in 100 µl PBS and briefly sonified (2 sec, intensity 3, on ice) before the protein concentrations of both fractions were determined using a BCA protein assay kit (2.7.5.1). To release LTBP from DOC-insoluble fractions, a plasmin digest was performed. To this end, 0.3 U / ml plasmin were added to the DOC-insoluble fraction, and the sample was subsequently incubated for 1.5 h at 37°C. Shortly after protein concentrations had been adjusted, lysates were either snap-frozen in liquid N_2 and stored at -80°C, or directly processed for SDS-PAGE (2.7.6) under non-reducing conditions.

Plasmin: Sigma, #P1867

2.7.4 In vitro assays on three dimensional FN matrix (FN 3D)

In order to mimic the three dimensional (3D) environment of cells *in vivo*, 3D fibronectin matrices were prepared *in vitro.* Thereby it was possible to perform *in vitro* analyses of cell signaling events that are triggered by 3D fibronectin–cell interactions.

2.7.4.1 Preparation of cell-free FN 3D matrices

3 x 10^5 cells were plated on a pre-coated 6 well cell culture plate and incubated at 37°C for 4–5 days (5% CO_2, 95% H_2O) to produce sufficient amounts of FN matrix. Afterwards, the cells were selectively removed by sequential washes and incubations with hypo- and hyper-osmotic solutions, while the matrix remained unaffected. To this end, the medium was removed and cells were washed twice with wash buffer I prior to incubation with 3D lysis buffer for 15 min at 37°C. Subsequently, the 3D lysis buffer was replaced with fresh lysis buffer, followed by 45 min incubation at 37°C. Next, 3D matrices were washed twice with wash buffer II, 4 x with ddH2O and were finally stored at 4°C in PBS.

3D lysis buffer: 1% NP-40 in 8 mM Na_2HPO_4 pH 9.6

Wash buffer I: 2 mM $MgCl_2$, 2 mM EGTA in 100 mM Na_2HPO_4 pH9.6

Wash buffer II: 300 mM KCl in 10 mM Na_2HPO_4 pH 7.5

2.7.4.2 Cell signaling assays on FN 3D matrices

In order to study the effects of cell – 3D FN interactions on selected cell signaling pathways *in vitro*, cells were starved in DMEM (w/o supplements) for 6 h. Next, cells were trypsinized (2.5.4.1) and washed once with Trypsin–Inhibitor solution (50 µg / ml in PBS) to block the trypsin activity. Subsequently, the cells were re-suspended in DMEM, transferred into a polystyrene tube and incubated in suspension for 1 h at 37°C (5% CO_2 and 95% H_2O). Starving and incubation of cells in suspension causes extensive inactivation of signaling pathways related to cell adhesion. The cell signaling activity increases again, when cells are replated. Aliquots of the cell suspension (~ 5 x 10^4 cells / aliquot) were seeded on prepared 3D FN matrices (2.7.4.1), were incubated for indicated times at 37°C and subsequently lysed in 100 µl cell lysis buffer (RIPA) (2.7.2.2) on ice. After lysis, samples were spun down briefly, followed by determination of the protein concentration in the supernatant using a BCA protein assay kit (2.7.5.1). Finally the lysates were snap-frozen in liquid N_2 and stored at -80°C, or directly prepared for SDS-PAGE (2.7.6).

Trypsin Inhibitor (from soybean): Roche, #10-109-886-001

2.7.5 Determination of the protein concentration

2.7.5.1 BCA protein assay

Proteins are able to reduce Cu^{2+} to Cu^{+} under alkaline conditions (Biuret-reaction). Cu^{+} is readily chelated by bicinchoninic acid, forming a complex with high spectro-

photometric absorbance at 562 nm. The assay was performed according to the manufacturer's instructions.

BCA Protein Assay Kit: Pierce, #23225

2.7.5.2 UV spectroscopic protein determination

The concentration of purified proteins in solution in this study was determined with sufficient accuracy by measurement of their photometric absorbance A_{280} at 280 nm. Aromatic side chains of proteins, such as tryptophan, tyrosine and phenylalanine, absorb light at this particular wavelength. The concentration of a protein is related to the amount of light absorbed by the protein solution by the Beer-Lambert Law:

$$A = \varepsilon \, c \, l$$

In this equation, A is absorbance, ε is the molar extinction coefficient (L / mol x cm), l is the path length of the sample cuvette (cm) and c is the concentration of the protein solution. Notice, that ε and l must be known to directly calculate c from A. The specific value of ε for each protein sequence was obtained by using the Peptide Property Calculator (www.basic.northwestern.edu/biotools/proteincalc.html).

2.7.6 SDS-polyacrylamide-gelelectrophoresis (SDS-PAGE)

SDS-PAGE is probably the most commonly used method to separate proteins under denaturizing conditions. The negatively charged detergent sodium dodecyl sulphate (SDS) becomes associated with the proteins and promotes their solubilisation. Thus, the proteins become negatively charged and can be electrophoretically separated in the meshwork of a polyacrylamide-gel according to their individual molecular size and shape. Defined protein standards are used as a reference to determine the size of the separated proteins. In order to prepare proteins for SDS-PAGE, a boiling step in presence of SDS has to be performed. Where indicated, 2-mercaptoethanol or di-thiothreitol (DTT) was added in some experiments to reduce disulfide bonds. After separation, proteins in a gel can be visualized by means of protein dyes, silver staining or western blotting. All SDS-PAGE protein separations in this study were performed with the so called discontinuous method. Here, a stacking gel is poured on top of a resolving gel. Both gels differ in terms of pH and acrylamide concentration. The stacking gel, which is passed first by the proteins, facilitates the concentration of all proteins at the interface between the two gels, whereas the resolving gel allows the separation of proteins according to their molecular size and shape. The content of acrylamide in the resolving gel is considered to be inversely proportional to the size of proteins to be separated. Proteins were separated using a mini-gel system featuring the measures 73 x 83 x 1.5 mm. Samples were mixed with 4 x SDS sample-buffer (4 x SDS-SB), boiled 3–5 min at 95°C and subsequently chilled on ice. After a brief centrifugation step, the samples were loaded on the stacking gel. The electrophoresis module was filled with 1 x SDS running buffer and the electrophoresis carried out at 20 mA (stacking gel) to 40 mA (resolving gel), respectively.

Resolving gels	6.5%	9%	stacking gel 4%
30% acrylamide	4.34 ml	6 ml	1.33ml
1.5 M Tris-HCl pH 8.8	5 ml	5 ml	2.52 ml (pH 6.8)
10% SDS	0.2ml	0.2 ml	0.1ml
10% APS	0.2 ml	0.2 ml	0.1ml
TEMED	16 µl	20 µl	10 µl
ddH_2O	10.24 ml	8.6 ml	5.94 ml

for 4 mini-gels

Mini-gel system: BioRad, Mini Protean III System, #165-3301

10 x SDS running buffer: 144 g Glycine, 33.3 g Tris, 10 g SDS

N,N,N',N'-Tetramethylethylenediamine (TEMED): Serva, #35925

2.7.7 Western blotting and Immunodetection

Western blotting is a very sensitive method to detect and quantify specific proteins by means of antibodies. Proteins are first resolved by SDS-PAGE (2.7.6) and subsequently electrophoretically transferred on a PVDF membrane. Proteins tightly bound to this membrane can then be visualized applying immunodetection reagents. After SDS-PAGE (2.7.6) the stacking gel was removed, and the resolving gel, together with a methanol-activated PVDF membrane, was assembled into a transfer-sandwich. Thereby, air bubbles between the layers, especially between gel and membrane, were thoroughly removed. Proteins were electrically transferred on the membrane overnight at 4°C and 55 mA / gel, or for 3 h at 4°C and 150 mA / gel, with the gel side of the transfer-sandwich connected to the cathode. After the transfer, the membrane was removed from the transfer-sandwich and blocked for 1 h in blocking buffer (see table of antibodies, 2.4.1). Blocking, as well as all subsequent washing and antibody incubation steps were performed under continuous shaking on a laboratory rocker (ELMI, Shaker S-4, and 20 RPM). Next, the membrane was incubated with the primary antibody (2.4.1) diluted in blocking buffer for either 3 - 4 h at RT, or overnight at 4°C. Subsequently, the membrane was washed 3 x 10 min with TBS-T (2.4.3) before the appropriate secondary antibody (2.4.1) in blocking buffer was added for 1–2 h incubation. After 3 further washes (2 x TBS-T, 1 x TBS (2.4.3) the membrane was subjected to a chemoluminiscence-based detection kit (ECL kit).

*Western blotting transfer buffer: 10 mM $Na_2B_4O_7$ * 10 H_2O in H_2O*

Blocking buffer: 5% Skim milk powder in TBS-T or 5% BSA in TBS-T

ECL kit: Millipore, Immobilon™ Western, #WBKLS0500

PVDF membrane: Millipore, Immobilon™ Transfer membranes, #IPVH00010

2.7.8 Expression of FN fragments in E.coli

The expression of recombinant FN fragments was performed in the E.coli strain BL21(DE3) (2.8.2.1) using the pET-15b expression vector (2.8.8). Transformations of bacteria with the desired expression vectors were routinely performed one day in advance. All incubation steps to grow the bacteria were performed in LB_{Amp} medium (2.8.2) at 37°C in a bacterial shaker (200 RPM). In order to start the protein expression, a bacterial colony was inoculated in 2 ml LB_{Amp} medium and incubated for 8–9 h. Subsequently, 50 µl of this starter culture were transferred into 100 ml of LB_{Amp} medium for overnight incubation. Next day, 20 ml of the overnight culture were mixed with 230 ml fresh LB_{AMP} medium and incubated until an optical density at 578 nm (OD_{578}) of 0.8 was reached (collect sample: - IPTG). Shortly after, the protein expression was induced by addition of isopropyl-β-D-thiogalactopyranoside (IPTG) to a final concentration of 0.4 mM. Following IPTG induction, the culture was further incubated for ~ 3 h (final OD_{578}: ~ 1.8; collect sample: + IPTG). Next, bacteria were pelleted by 10 min centrifugation at 5000 x g (4°C), and the obtained pellet was re-suspended in 200 ml ice-cold pellet wash buffer. Subsequently, the bacterial suspension was spun down again (5000 x g, 10 min, at 4°C) and the obtained pellet re-suspended in the appropriate amount of lysis buffer (10 ml lysis buffer / g pellet). Lysis was allowed to occur during 30 min with continuous stirring at 4°C. Afterwards, the lysate was sonified for 3 x 15 sec. (intensity 5, on ice) to further improve the lysis efficiency (collect sample: crude lysate). The obtained crude lysate was cleared by 30 min centrifugation at 20000 x g (at 4°C). To adjust the ionic-strength of the cleared lysate for Mn^{2+}-NTA affinity chromatography, NaCl and $MgCl_2$ were added to final concentrations of 150 mM and 2 mM, respectively (collect sample: cleared lysate). In order to purify the expressed protein, 2 ml of Mn^{2+}- NTA resin was equilibrated with 2 x 10 ml column wash buffer and shortly after added to the cleared lysate. The resin was allowed to bind the protein for 20 min at RT in a rotating tube. Thereafter, the resin was spun down for 3 min at 1500 RPM, the supernatant was removed and the resin was washed with 2 x 10 ml column wash buffer (collect sample: wash 1 & 2). Finally, the resin was packed on a column and washed with 5 ml column wash buffer before 5 ml of elution buffer were applied to elute the protein. The eluate was collected in 500 µl fractions and protein concentrations of all fractions were determined by UV spectrophotometric means (2.7.5.2). Most concentrated fractions were pooled and dialysed twice against 500 ml TBS overnight at 4°C.

Isopropyl-β-D-thiogalactopyranoside (IPTG):Sigma, #I-6758

Pellet wash buffer: 150 mM NaCl, 1 mM EDTA in 20 mM Tris-HCl pH 8.0

Lysis buffer: 1 mM PMSF, 0.1 mg/ml Lysozyme, 1 mM EDTA in 20 mM Tris-HCl pH 8.0

Lysozyme: Sigma, #L-6876

PMSF (Phenylmethanesulfonyl fluoride): Sigma, #P-7626

Column wash buffer: 150 mM NaCl, 10 mM Imidazole in 20 mM Tris-HCl pH 8.0

Elution buffer: 150 mM NaCl, 200 mM Imidazole in 20 mM Tris-HCl pH 8.0

2.7.9 Solid phase binding assay

The solid phase binding assay is a highly sensitive method to detect protein–protein interactions. The functional principle is similar to an ELISA assay: A protein is absorbed on a microtiter plate, whereas its supposed interaction partner is washed over the plate and is allowed to bind specifically. Finally, the binding complexes can be detected using antibodies. In order to map integrin binding sites on FN, various FN fragments of indicated concentration were absorbed on a microtiter plate overnight at 4°C. Next day, the plate was blocked with SP blocking buffer for 1 h at RT. After blocking, serial dilutions of biotinylated integrins were added (50 µl / well, diluted in SP binding buffer) and incubated for 5 h at RT. The plate was subsequently washed 3 x with SP washing buffer (200 µl / well) prior to application of a Streptavidin–HRP solution (50 µl / well, diluted 1:1000 in SP binding buffer) for 15 min at RT. Finally, the plate was washed 4 times with SP washing buffer and bound integrins were detected using ABTS reagent. Therefore, ABTS solution (100 µl / well) was added to the plate and incubated for 45 min. Subsequently, the absorbance at 405 nm was measured in a spectrophotometer.

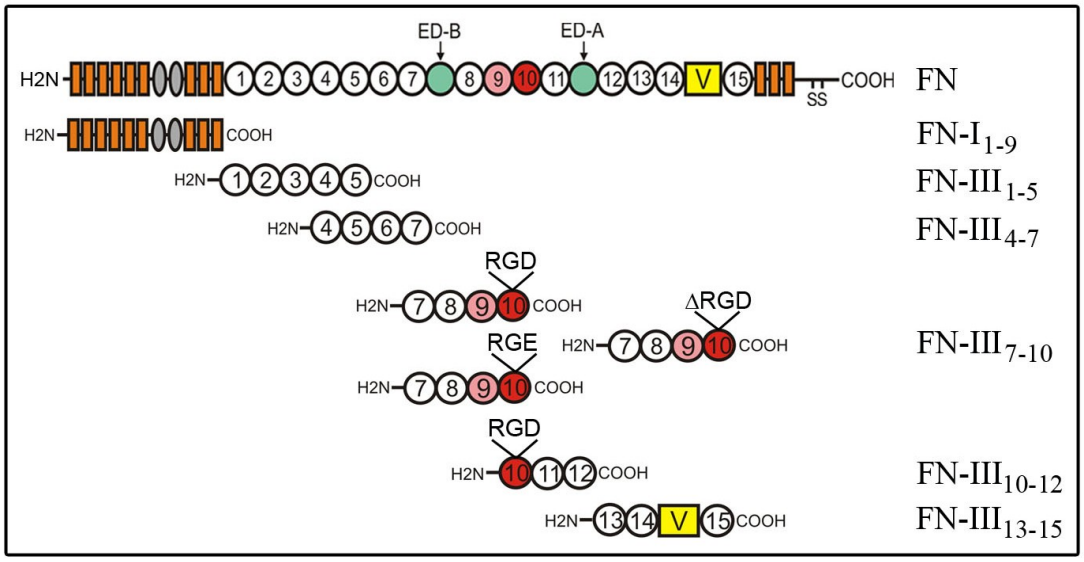

Fig 2.1. ***Schematic depiction of FN fragments utilized in solid phase binding assays****. The full-length FN is shown on top. Type I domains are depicted as orange rectangles, Type II domains as grey ovals and type III domains as white circles. Domain FN-III$_9$ (pink) contains the synergy region; FN-III$_{10}$ (red) the RGD motif. The v-region is depicted in yellow. Note that in two FN-III$_{7-10}$ fragments the RGD motif was either mutated to RGE or completely removed, respectively.*

Peroxidase Substrate Kit 2,2'-azino-bis(3-ethylbenzthiazoline-6-sulphonic acid) (ABTS): Vector Laboratories, #SK-4500

Microtiter plate: Nunc, MaxiSorp^{TM}, #439454

SP blocking buffer: 1% BSA, 150 mM NaCl in 20 mM Tris-HCl pH 7.5

SP binding buffer: 0.1% BSA, 1 mM $MgCl_2$, 150 mM NaCl in 20 mM Tris-HCl pH 7.5

SP washing buffer: 1 mM $MgCl_2$, 150 mM NaCl in 20 mM Tris-HCl pH 7.5

Rec. biotinylated αvβ3 and α5β1 integrins: Gift from Junichi Takagi, Osaka University, Japan

2.7.10 Luciferase based TGF-β reporter assay

A major fraction of TGF-β is bound to the ECM in a so called latent form, which can be experimentally released and activated by a heat step. Cells stably transfected with a Luciferase gene fused to the Plasminogen Activator Inhibitor I promoter provide a very sensitive tool to assay the amount of active TGF-β (Abe, Harpel et al. 1994) in conditioned medium. Addition of active TGF-β to these cells induces the expression of the reporter enzyme firefly luciferase. This enzyme catalyses a luminescent reaction, in which light is produced through oxidation of beetle luciferin to oxyluficerin. Quantification of the emitted photons by means of a luminometer allows the indirect determination of the amount of active TGF-β. In this study, conditioned medium from equal amounts of fibroblasts (150000 fibroblasts / 6 cm dish) was analysed for TGF-β activity. To perform the assay, Mink lung epithelial cells (MLEC), stably transfected with the reporter construct p800neoLuc, were seeded on a 96 well plate (~ 20000 / well) and incubated overnight at 37°C (5% CO_2, 95% H_2O) in growth medium supplemented with 1 mg / ml neomycin. Next day, the MLECs were washed once with PBS and conditioned medium from fibroblasts after 3, 4 and 5 days in culture (100 µl / well) was added. Subsequently, the fibroblasts were incubated for 10 min at 80°C in order to release all latent TGF-β (heat-step) and cooled to RT. Aliquots of this heat-treated conditioned medium (100 µl / well) were also added to controlswells with MLECs and incubated for 24 h at 37°C (5% CO_2, 95% H_2O). Finally, a luciferase assay was performed according to the manufacturer's instructions.

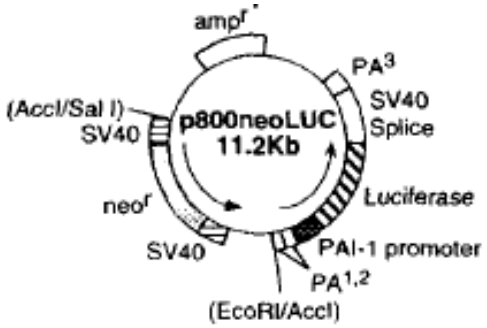

Fig 2.2. ***Map of p800neoLuc****. The construct contains a plasminogen activator inhibitor I promoter fused to the luciferase reporter gene. A neomycin resistance cassette allows positive selection of transfectants (Taken from Abe et al.1994).*

Luciferase assay: Promega, Bright-Glo™ Luciferase Assay System, #TM052

Luminometer: Promega, GloMax™

Luminometer 96 well plates: Nunc, Nunclon Delta white, #136101

Neomycin (G-418 sulphate): PAA, #P31-011

TGF-β inhibitor, SB 431542: BIOTREND, #BS0216

2.8 Molecular Biological Methods

2.8.1 Material Molecular Biology

Autoclave: KSG, KSG-12

Centrifuge: Eppendorff, 5417C

Centrifuge: Beckmann Coulter, Avanti J-25 with rotors J 14 and J 25.50

Microwave: Daewoo, KOR 63D7

Thermocycler: BioRad, DNAEngine

Thermomixer: Eppendorff, 5350

2.8.1.1 Phenol / Chloroform extraction of tail DNA

In order to isolate murine genomic DNA for genotyping, ~ 5 mm of a tail tip biopsy were subjected to an overnight digestion with proteinase K (100 µg / ml) in 250 µl lysis buffer at 55°C in a shaker. Next day, 250µl Phenol/Chloroform (1:1) was added to the digest. After brief mixing, the DNA solution was spun down for 5 min at 15000 x g. The upper phase was collected and carefully mixed with 1 ml of 100% ethanol and 20 µl of 3 M sodium acetate and spun down again (2 min at 15000 x g). The obtained pellet was washed once with ~ 200µl of 70% ethanol, air-dried and finally dissolved in 50 – 150 µl ddH_2O.

Phenol / Chloroform / Isoamyl Alcohol (25 : 24 : 1): Calbiochem, #KP31757

2.8.1.2 Preparation of yolk sac DNA for genotyping

Small pieces of yolk sac tissue were transferred to 25 µl of 1 x PCR buffer and digested overnight at 55°C with 400 µg / ml proteinase K. Next day, 1 µl of the digest was used for the genotyping PCR (2.8.5.2).

2.8.2 Bacteriological tools

Two Escherichia coli (E.coli) strains were used in this study: For all cloning steps the strain XL-1 blue was utilized, whereas the strain BL21(DE3) was used for recombinant protein expression purposes. Both strains were grown in lysogeny broth (LB) rich medium at 37°C in a bacteria shaker (Buchner Laboratories). The medium was autoclaved for 20 min at 120°C shortly after preparation. If indicated, antibiotics were added to the autoclaved, cooling medium after a temperature below 50°C was reached. For preparation of LB plates, about 20 ml of a sterile, ~ 50°C warm LB–Agar mixture was poured into 100 mm plates (Greiner bio-one) and stored at 4°C after gelling had occurred.

LB medium: 10 g NaCl, 10 g trypton, 5 g yeast extract filled up to 1 l with ddH2O, autoclaved and stored at 4°C

Agar: 15 g of Agar in LB, autoclaved and poured into 100 mm dishes, stored at 4°C

Concentration of antibiotics used: 12.5 µg / ml Tetracycline; 75 µg / ml Ampicillin

2.8.2.1 Preparation of competent E.coli strains

One colony of the E.coli strain XL-1 blue was inoculated in 10 ml LB, supplemented with Tetracycline, and incubated overnight at 37°C under shaking (185 RPM). Next, 2 ml of the overnight culture were inoculated in 100 ml LB + Tetracycline and grown until an optical density of 0.5 at 550 nm (OD_{550}) was reached. The culture was chilled on ice for 10 min, and subsequently spun down for 15 min at 4°C with 1000 x g. The pellet was re-suspended in 10 ml TSS and 2.9 ml Glycerol (87%) and shortly after frozen on dry-ice in 100 µl aliquots. Aliquots of competent bacteria were stored at -80°C until usage.

TSS: 50 g polyethylenglycol, 5 g tryptone, 2.5 g yeast extract, 2.5 g NaCl, 25 ml DMSO, 25 ml $MgCl_2$ (1 M) filled up to 500 ml with ddH_2O and sterile filtered. Store at 4°C

To prepare competent bacteria of the E.coli high-efficiency protein expression strain BL21(DE3), a starter culture was inoculated in 5 ml LB, supplemented with 0.02 M $MgCl_2$ and 0.01 M KCl. After overnight incubation at 37°C in a shaker (180 RPM), the bacteria were transferred into 150 ml LB + 0.02 M $MgCl_2$ + 0.01 M KCl and grown at 37°C until an OD_{550} of 0.3–0.4 was reached. After 10 min incubation on ice, the bacteria were pelleted (15 min, 4°C, 1000 x g) and re-suspended in an equal volume of

ice-cold TFB1 and incubated on ice for further 10 min. Subsequently, the bacteria were spun down again, the pellet was re-suspended in 1/10 volume of TFB2 and shortly after snap-frozen on dry-ice in 200 µl aliquots. Competent bacteria were stored at -80°C until usage.

TFB1: 1 ml KAc (5 M), 10 ml $MgCl_2$ (1 M), 20 ml RbCl (1 M), 2 ml $CaCl_2$, 132 ml ddH_2O, the solution was sterile filtered and 34.5 ml of 87% glycerol was added

TFB2: 0.5 ml MOPS (1 M), 3.75 ml $CaCl_2$ (1 M), 0.5 ml RbCl (1 M), 8.75 ml 87% glycerol, filled up to 40 ml with ddH_2O and autoclaved

2.8.2.2 Transformation of competent E.coli

Shortly after the competent bacteria had thawed, 10-50 ng of desired DNA was added. The bacteria / DNA suspension was mixed by gently flicking the tube and was then incubated on ice for 30 min. Next, a heat-shock (90 sec at 42°C) was performed to promote the up-take of DNA. After the heat shock, bacteria were again placed on ice for at least 2 min before 1 ml of LB medium (w/o antibiotics) was added. The bacterial suspension was incubated at 37°C for 1 h in a shaker (200 RPM). Finally, bacteria were spun down (30 sec at 3000 x g) and re-suspended in 100 µl of LB medium and immediately spread on LB plates. Plates were incubated overnight at 37°C. Successful transformation was indicated by the appearance of colonies after 10–14 h.

2.8.3 Preparation of plasmid DNA from bacterial cultures

A single colony grown on a plate after transformation (2.8.2.2) was picked and inoculated in 2–5 ml LB medium (2.8.2) and bacteria were grown for 8–16 h (37°C, 200 RPM). Next, ~ 2 ml of the culture was spun down for 30 sec at 15000 x g. The bacterial pellet was used for plasmid DNA isolation using the Qiagen Plasmid Mini Kit following the manufacturer's instructions. For preparations of larger amounts of plasmid DNA (up to 500 µg), a larger volume of bacterial culture (~ 100 ml) was processed using a Qiagen Plasmid Maxi Kit. Purified plasmid DNA was photometrically quantified at 260 nm and stored at -20°C.

Qiagen Plasmid Mini Kit, Qiagen, #12125

Qiagen Plasmid Maxi Kit, Qiagen, #12162

2.8.4 Molecular cloning of DNA

Restriction enzymes are commonly used tools for the generation of DNA constructs. These enzymes are able to specifically bind to mainly palindromic recognition sequences within the DNA and cut it by hydrolysation of two phosphodiester bonds. Thereby, they leave a phosphate group in 5' prime and a hydroxyl group in 3' prime of the cleaved DNA, which allows the ligation with other DNA fragments cleaved by the same enzyme.

2.8.4.1 Enzymatic digestion of DNA with restriction enzymes

The restriction enzymes used in this study were all purchased form New England Biolabs (NEB). All digestion-reactions were performed according to the manufacturer's instructions. In general, a total volume of 20–30 µl containing 10 U enzyme / µg DNA dissolved in ddH_2O was incubated at 37°C in presence of the appropriate buffer recommended by the manufacturer. In some cases, the reaction-mix was supplemented with BSA to improve the restriction efficiency of certain enzymes.

2.8.4.2 Dephosphorylation of plasmid DNA

Digestion of plasmids with restriction enzymes creates a reactive phosphate group in 5'-prime of the linearized plasmid, which readily ligates with the corresponding 3'-hydroxyl group of the same plasmid during subsequent ligation reactions. In most cases, this self-ligation competes with the insertion of the insert during a ligation reaction and thus strongly reduces the yield of the desired ligation product. To prevent self-ligation of linearized plasmids, the 5' –phosphate group can be removed by utilization of alkaline phosphatases. In this study, shrimp alkaline phosphatase was used for this purpose (sAP). Dephosphorylation was achieved by incubating 3–5 µg linearized plasmid DNA with 5 U sAP in 1 x sAP reaction buffer in a total volume of 30 µl for 60 min at 37°C. After the reaction, sAP was heat inactivated for 15 min at 65°C according to the manufacturer's instructions.

Shrimp Alkaline Phosphatase: Roche, #11 758 250 001

2.8.4.3 Ligation of DNA fragments

The ligation reaction generates a phosphodiester bond between the 5'- phospho - and 3' – hydroxyl groups of two DNA segments that have been cut with the same restriction enzyme. Usually, the following protocol for ligation was used: ~ 100 ng of linearized and dephosphorylized vector were mixed with ~ 50 ng of the insert, 1.5 µl ATP (10 mM), 1.5 µl Fast-Link Ligase buffer and 1 µl Fast-Link Ligase. The reaction was filled up to 15 µl with ddH_2O and incubated for 30 min at RT. 1–5 µl of the reaction were used for DNA transformation (2.8.2.2).

Fast-Link DNA Ligation Kit: Epicentre Biotechnologies, #LK6201H

2.8.4.4 Sequencing of DNA

To verify the sequence of cloned plasmid DNA, ~ 500 ng DNA was mixed with 2 µl Big Dye terminator mixture and 1 µl of an appropriate sequencing primer (10 pmol) in a total volume of 10 µl. Subsequently, the sample was subjected to a PCR (2.8.5.2). The PCR product was stored at 4°C prior to sequencing at the core-facility of the Max-Planck-Institute (Martinsried, Germany). The sequence data was processed by using Chromas Lite 2.01 software (www.technelysium.com.au).

2.8.5 Polymerase chain reaction (PCR)

PCR is the method of choice for enzymatic DNA amplification. Typically, a PCR reaction mix contains five components: The DNA strand to be amplified (template), two primers, dNTPs and a heat-stable DNA polymerase (Taq or high fidelity polymerase). The reaction starts with DNA denaturation at 95°C, which is followed by annealing of the primers to the DNA template at lower temperatures (55°C – 68°C, depending on the primers), and finally ends with DNA synthesis at 68°C – 72°C.

2.8.5.1 Oligonucleotides (primer)

All oligonucleotides were synthesised and purified by Metabion international (Martinsried, Germany). Those used for cloning of siRNA constructs were 5'-prime phosphorylated and HPLC purified by the manufacturer.

Name	5' - 3' sequence	application
Rb2	GTG GAG ATT TGT GTC ACA GGT G	genotyping $FN^{CC>SS}$
Fb (HpaI BamHIF)	CGG GAT CCG CTC ATG AAC AAA GCA GAC AGC	genotyping $FN^{CC>SS}$
RGEGenof	CAA AGA AGA CCC CAA GAG CA	genotyping $FN^{RGE/RGE}$
RGEGenoR	ACA AGCCCTGGCCTTTAGTT	genotyping $FN^{RGE/RGE}$
RGD>RGEki fw	CAC TGG CCG TGG AGA GAG CCC CGC AAG CAG	FN III 7-10 mutagenesis
RGD>RGEki rev	CTG CTT GCG GGG CTC TCT CCA CGG CCA GTG A	FN III 7-10 mutagenesis
deltaRGDki fw	GTG TAT GCT GTC ACT GGC AGC CCC GCA AGC AGC AAG C	FN III 7-10 mutagenesis
deltaRGDki rev	GCT TGC TGC TTG CGG GGC TGC CAG TGA CAG CAT ACA C	FN III 7-10 mutagenesis
Int avkdown 1fw	GAT CCC CCA ACA GGC AAT CGA GAT TAT TCA AGA GAT AAT CTC GAT TGC CTG TTG TTT TTA	cloning αv integrin-siRNA
Int avkdown 1rev	AGC TTA AAA ACA ACA GGC AAT CGA GAT TAT CTC TTG AAT AAT CTC GAT TGC CTG TTG GGG	cloning αv integrin-siRNA
Int avkdown 2fw	GAT CCC CCG GAC TGC ACA AGC AAT TTT TCA AGA GAA AAT TGC TTG TGC AGT CCG TTT TTA	cloning αv integrin-siRNA
Int avkdown 2rev	AGC TTA AAA ACG GAC TGC ACA AGC AAT TTT CTC TTG AAA AAT TGC TTG TGC AGT CCG GGG	cloning αv integrin-siRNA
Int avkdown 3fw	GAT CCC CGC TTC AAT GAT ATT GCA ATT TCA AGA GAA TTG CAA TAT CAT TGA AGC TTT TTA	cloning αv integrin-siRNA
Int avkdown 3rev	AGC TTA AAA AGC TTC AAT GAT ATT GCA ATT CTC TTG AAA TTG CAA TAT CAT TGA AGC GGG	cloning αv integrin-siRNA
Int avkdown 4fw	GAT CCC CGC AGG CTC ATA TTC TAC TTT TCA AGA GAA AGT AGA ATA TGA GCC TGC TTT TTA	cloning αv integrin-siRNA
Int avkdown 4rev	AGC TTA AAA AGC AGG CTC ATA TTC TAC TTT CTC TTG AAA AGT AGA ATA TGA GCC TGC GGG	cloning αv integrin-siRNA

Int av kdown 5fw	GAT CCC CCG TTA GGG CAA TTA GGA TTT TCA AGA GAA ATC CTA ATT GCC CTA ACG TTT TTA	cloning αv integrin-siRNA
Int av kdown 5rev	AGC TTA AAA ACG TTA GGG CAA TTA GGA TTT CTC TTG AAA ATC CTA ATT GCC CTA ACG GGG	cloning αv integrin-siRNA
>pET 11 seq fw	GGA TAA CAA TTC CCC TCT AG	sequencing
>pET 11 seq rev	GTT ATG CTA GTT ATT GCT CAG	sequencing

2.8.5.2 PCR reactions

The following PCR reactions were performed in this study: 1) genotyping PCR using tail or yolk sac DNA and 2) cloning PCR using purified plasmid DNA (2.8.3) and high fidelity polymerase featuring proof reading activity.

Genotyping PCR (1)

Isolated tail or yolk sac DNA .....1 µl

Primer 1 (100 pM) .....0.5 µl

Primer 2 (100 pM) .....0.5 µl

dNTPs (10 mM).....0.5 µl

$MgCl_2$ (50 mM):..... 0.75 µl

10 x PCR buffer: .....2.5 µl

Taq polymerase: .....0.5 µl

Filled up to 25 µl with ddH_2O and subjected to PCR

Cloning PCR (2)

Plasmid DNA (~ 200 ng) .....1 µl

Primer 1 (100 pM) .....1 µl

Primer 2 (100 pM) .....1 µl

dNTPs (10 mM).....1 µl

$MgCl_2$ (50 mM):.....1.5 µl

10 x PCR buffer: .....5 µl

High fidelity polymerase:.....1 µl

Filled up to 50 µl with ddH_2O and subjected to PCR

2.8.5.3 PCR programs

The following PCR programs were used in this study:

Genotyping $FN^{RGE/RGE}$ and $FN^{CC>SS}$ PCR:

Step	*time (sec.)*	*temp. (°C)*
1	*30*	*95*
2	*30*	*95*
3	*30*	*58*
4	*45*	*72*
5	*300*	*72*
6	*∞*	*4*

Cloning PCR:

Step	*time (sec.)*	*temp. (°C)*
1	*300*	*95*
2	*30*	*95*
3	*30*	*63*
4	*120*	*72*
5	*30*	*95*
6	*30*	*58*
7	*120*	*72*
8	*420*	*72*
9	*∞*	*4*

Genotyping PCR's were performed for 35 cycles (step 2 – 4). Cloning PCR's were performed for 27 cycles (step 5-7), including 8 additional cycles with higher annealing temperature (63°C, step 2 – 4).

Pwo SuperYield DNA Polymerase: Roche, #04 340 868 001

2.8.6 PCR based Site directed mutagenesis

Site directed mutagenesis is a commonly used approach to study protein functions. This method allows the selective introduction of point mutations into the coding DNA sequence of a gene of interest. As a result, deletion, insertion or swap of amino acids in the translated protein is achieved. In the present work, point mutations were introduced into FN fragments utilizing a QuikChange Site-Directed Mutagenesis kit. In order to perform a site directed mutagenesis, the gene of interest must be inserted in a circular DNA vector, which is used as template for the mutagenesis PCR reaction. Two oligonucleotide primers, encoding for the desired mutation, are extended during this PCR, thereby generating a mutant plasmid *in vitro*. Unlike the E.coli derived template DNA, the mutant plasmid lacks DNA methylations. Final application of an endonuclease (DpnI), which only targets methylated DNA, allows selective digestion of the template DNA, whereas the mutant plasmid remains unaffected.

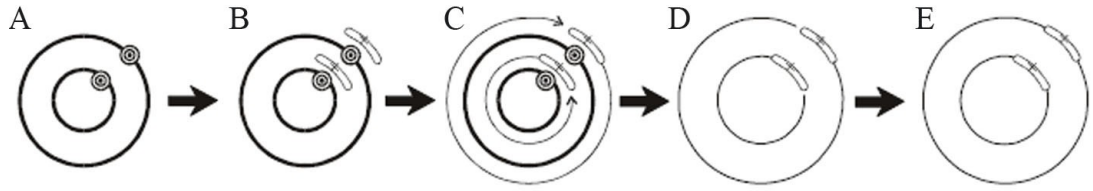

Fig 2.3. ***Principle of site directed mutagenesis.*** ***A****. Gene in a plasmid with target site for mutation.* ***B****. Annealing with oligonucleotides containing the desired mutation.* ***C****. PCR*

generated extension of the mutagenic primers, resulting in a mutant plasmid. ***D****. Digestion of the methylated, parental plasmid with Dpn I.* ***E****. Mutant plasmid, ready for transformation (Taken from the QuikChange Site-Directed Mutagenesis Kit manual (Stratagene) and modified).*

QuikChange® Site-Directed Mutagenesis Kit: Stratagene, #200518

2.8.6.1 Design of mutagenesis primers

All primers used for mutagenesis were HPLC purified and designed according to the manufacturer's instructions (Stratagene, QuickChange Site-Directed Mutagenesis Kit). The desired mutational sequence was flanked by 10–15 nucleotide bases of the correct sequence at both ends of the oligonucleotide. The maximum length of the designed primers was limited by their calculated melting temperature T_m (see formula below), which was not allowed to exceed 78°C.

$$Tm = 81.5 + 0.41 (x \% \text{ GC content}) – 675 / N - \% \text{ mismatch}$$

N: primer length in bases

2.8.6.2 Mutagenesis PCR reactions

Mutagenesis Mix 1:	*Mutagenesis Mix 2:*
Plasmid DNA (~ 25 ng) ..... 0.5 µl	*Plasmid DNA (~ 25 ng)..... 0.5 µl*
Primer 1 (100 pM) ..... 1 µl	*Primer 2 (100 pM) ..... 1 µl*
dNTPs (25 mM)..... 2 µl	*dNTPs (25 mM)..... 2 µl*
10 x PCR buffer..... 5 µl	*10 x PCR buffer..... 5 µl*
PfuTurbo DNA polymerase..... 1 µl	*PfuTurbo DNA polymerase..... 1 µl*

Each mix was filled up to 50 µl with ddH_2O and subjected to mutagenesis PCR (2.8.6.3).

2.8.6.3 Mutagenesis PCR program

The following PCR program was used for site directed mutagenesis

Step	*time (sec.)*	*temp. (°C)*
1	*30*	*95*
2	*30*	*95*
3	*60*	*65*
4	*420*	*72*
5	*∞*	*4*
6	*30*	*95*
7	*30*	*95*
8	*60*	*63*

9.....900..... 72

10..... ∞ 4

The mutagenesis PCR was performed for 10 cycles (step 2 – 4) for each mutagenesis mix separately. At step 5, 25 µl of both mixes were combined and subjected to the next PCR (step 7 – 9) for 18 cycles. Subsequently, 1 µl of DpnI was added to 50 µl of the PCR product and incubated for 1 h at 37°C. 5–20 µl of the digest were used for DNA transformation (2.8.2.2).

2.8.7 Agarose gel electrophoresis

In this study, agarose gel electrophoresis was routinely used for separation, purification and identification of DNA fragments. In order to prepare an agarose gel, 1–3 mg of Ultra pure Agarose was added to 150 ml 1 x TAE buffer (final agarose concentration 0.07-2%, dependent on the sizes of separated DNA fragments) and boiled in a microwave. As soon as the agarose was dissolved, 10 µl of ethidium bromide solution was mixed with the hot solution to allow visualization of DNA under UV-light. The melted agarose was poured into a casting mould and allowed to gel at RT. After gelling had occurred, the agarose gel was placed in an electrophoresis chamber containing 1 x TAE buffer. The DNA sample solution was mixed with 6 x DNA loading buffer and loaded on the agarose gel. Electrophoresis was performed at 70 – 120 V at RT. As a size reference, the 1 kb DNA Ladder was regularly used. DNA fragment bands were visualized by means of UV-light of 366 nm wavelength.

TAE x 50: 242 g Tris-base, 57.1 ml glacial acetic acid, 100 ml EDTA (0.5 M, pH 8.0) filled up to 1 l with H_2O

Agarose: Invitrogen, UltraPureTM Agarose, #15510-027

Ethidium bromide: Roth, #2218.1

1 kb Ladder: Invitrogen, #15615-016

2.8.7.1 Extraction of DNA from agarose gels

For cloning purposes, it was necessary to extract the desired DNA bands from agarose gels after separation. Therefore, the corresponding DNA band was excised from the gel under UV-light with a scalpel and extracted from the agarose block using a Qiagen Gel Extraction Kit according to the manufacturer's instructions.

Qiagen Gel Extraction Kit, Qiagen, #20021

2.8.8 Generation of FN fragment expression constructs

FN-III$_{7\text{-}10}$ RGE, FN-III$_{7\text{-}10}$ ΔRGD: A fragment of the FN-III$_{7\text{-}10}$ cDNA (inserted in pET-15b) was released by digestion with BamHI and subcloned into pBS that was cut before with the same enzyme and dephosphorylated. Site directed mutagenesis was performed (2.8.6) and the correct mutation was checked by sequencing. Subsequently,

the FN fragment was released form pBS by BamHI digest and inserted back into BamHI cut and dephosphorylated pET-15b FN-III$_{7\text{-}10}$. The orientation was checked by PCR using a primer pair annealing 3'-prime in pET-15b and 5'-prime in the cDNA. Finally, correctness of the mutated cDNA was verified by sequencing.

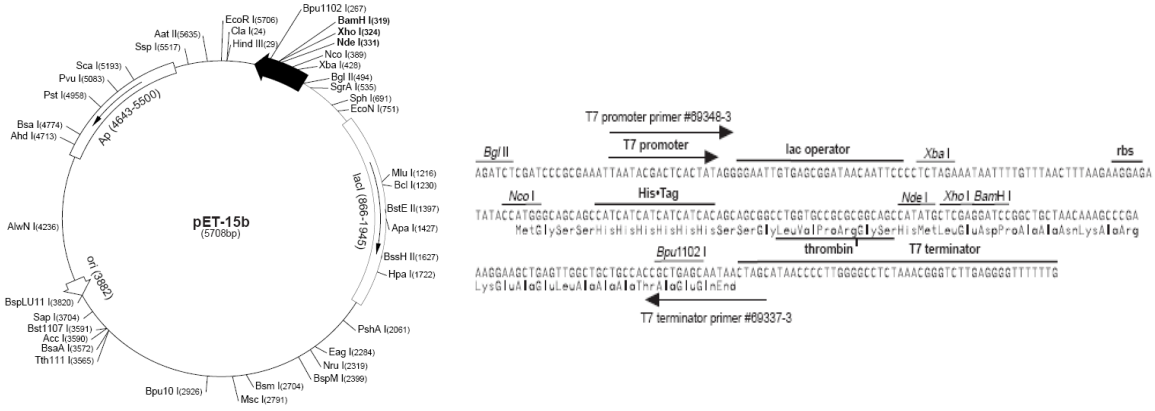

Fig 2.4. ***Map of the cloning / expression vector pET-15b****. The cDNAs of the FN fragments were cloned into the vector by Nde I / BamH I sites. Recombinant FN fragments exhibit a N-terminal His-Tag (Taken from the pET-15b map (Novagen)and modified).*

2.8.9 Generation of siRNA constructs

Small synthetic interfering RNAs (siRNAs) are a highly specific tool to silence genes on the post-transcriptional level. The effect of many RNAi mediated gene silencing approaches is short-lived, since many of them utilize only transiently transfected expression systems. To overcome this problem, a stably transfected siRNA expression system (pSuper RNAi vector) was used in this study to provide permanent and effective silencing of the gene of interest. The pSuper RNAi (Brummelkamp, Bernards et al. 2002) system facilitates the transcription of RNA transcripts that readily form pair stem loop structures. These structures are rapidly cleaved within the cell, thereby producing a functional siRNA.

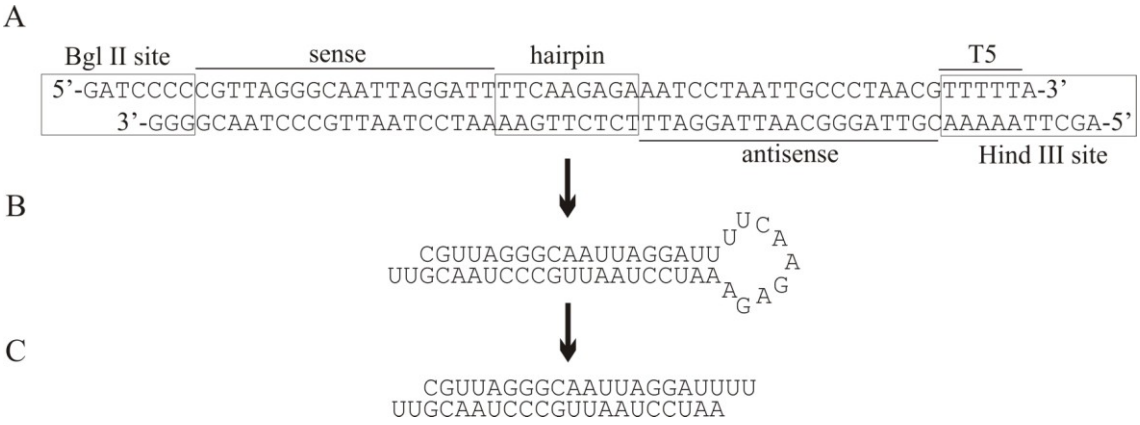

Fig 2.5. ***Principle of pSuper driven siRNA expression. A****. Annealed primers containing the targeting sequence, the hairpin loop, a termination signal (T5) and pSuper compatible*

overhangs (Bgl II and Hind III). ***B****. The RNA transcript forms a pair stem loop structure.* ***C****. Cell mediated processing of the RNA transcript results in a functional siRNA.(Modified from the pSuper.Retro Instruction manual, OligoEngine. Shown here: Construct #5 for αv integrin knockdown, which produced a highly efficient knockdown.*

2.8.9.1 Design of siRNA constructs

siRNA constructs were designed according to the protocols of (Ui-Tei, Naito et al. 2004) and (Naito, Yamada et al. 2004). The constructs had to meet the following requirements: The sense-strand should contain G/C nucleotides in 5'- prime and an A/T rich region ending with A/T must be located at its 3'-prime end. There should be no G/C stretches longer than 9bp and the overall G/C content should not exceed 60%. Appropriate 19mers matching these requirements were identified through processing the target gene's full length mRNA sequence with siDirect software. For each knockdown, five different knockdown constructs were designed and subsequently cloned into the pSuper.Retro vector.

2.8.9.2 Cloning of knockdown constructs

In order to prepare the knockdown insert for pSuper.Retro, the forward and reverse strands of the oligonucleotides (5'-prime phosphorylated and HPLC purified) had to be annealed. Therefore, 3 µg of each, the forward and the reverse strand were combined and filled up to 50 µl with annealing buffer. Primer denaturation was achieved through a heat-step. Subsequently the solution was allowed to cool down slowly to allow proper annealing of both strands. The denaturation and annealing procedure was performed as listed in the table below:

Step	time (sec.)	temp. (°C)	
1	240	90	
2	600	70	-1°C / min
3	900	15	
4	∞	10	

Annealed oligonucleotides were kept on ice until ligation was performed. In order to prepare pSuper.Retro for ligation, the vector was digested with Bgl II and Hind III (2.8.4.1), followed by dephosphorylation (2.8.4.2). Finally, 4 µg of linearized pSuper.Retro were ligated (2.8.4.3) with 2 µl of the annealed oligonucleotides. Successful ligation results in destruction of the Bgl II restriction site. To reduce the amount of re-ligated vector, a additional Bgl II digest (2.8.4.1) of the ligation reaction was performed. 2 µl of the reaction were used for transformation.

Annealing buffer: 100 mM NaCl in 50 mM HEPES pH 7.4

2.8.10 Preparation of retrovirus

Retrovirus preparations were done in collaboration with Prof. Dr. Alexander Pfeiffer (University of Bonn, Germany). For production of vesicular stomatitis virus G (VSV-G) pseudo typed retroviral vectors, human embryonic kidney cells (HEK293T) were transfected with the pSuper.Retro knockdown construct, packaging plasmids (encoding HIV *gag*, *pol* and *rev*) and a plasmid encoding for the envelope of VSV-G by a calcium-phosphate method. Supernatant containing the VSV-G pseudo typed retrovirus was harvested, enriched by centrifugation and directly used for infection of $FN^{RGE/RGE}$ fibroblasts.

2.8.11 Plasmids and cDNAs

cDNA	backbone	provided by	reference
FN-III_{1-5} (human)	pET-15b	H.P. Erickson	(Ohashi et al., 2005)
FN-III_{4-7} (human)	pET-15b	H.P. Erickson	(Ohashi et al., 2005)
FN-III_{7-10} (human)	pET-15b	H.P. Erickson	(Ohashi et al., 2005)
FN-III_{7-10}RGE (human)	pET-15b	H.P. Erickson	(Ohashi et al., 2005)
FN-III_{7-10}ΔRGD (human)	pET-15b	H.P. Erickson	(Ohashi et al., 2005)
FN-III_{10-12} (human)	pET-15b	H.P. Erickson	(Ohashi et al., 2005)
FN-III_{13-15} (human)	pET-15b	H.P. Erickson	(Ohashi et al., 2005)

2.9 Microscopy

2.9.1 Confocal microscopy

Confocal images were taken using a confocal microscope (Leica, DMIRE2) with immersion oil objectives HCX PL APO 100 x/1.4-0.70, HCX PL APO 63 x/1.4-0.60 and a HC PL 40 x/0.70 dry objective at RT. Images were acquired, processed and evaluated using Leica Confocal Software (version 2.5, Build 1227).

2.9.2 Epifluorescence microscopy

Fluorescence images were taken at RT with an epifluorescence microscope (Leica, DMRA2) equipped with a NPLAN 40/0.65 NA objective and a CCD camera (Hamamatsu, ORCA-ER).

2.9.3 Light microscopy of living cells

Images of living cells were taken using an inverted light microscope (Zeiss, Axiovert 40 CFL) equipped with a A – PLAN 10 x / 0.25 objective and a LCD camera (Prosilica).

Images were acquired and evaluated using the software Fire wire recorder (SVS – Visitek GmbH).

2.9.4 Light microscopy of histological sections

Images of histological sections were taken using a light microscope (Zeiss, Axioskop) equipped with a 5 x / 0.15 and 10 x / 0.30 objective (Zeiss, Plan-NEOFLUAR) equipped with a LCD camera (Leica, DCC500).

2.9.5 Stereo microscopy of macroscopic structures

Embryos were dissected and visualized using a stereomicroscope (Leica, MZFLIII) equipped with a LCD camera (Jenoptik, ProgRes C14).

3 Results

3.1 Functional analysis of FN's RGD motif *in vivo* and *in vitro*

The generation of the FN RGD>RGE targeting construct as well as the generation of $FN^{RGE/+}$ knockin ES cells was done by Drs. Fässler and Seiichiro Takahashi. Mouse-blastocyst injection of selected ES cells to obtain germ line chimeras was performed by Dr. Bösl (Max-Planck-Institute of Biochemistry, Martinsried, Germany). The *in vivo* analysis of $FN^{RGE/RGE}$ mice described in this study was performed in cooperation with Dr. Seiichiro Takahashi.

3.1.1 Generation of $FN^{RGE/RGE}$ knockin mice

Murine fibronectin is encoded by a single gene (Fn1) that consists of 46 exons located on chromosome 1. Translation of its ~ 8.3 kbps long transcript gives rise to a protein composed of 2477 amino acid residues. The RGD motif is located in exon 30. Substitution of the aspartate (D^{1616}) to glutamate (E) leads to abrogation of integrin binding (Pierschbacher and Ruoslahti 1984). In order to study the impact of the RGD>RGE mutation *in vivo*, mice with the corresponding mutation in the fibronectin gene were generated using homologous recombination techniques. Therefore, a fragment of the FN gene containing exon 30 was cloned into a pKS vector backbone. The amino acid substitution was achieved by site directed mutagenesis, resulting in a change of the aspartate (D) encoded by the codon GAC to GAG, which codes for glutamate (E). The C>G nucleotide change additionally created a novel HinfI restriction site in the mutant FN gene, which was used to identify mice carrying the mutated allele. (Fig 3.2). The resultant targeting construct $FN\text{-}RGE^{neo}$ was used for gene targeting (Fig 3.1).

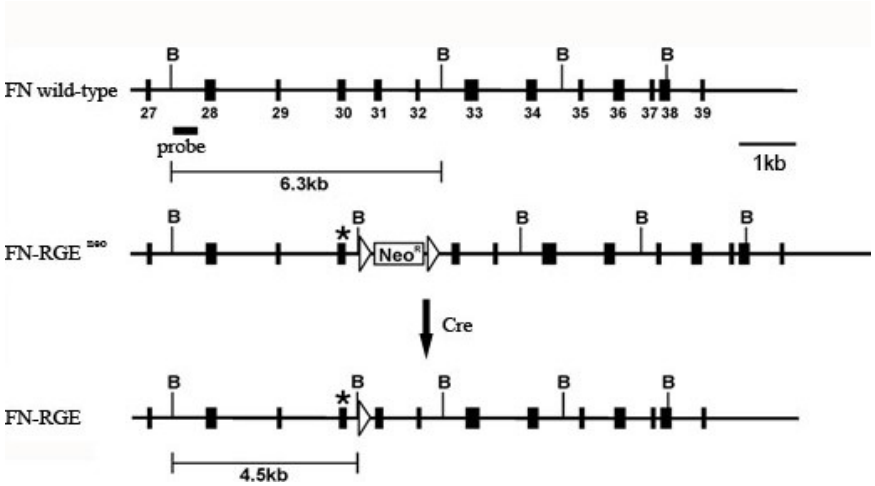

Fig 3.1. ***Schematic representation of the FN-RGE knockin strategy****. Depicted is the cloned FN fragment containing exon 30, which was targeted by the point mutation (*****). Additionally, a loxP flanked neomycin resistance (Neo^R) cassette was inserted into intron 30 to allow positive selection of ES cell clones that incorporated the mutated allele by recombination. The resultant targeted allele is depicted as FN-RGE^{neo}. The removal of the selection cassette from the targeted allele was later achieved by intercrossing heterozygous mice with a strain expressing deleter-Cre recombinase. B marks BamHI restriction sites.* (*Modified from Takahashi et al.).*

Electroporation of the targeting construct into ES cells (derived form 129/Sv mice) and subsequent selection with neomycin yielded two clones whose chromosomal DNA had incorporated the mutant allele by homologous recombination. Both clones were identified by Southern blot analysis. Therefore, genomic ES cell DNA was subjected to a BamHI digest and hybridized with an external probe which recognized the wild-type (6.3 kbps) and the mutant allele (4.2 kbps). In order to generate germ-line chimeras, the two ES cell clones carrying the FN-RGE allele were injected into blastocysts, which were subsequently transferred into foster mice. Highly chimeric male offspring were mated to female C57BL6 mice to assess germ-line transmission and to obtain FN-RGE heterozygous mice (FN$^{RGE/+}$). The FN$^{RGE/+}$ progeny were viable and of normal appearance. In order to remove the neomycin selection cassette, FN$^{RGE/+}$ males were mated to deleter-Cre expressing C57BL6 females. The successful introduction of the FN-gene mutation in mice was finally confirmed by Southern blot analysis of DNA derived from tail biopsies as previously described for the ES cells. In addition, the mice were genotyped by PCR, which facilitated the detection of the mutant and the wild-type allele with the corresponding amplicon-sizes of 380 bps and 330 bps, respectively (Fig 3.2).

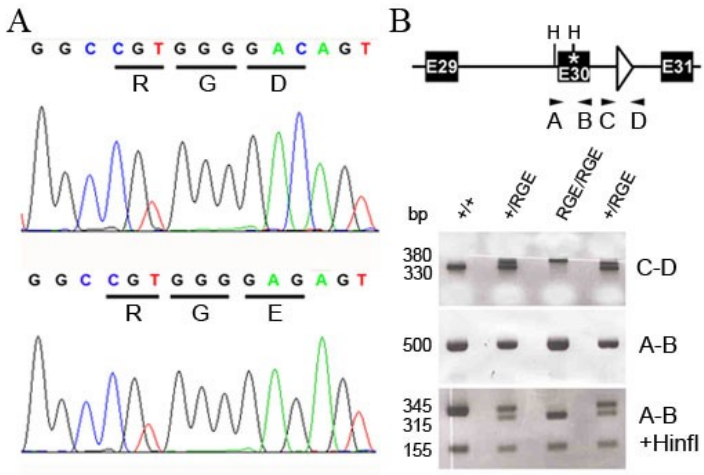

Fig 3.2. ***Confirmation of the FN-RGE mutation in mice****. **A**. Sequenced amplicon of a genotyping PCR: Confirmation of the knockin mutation. **B**. HinfI digest of amplicons, derived from genotyping PCR using the primer pair genoRGE fw and genoRGE rev (2.8.5.1), results in the expected fragmentation of the mutant amplicon. (Taken from Takahashi et al. and modified).*

Intercrossings of $FN^{RGE/+}$ mice revealed no viable homozygous ($FN^{RGE/RGE}$) progeny. Out of 157 viable offspring, 65% heterozygous and 35% wild-type, but no homozygous were obtained (Fig 3.3). This clearly indicates that the FN-RGE mutation represents a recessive embryonic lethal trait. In order to assess the time point of lethality, embryos derived from heterozygous intercrosses were dissected at different stages of embryonic development. Each dissected embryo was genotyped by PCR of DNA-extracts from yolk sac biopsies or embryonic tissue. Until E10.5, all embryos were alive and the determined genotypes showed normal Mendelian distribution. Beyond E10.5, no $FN^{RGE/RGE}$ embryo survived, which was indicated by lacking heartbeat. One day later (E11.5), all homozygous mutants were already partially disintegrated and started to become resorbed.

		wild-type		$FN^{RGE/+}$		$FN^{RGE/RGE}$	
Stage	Total	*n*	%	*n*	%	*n*	%
E7.5	16	5	31.2	8	50.0	3	18.8
E8.5	170	46	27.1	81	47.6	43	25.3
E9.5	95	26	27.3	46	48.4	23	24.2
E10.5	46	12	26.1	21	45.7	13	28.3
E11.5	26	11	42.3	15	57.7	3[a]	11.5
E12.5	15	4	26.6	11	73.3	0	0.0
E13.5	4	2	50.0	2	50.0	0	0.0
P21	157	55	35.0	102	65.0	0	0.0

Fig 3.3. ***Genotypes of progeny derived from heterozygous intercrosses****. The genotypes show Mendelian distribution. Homozygous mutants die around E10.5. ([a]) assigns embryos without beating heart. (Taken from Takahashi et al. and modified).*

3.1.2 $FN^{RGE/RGE}$ embryos display multiple abnormalities

To analyse the cause of lethality and the defects caused by the FN-RGE mutation, embryos derived from heterozygous intercrosses were dissected at different developmental stages. $FN^{RGE/RGE}$ embryos displayed the first subtle defects at E8.5,

which was manifested in a slightly shorter anterior–posterior axis. With respect to the development of the neural tube, the head fold and the number of present somites (three to four pairs), $FN^{RGE/RGE}$ embryos were indistinguishable from their wild-type littermates. The defects caused by the FN mutation became explicitly evident at E9.5. While wild-type embryos at this stage completed turning (Fig 3.4) into the fetal position, $FN^{RGE/RGE}$ mutants were only partially turned, the limb buds were missing and their neural tube exhibited a notable kink. Furthermore, $FN^{RGE/RGE}$ embryos had a shortened posterior trunk whose appearance differed markedly from the elongated and C-shaped trunk of wild-type embryos.

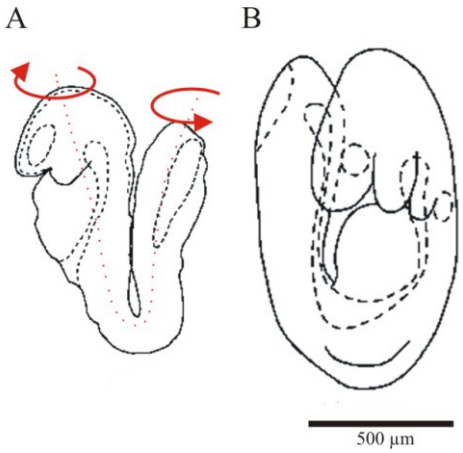

Fig 3.4. ***Turning of the embryo****. Between E8.5 (**A**) and E9.0 (**B**), embryos turn by rotation around their longitudinal axis.* $FN^{RGE/RGE}$ *mice fail to complete this rotation in time. (Pictures taken from emap Edinburgh mouse atlas project and modified).*

A characteristic feature of all $FN^{RGE/RGE}$ embryos at E9.5 was the complete absence of somite blocks in the severely shortened posterior trunk, which resulted in a low total number of only 12 – 13 somite pairs compared to ~ 21 in wild-type littermates. At E10.5, $FN^{RGE/RGE}$ embryos displayed some further progression in heart and head development. However, the formation of somite blocks in $FN^{RGE/RGE}$ embryos stopped around E9.0 with a number of 12 – 13 pairs, which did not increase any further at later stages.

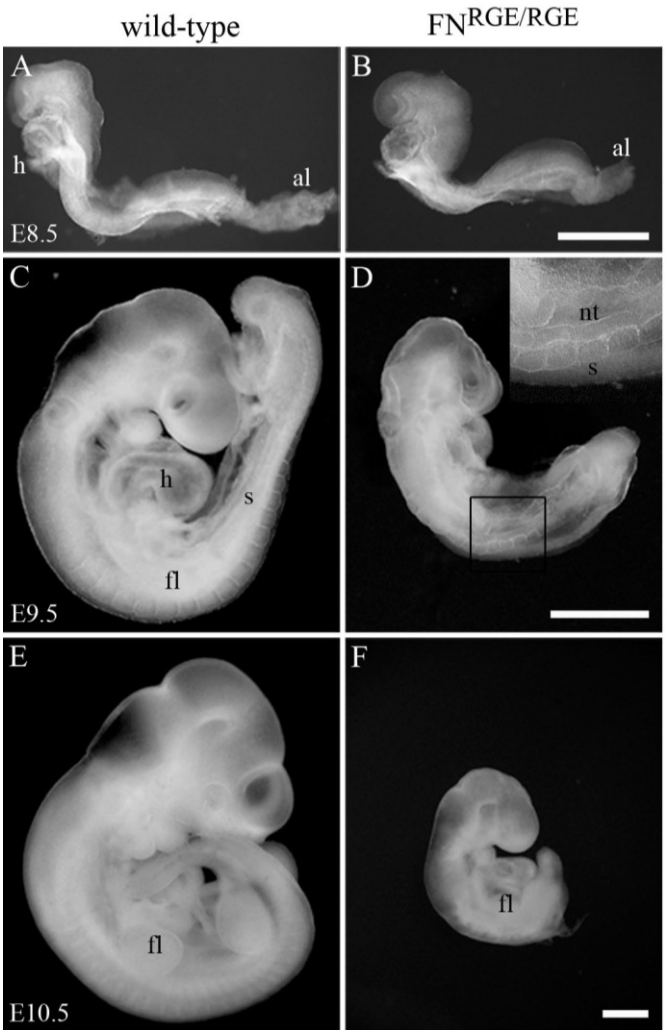

Fig 3.5. ***Whole-mount images of wild-type and FN$^{RGE/RGE}$ embryos****. **A and B**. Side view of E8.5 embryos, both with four pairs of somites and a well developed allantois (al). The FN$^{RGE/RGE}$ embryo is slightly smaller. **C and D**. The wild-type embryo has turned into fetal position and contains 21 pairs of somites (C). The E9.5 FN$^{RGE/RGE}$ embryo has not completed turning, has a kinked neural tube and a shortened posterior trunk region with only 13 pairs of somites (D). The inset shows the anterior somites in higher magnification. The headregion of the mutant embryo is normally developed. **E and F**. Side view of an E10.5 wild-type embryo with 29 somite pairs (E) and an FN$^{RGE/RGE}$ embryo with 13 (F). The fore limb buds and the first branchial arch are developed, but the second branchial arch is missing (F). al, allantois; fl, fore limb bud; h, heart; nt, neural tube; s, somites; Scale bars: (B, D, F) 500 µm. (Taken from Takahashi et al. and modified).*

The observed defects in FN$^{RGE/RGE}$ embryos suggested implications of aberrant apoptotic and cell proliferation processes. In order to test this assumption, markers for cell apoptosis and proliferation were analysed by immunohistochemistry. Analysis of the apoptotic markers TUNEL and cleaved Caspase 3 revealed, that FN$^{RGE/RGE}$ embryos exhibited markedly elevated levels of apoptotic cell death, particularly in tail bud

derived mesodermal cells located in the posterior trunk region. In contrast, cell proliferation tested by Ki67 staining was similar in wild-type and $FN^{RGE/RGE}$ embryos.

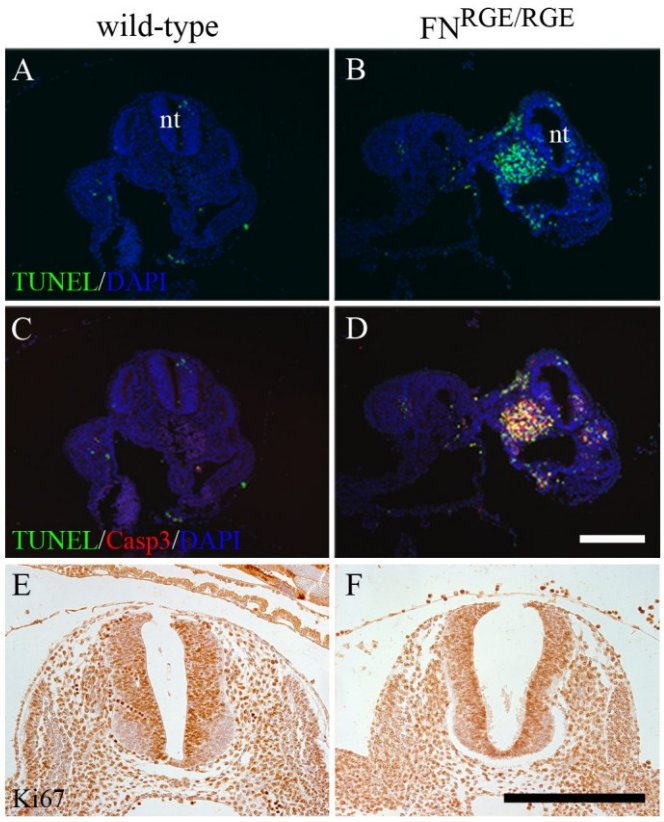

Fig 3.6. ***Analysis of apoptotic cell death and cell proliferation in E9.5 embryos****.* ***A to D****. TUNEL and cleaved form of caspase-3 staining reveal massive apoptosis in the posterior trunk region of* $FN^{RGE/RGE}$ *embryos in comparison with very few positive cells in the wild-type control embryo. Sites of co-localization of TUNEL (green) and cCasp3 (red) are colored in yellow.* ***E and F****. Analysis of cell proliferation by staining for the cell proliferation marker Ki67 revealed no notable difference between controls and* $FN^{RGE/RGE}$ *embryos. nt, neural tube; Scale bars: (D and F) 100 µm (Taken from Takahashi et al. and modified).*

3.1.3 FN-RGE is normaly distributed and assembled *in vivo*

It is a widely accepted notion, that FN's RGD motif is essential for FN matrix assembly to occur (Schwarzbauer 1991). Thus it was obvious to expect that mutation of this motif abrogates FN fibril assembly. To determine whether FN-RGE was assembled into a fibrillar matrix, immunostaining and Western blot analysis of E9.5 embryos were performed. Immunofluorescence staining for FN of parasagittal paraffin-sections from PFA fixed E9.5 embryos revealed a wide expression of FN-RGE. $FN^{RGE/RGE}$ embryos exhibited a strong FN-RGE matrix surrounding large vessels, the nervous tissue and somite blocks. A fine meshwork was visible within the heart, somites, tail bud mesoderm and the developing facial and trunk mesenchyme (Fig 3.7.A). There was no detectable difference of the FN immunosignal between $FN^{RGE/RGE}$ and wild-type control

embryos. The apparently normal expression levels of FN-RGE assessed by immunofluorescence could be confirmed by a comparative Western blot analysis of whole embryo lysates (Fig 3.7.B).

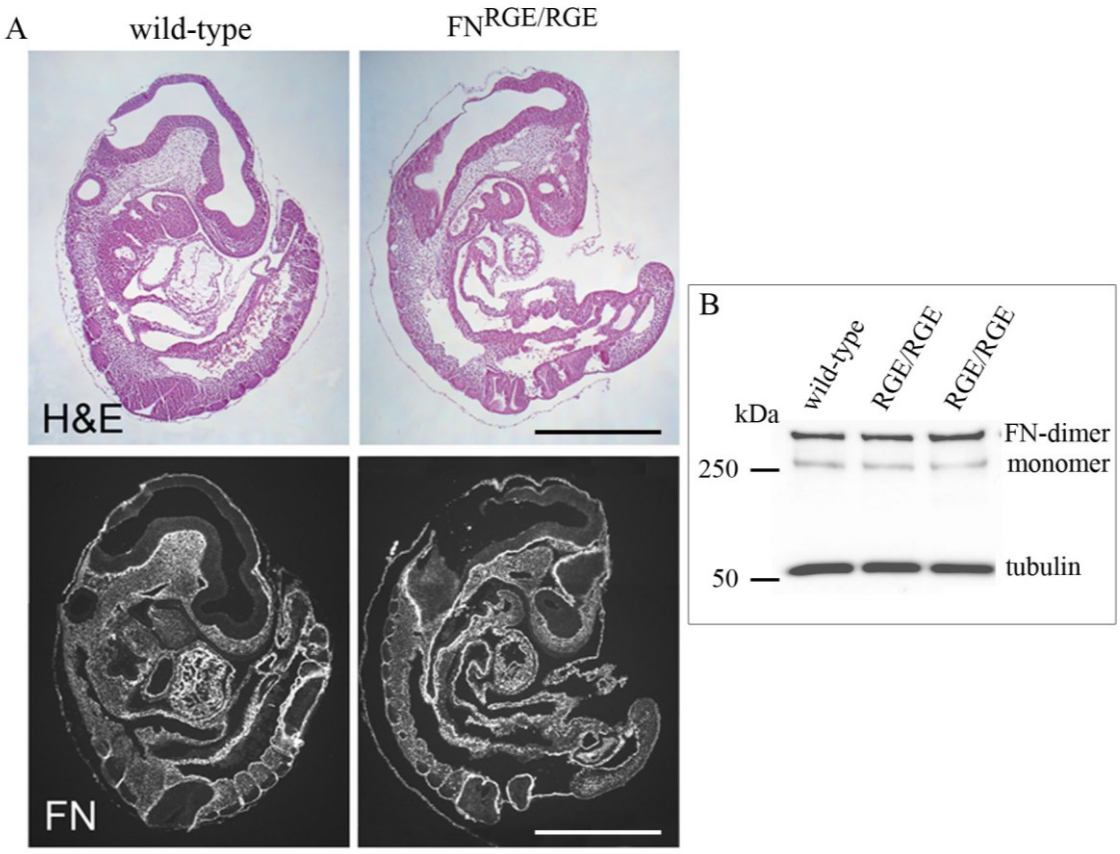

Fig 3.7. ***FN-RGE expression in FN$^{RGE/RGE}$ embryos****. **A**. Sagittal paraffin sections of E9.5 embryos stained with hematoxylin-eosin (H&E, top) and anti-serum against FN (bottom). FN$^{RGE/RGE}$ embryos display a notably shortened posterior trunk region. **B**. Western blot of E8.5 embryo lysates shows similar levels of FN expression levels in wild-type and FN$^{RGE/RGE}$ littermates. Scale bars: 500 µm (Taken from Takahashi et al. and modified).*

In vitro studies reported that α4 integrin is capable to trigger FN fibril formation in an RGD independent manner (Sechler, Cumiskey et al. 2000). Thus, the unexpected finding of apparently normal FN-RGE fibrils could be explained by the possibility of α4β1 integrin dependent assembly or, alternatively, by a cross-linking artefact induced by PFA fixation. In order to test these possibilities, native cryo-sections derived from E9.5 embryos were immunostained for FN and α4 integrin expression. The FN staining revealed a similar amount and distribution of FN fibrils in FN$^{RGE/RGE}$ embryos and wild-type controls. Integrin α4 was expressed at low levels and signals were only detectable in the cranial region, the epicardium and the proepicardial serosa of controls and FN$^{RGE/RGE}$ embryos. Importantly, α4 integrin positive cells in the cranial region or in the heart did not co-localize with FN signals, suggesting the existence of a novel, RGD and α4 integrin independent FN fibrillogenesis mechanism (Fig 3.8.A). In order to test

whether the absence of RGD-integrin interactions leads to a compensatory up-regulation of non-RGD binding α4 integrin expression, fluorescence activated cell sorter (FACS) analysis of single cell suspensions derived from collagenase treated E9.5 embryos was performed. It revealed that both, $FN^{RGE/RGE}$ and control embryos exhibited only a small population of α4 integrin positive cells of indistinguishable size and similar expression levels, demonstrating that α4 integrin expression was not altered in $FN^{RGE/RGE}$ mice (Fig 3.8.B).

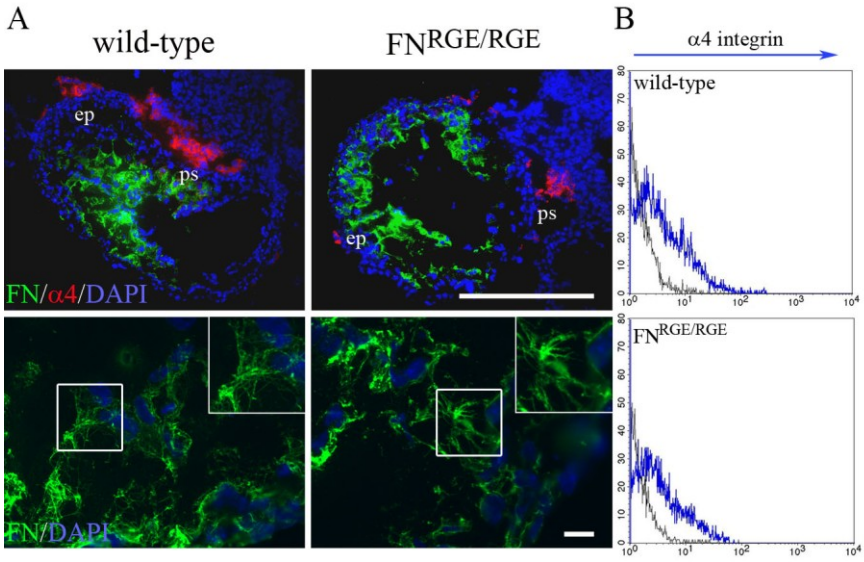

Fig 3.8. ***FN-RGE fibrillar network in $FN^{RGE/RGE}$ embryos****. **A**. Native cryosections of unfixed E9.0 embryos were stained for FN and α4 integrin. Image of the heart ventricle (top): Note that α4 integrin immunosignals are not co-localizing with FN signals. Higher magnifications show similar FN fibril-thickness and ramifications in wild-type and $FN^{RGE/RGE}$ embryos (bottom and inset). **B**. FACS analysis of single cell suspensions derived from E9.5 embryos shows comparable levels of α4 integrin expression. ep, epicardium; ps, proepicardial serosa; Scale bars: 100 µm. (Taken from Takahashi et al. and modified).*

3.1.4 $FN^{RGE/RGE}$ cells assemble FN-RGE in an αv integrin-dependent manner

In order to identify the mechanism underlying FN-RGE matrix assembly, several clonal fibroblast-like cell lines derived from E9.5 $FN^{RGE/RGE}$ and control embryos were established. The obtained cell lines were assayed for the cell surface expression levels of α2, α5, α6, αv, α4, β1 and β3 integrin by FACS analysis (Fig 3.9.A). Only cell lines with comparable integrin expression levels were chosen for subsequent assays. To rule out α4 integrin mediated FN assembly, only clones lacking α4 integrin were used. Addition of labelled wild-type plasma FN (pFN) to $FN^{RGE/RGE}$ cells in serum replacement medium resulted in the assembly of a normal fibrillar network with α5 integrin co-localized in fibrillar adhesions (Fig 3.9.B). This preliminary test confirmed that FN binding integrins on the surface of $FN^{RGE/RGE}$ clones were fully functional.

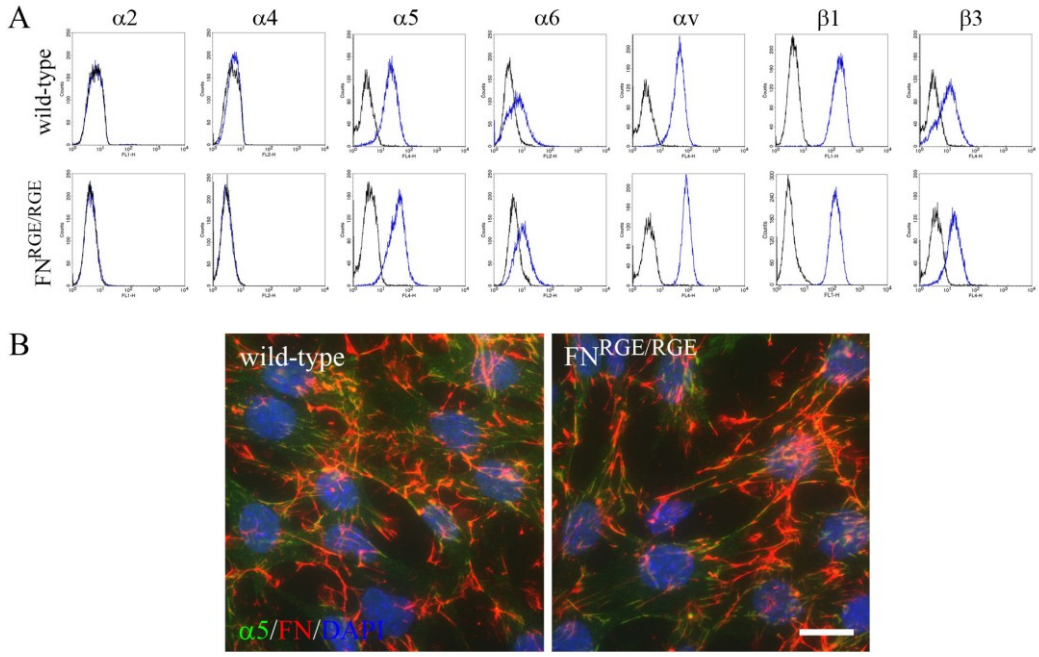

Fig 3.9. ***Integrin expression profile and plasma FN assembly assay***. ***A***. *Integrin expression profile of a selected wild-type and* $FN^{RGE/RGE}$ *clone determined by flow cytometry. Cell lines were incubated with antibodies to α2, α4, α5, αv, α6, β1 and β3 integrin subunits (blue histogram). Note that α5, αv, β1 and β3 integrins are expressed at comparable levels, while both clones lack α4 integrins. (Isotype controls are depicted in black).* ***B***. *Wild-type and* $FN^{RGE/RGE}$ *cells cultured in presence of exogenous plasma FN (60 nM). Note that* $FN^{RGE/RGE}$ *cells are capable to assemble exogenously added pFN. Scale Bar: 15 µm (Taken from Takahashi et al. and modified).*

In order to test whether $FN^{RGE/RGE}$ cells were also capable to assemble their endogenously produced mutant FN-RGE, it was necessary to grow them in serum-replacement medium to avoid contaminations with exogenous FN derived from serum. Serum is a widely used supplement of most cell growth media and a major source for exogenous FN. Assembly assays of endogenous FN critically depend on the absence of serum-derived FN. As cells in serum-replacement medium lack ECM components usually provided by the serum, they had to be seeded on defined substrates, such as Laminin 111 (LM111) or Vitronectin (VN). Wild-type and $FN^{RGE/RGE}$ cells plated on LM 111 adhered via their laminin binding α6β1integrin. Thus, α5β1 integrin, as well as αv integrins, were left unoccupied to the assembly of the secreted FN. In contrast to the previously mentioned notion that FN's RGD motif is essential for the initiation of FN matrix assembly, $FN^{RGE/RGE}$ cells were found to initiate and complete the assembly of FN-RGE into a dense network of fibrils on their cell-surface. The morphology of the fibrillar FN-RGE network was similar to that observed in $FN^{RGE/RGE}$ embryos. Although the kinetics of fibril formation was comparable between wild-type and $FN^{RGE/RGE}$ cells, the size and the distribution of the fibrils differed between the two cell lines. Wild-type cells produced an elaborate network of long and thin fibers, while the appearance of

FN-RGE fibrils assembled by $FN^{RGE/RGE}$ cells was rather short and thick (Fig 3.10.A). To determine which integrin, α5 or αv, mediates the assembly of FN-RGE, cells were plated on VN. On VN, wild-type and $FN^{RGE/RGE}$ cells adhered via their αv integrins. A previous study has shown that this depletes αvβ3 integrins from the apical cell surface but leaves α5β1 integrin diffusely distributed on the cell surface and presumably free to participate in FN matrix assembly (Fath, Edgell et al. 1989). When plated on VN, control cells developed a regular FN network, while $FN^{RGE/RGE}$ failed to form FN-RGE fibrils (Fig 3.10.B). This suggests that αv, but not α5β1 integrin, mediates the assembly of FN-RGE into a matrix network.

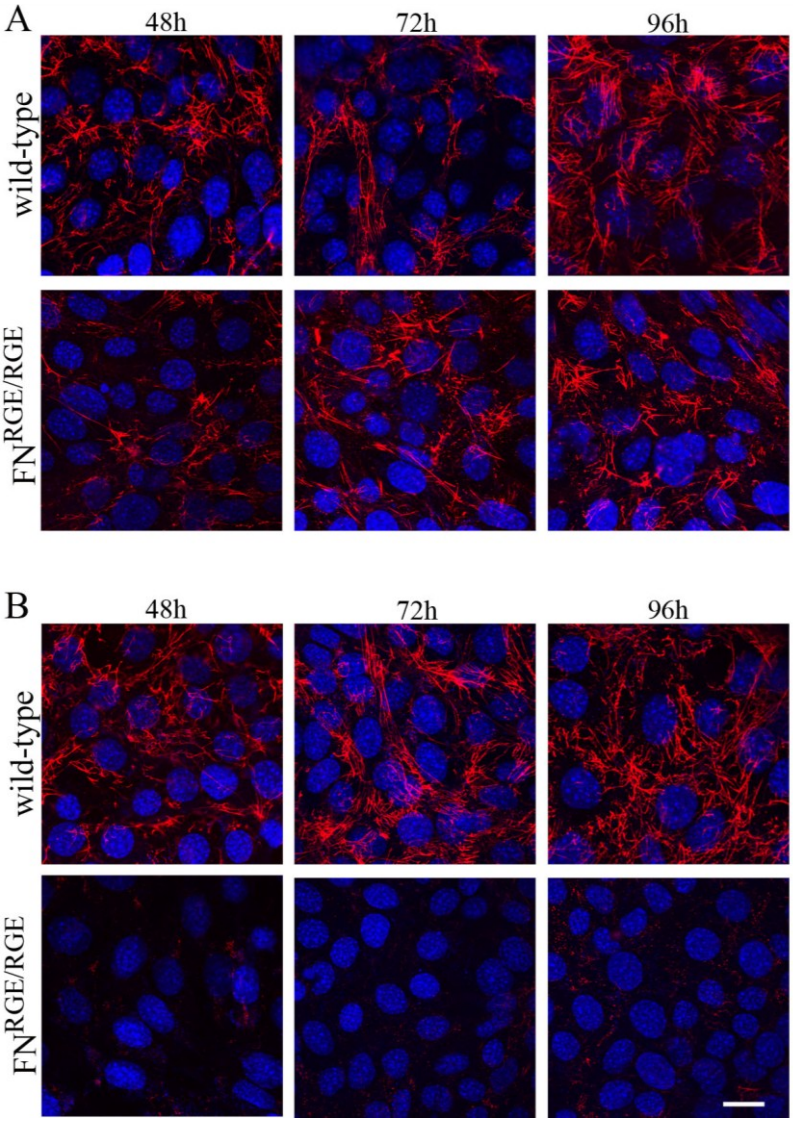

Fig 3.10. ***FN-RGE fibril assembly on LM111 and VN. A and B****. Wild-type and $FN^{RGE/RGE}$ cells grown in serum replacement medium and either plated on LM111 (A) or VN (B). Cells were fixed after 48, 72 and 96 h and stained for FN (red, DAPI stained cell-nuclei are depicted in blue). Note that $FN^{RGE/RGE}$ cells are able to form FN-RGE fibrils on LM111 (A, bottom), but not on VN (B, bottom). Scale bar: 15 µm (Taken from Takahashi et al. and modified).*

3.1.5 αv integrins can trigger an RGD-independent FN assembly pathway

Since the data obtained with $FN^{RGE/RGE}$ cells on VN (shown in Fig 3.10. B) suggested that αv integrins play an essential role in FN-RGE fibril formation, it was further investigated whether α5β1 integrins were indeed not involved in this process. Therefore, wild-type and $FN^{RGE/RGE}$ cells were grown on LM111 and stained with antibodies against FN and the α5 integrin subunit. Fig 3.11.A demonstrates that wild-type cells showed co-alignment of α5 integrin with the thin and elaborate FN network. In contrast, $FN^{RGE/RGE}$ cells failed to align α5 integrin with FN-RGE fibrils. Instead, the α5 signal on $FN^{RGE/RGE}$ cells was diffusely distributed over the whole cell surface further indicating that this integrin was not able to bind to FN-RGE (Fig 3.11.A). Unfortunately, due to the poor quality of available anti-αv antibodies, it was not possible to directly demonstrate the co-localization of αv integrin with FN-RGE. To further corroborate the particular importance of αv integrins for FN-RGE fibril formation, a knockdown of the αv subunit in $FN^{RGE/RGE}$ cells was performed. The depletion was achieved by retroviral transduction of a construct expressing αv specific siRNAs, and yielded a ~80% down-regulation of αv expression as determined by FACS (Fig 3.11.C). As a negative control, $FN^{RGE/RGE}$ cells were transduced with a construct expressing scrambled siRNA. In order to assess the consequences of the knockdown on FN-RGE assembly, the αv-depleted $FN^{RGE/RGE}$ cells were plated on LM111 and cultured in serum-replacement medium for up to 96 h. Despite the availability of free α5β1 integrins, the αv-depleted $FN^{RGE/RGE}$ cells were unable to form FN-RGE fibrils (Fig 3.11.B). Only after longer culture periods a few thick fibers could be occasionally observed, which was likely due to the remaining low levels of αv integrin expressed on αv-depleted $FN^{RGE/RGE}$ cells.

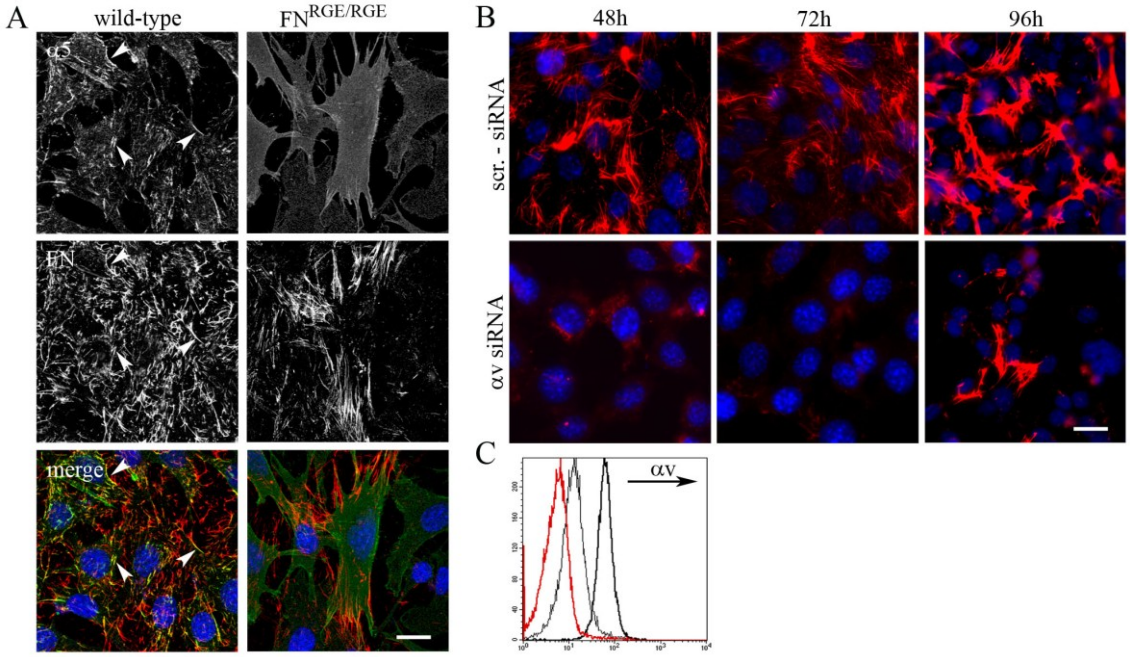

Fig 3.11. ***Distribution of α5 integrin and siRNA mediated depletion of αv integrin in $FN^{RGE/RGE}$ cells.*** ***A****. Distribution of α5 integrin and FN fibers on wild-type and $FN^{RGE/RGE}$ cells*

cultured on LM111 for 24 h in serum-replacement medium. Note that α5 and FN co-localize in fibrillar adhesions (white arrowheads) of wild-type cells, whereas α5 is diffusely distributed on $FN^{RGE/RGE}$ cells. ***B****. αv integrin depletion in $FN^{RGE/RGE}$ cells by retroviral transduction of anti-αv siRNA and control siRNA (scr.-siRNA) expression cassettes. Cells were cultured for 48, 72 and 96 h on LM111 in serum-replacement medium and stained for FN-RGE. Note that FN-RGE fibril formation is largely abrogated in αv-depleted $FN^{RGE/RGE}$ cells.* ***C****. Determination of αv integrin knockdown efficiency by FACS analysis. The siRNAs against αv integrins cause ~80% depletion (thin black histogram). The bold black histogram indicates normal expression levels of αv integrin in $FN^{RGE/RGE}$ cells expressing scrambled siRNAs. (red histogram: isotype-control). Scale bars: 15 µm. (Taken from Takahashi et al. and modified).*

To assess the importance of αv integrin's RGD-binding pocket for FN-RGE fibril formation, I performed FN assembly assays in presence of RGD containing peptides. The linear Gly-Arg-Gly-Asp-Ser-Pro (linRGD) peptide is a widely used compound to disrupt the interaction of RGD binding integrins, such as α5β1 and αvβ3, with their ligands. The more constrained cyclic *cyc*RGD (*cyclo* [-Arg-Gly-Asp-D-Phe-Val-]) was reported to preferentially bind to αvβ3 integrin (Pfaff, Tangemann et al. 1994). Incubation of wild-type and $FN^{RGE/RGE}$ cells with linRGD extensively inhibited assembly of wild-type as well as FN-RGE fibrils. In contrast, presence of *cyc*RGD had a strong inhibitory effect on the assembly of FN-RGE, while wild-type fibril formation was only marginally affected. Treatment of wild-type and $FN^{RGE/RGE}$ cells with control peptides, in which the RGD motif was mutated (linear Gly-Arg-Gly-Glu-Ser-Pro [linRGE] peptide or cyclic *cyclo*[-Arg-Ala-Asp-D-Phe-Val-] peptide [*cyc*RAD]) had no effect on assembly of wild-type FN or FN-RGE (Fig 3.12). Since FN contains domains that facilitate binding to cell surface proteoglycans, such as members of the syndecan family, it was further tested whether these receptors were involved in the promotion of FN-RGE assembly. Heparin treatment, which blocks the binding of FN to cell surface proteoglycans, marginally inhibited wild-type FN assembly but had almost no effect on FN-RGE fibril formation (Fig 3.12). These data demonstrated that the RGD binding pocket of αv integrin is essential for FN-RGE matrix assembly.

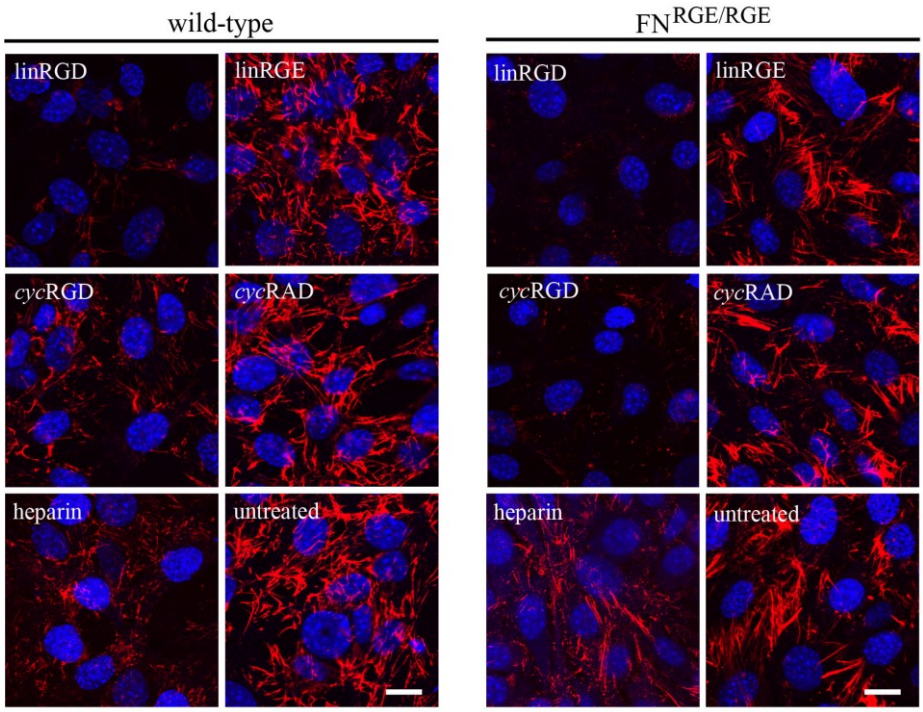

Fig 3.12. ***Effect of heparin, linear RGD or cyclic RGD peptides on FN-RGE assembly****. Wild-type and* $FN^{RGE/RGE}$ *cells were cultured on LM111 in serum-replacement medium for 2 h. Subsequently, heparin or peptides were added and cells were further incubated for 14 h. Finally, cells were stained with anti-FN antibodies (red signal) and DAPI to stain the nuclei (blue signal). The following compound concentrations were used: linRGD and linRGE 900 µM; cycRGD and cycRAD 410 µM; heparin 100 µg/ml; Scale bars: 15 µm. (Taken from Takahashi et al. and modified).*

3.1.6 The FN-I_{1-9} domains bind αvβ3 integrin with high affinity

The previous data demonstrated that αv integrins are essential for the formation of FN-RGE fibrils and suggested that these integrins are capable to bind to FN via a novel binding site. In order to map this novel αv binding / assembly site(s), wild-type and $FN^{RGE/RGE}$ cells cultured on LM111 were treated with recombinant FN fragments spanning almost the entire length of the FN molecule. As expected, all fragments containing the RGD motif (FN-III_{7-10} and FN-III_{10-12}) strongly inhibited the formation of wild-type FN as well as FN-RGE fibrils (Fig 3.13). In addition, a strong inhibitory effect was observed after treatment with FN's *N*-terminally derived fragment FN-I_{1-9}, which is generally recognized as a potent inhibitor of FN matrix assembly (Fig 3.13). The inhibitory effect of FN-I_{1-9} on FN matrix assembly is thought to be caused by its interaction with cell surface receptors. Another explanation for the inhibitory effect is its ability to bind to specific FN-III domains of other FN molecules, which results in lateral inhibition of FN self-association required for network formation (McKeown-Longo and Mosher 1984; Aguirre, McCormick et al. 1994; Hocking, Sottile et al. 1994; Bultmann, Santas et al. 1998). In contrast to the previously mentioned results, no

inhibitory effect on FN assembly, neither on wild-type nor on FN-RGE, was observed after cells had been treated with FN-III$_{1\text{-}5}$, FN-III$_{4\text{-}7}$, FN-III$_{13\text{-}15}$ and the control fragment FN-III$_{7\text{-}10}$RGE (Fig 3.13).

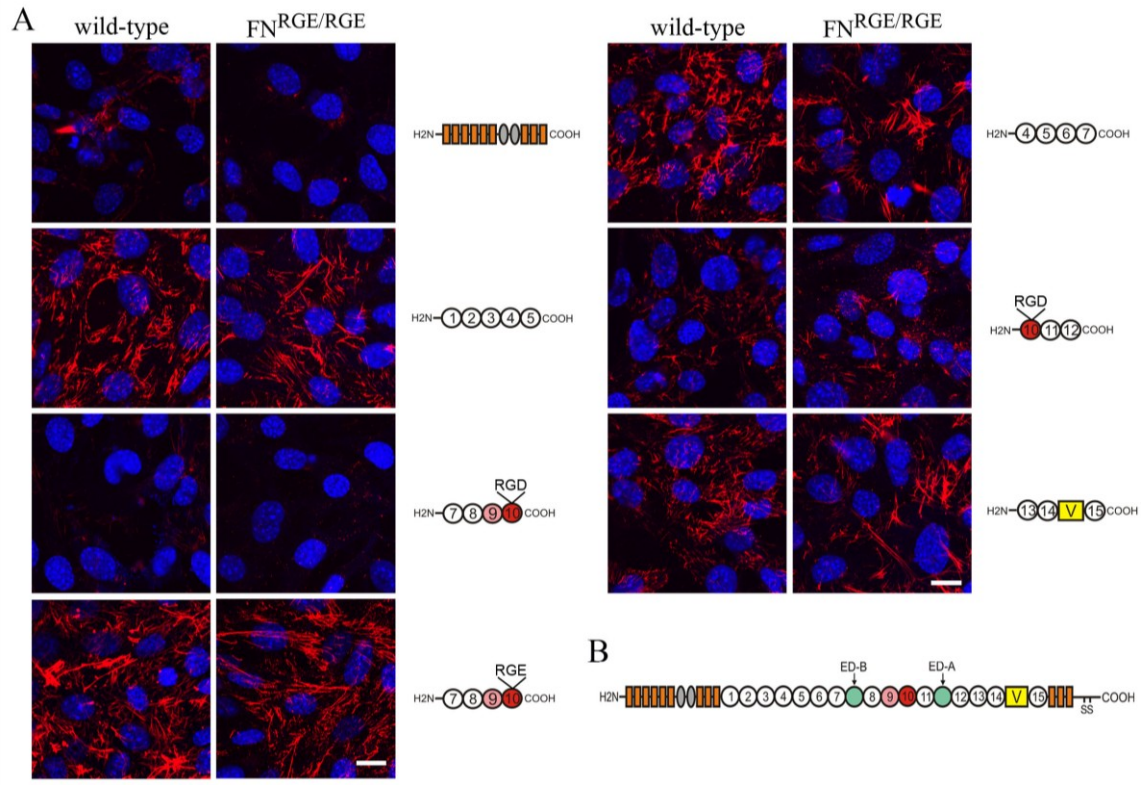

Fig 3.13. ***Effect of recFN fragments on FN assembly****. **A**. Wild-type and FN$^{RGE/RGE}$ cells were cultured on LM111-coated dishes in serum replacement medium for 2 h, recFN fragments were added (right) and cells were incubated for further 14 h. Finally, cells were PFA fixed and stained for FN using an anti-FN antibody. Note the strong inhibition of FN assembly when FN-III$_{7\text{-}10}$, FN-III$_{10\text{-}12}$ and FN-I$_{1\text{-}9}$ are applied. Final concentrations of recFN fragments: FN-I$_{1\text{-}9}$, 2.5 µM; FN-III$_{7\text{-}10}$ and FN-III$_{7\text{-}10}$RGE, 10 µM; all other fragments 25 µM. **B**. Schematic depiction of the modular domain composition of FN. Type I domains are depicted as orange rectangles, type II domains as grey ovals, and type III domains as circles. The integrin binding domains III$_9$ and III$_{10}$ have been highlighted in pink (synergy site) and red (RGD motif), respectively. The variable region is depicted as a yellow rectangle. Extradomains A and B are shown in green. Scale bars: 15 µm. (Taken from Takahashi et al. and modified).*

Treatment of wild-type and FN$^{RGE/RGE}$ cells with recFN-I$_{1\text{-}9}$ resulted in a strong inhibition on FN matrix assembly. Since assembly of FN-RGE depended on αvβ3 integrin, it was further examined whether this integrin was capable of binding to the recombinant FN-I$_{1\text{-}9}$ fragment. Therefore direct and competitive solid phase binding assays (2.7.9) were performed, in which the recombinant FN fragments were adsorbed to a microtiter plate and then incubated with serially diluted biotinylated αvβ3 integrins. Direct binding assays showed comparable binding of αvβ3 to FN-III$_{7\text{-}10}$, FN-III$_{10\text{-}12}$ and, surprisingly, to FN-I$_{1\text{-}9}$ (Fig 3.14.A). No binding of αvβ3 to the other fragment tested

was observed (Fig 3.14.B). In a similar assay, α5β1 integrin was applied. Although α5β1 lacked the ability to assemble FN-RGE, it exhibited the capability to bind to FN-I_{1-9} (Fig 3.14.C).

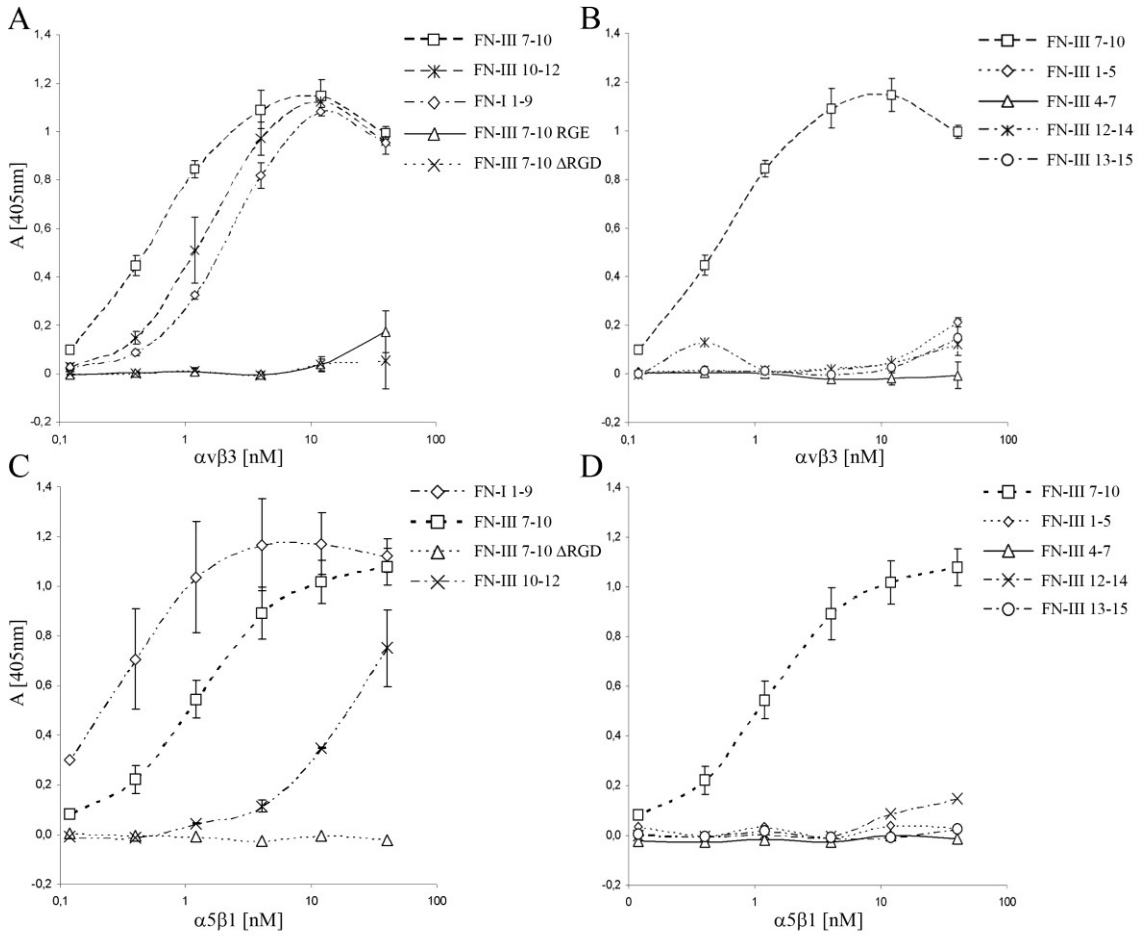

Fig 3.14. ***Direct solid-phase FN and integrin binding assay****.* ***A****. Titration curve of avb3 integrin bound to different recombinant FN fragments. FN fragments were adsorbed at 0.25 µM to microtiter plates. After blocking of non-specific binding with BSA, biotinylated αvβ3 was allowed to bind to immobilized FN fragments. In order to activate the integrins, the assay was performed in TBS buffer containing 1 mM $MnCl_2$. Note that αvβ3 bound with high affinity to FN-I_{1-9}. Fragments containing the RGD motif (FN-III_{7-10} and FN-III_{10-12}) served as positive controls. A FN-III_{7-10} fragment lacking the RGD motif served as negative control.* ***B****.αvβ3 integrin showed no binding to other fragments than FN-III_{7-10}, FN-III_{10-12} and FN-I_{1-9}.* ***C****. Same experimental procedure as mentioned in A and B, this time using biotinylated α5β1 for titration. Note that α5β1 binds to FN-I_{1-9}.* ***D****. Similarly to αvβ3, α5β1 did not bind to other fragments than FN-III_{7-10}, FN-III_{10-12} and FN-I_{1-9}. In all binding assays, the absorbance measured in BSA coated control wells was <15% relative to maximum absorbance values and was routinely subtracted. All binding was determined in duplicate. Mean ± SD (n = 3) (Taken from Takahashi et al. and modified).*

In order to reveal the role of the RGD binding pockets of the integrins αvβ3 and α5β1 for FN-I_{1-9} binding, competitive solid phase binding assays in presence of linRGD

peptides were performed. Treatment with linRGD resulted in strong inhibition of both, αvβ3 and α5β1 binding to the FN-I_{1-9} fragment (Fig 3.15.A and B).

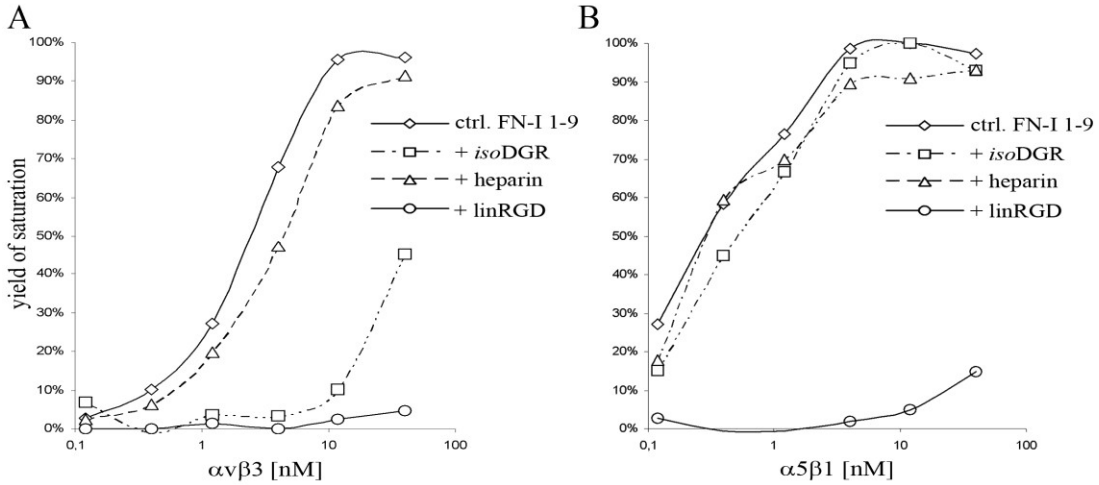

Fig 3.15. ***Competitive solid-phase binding assay****. FN-I_{1-9} was immobilized at 0.25 µM. The same experimental procedure was performed as mentioned in Fig 3.14. Integrins were allowed to bind in presence of 100 µg/ml heparin (triangles), 750 µM isoDGR-2C peptide (squares) or 850 µM linRGD peptide (circles). The values plotted are normalized to the maximal binding value to give the yield of saturation.* ***A****. The maximal binding value of αvβ3 integrin to FN-I_{1-9} corresponds to an OD (405 nm) of 1.08. Note that αvβ3 binding to FN-I_{1-9} is inhibited by both linRGD and isoDGR-2C peptides.* ***B****. Maximal binding of α5β1 corresponds to an OD (405 nm) of 1.04. Note that α5β1 binding to FN-I_{1-9} is inhibited by linRGD peptides but not by isoDGR-2C peptides.*

3.1.7 The GNGRG motif in FN-I_5 represents a novel αvβ3 binding and assembly site for FN

Structural studies have shown that murine FN contains four GNGRG motifs within the FN-I_{1-9} fragment that are well conserved in human, rat, bovine, amphibian and fish (Di Matteo, Curnis et al. 2006). In a more recent study it was demonstrated that a single GNGRG motif located in the FN-I_5 domain can convert into G*iso*DGRG (where *iso*D is *iso*-aspartate) and GDGRG by spontaneously occurring deamidation of the asparagine and that particularly G*iso*DGRG exhibits a high binding affinity to αvβ3 integrin. This finding was further supported by structural studies, which revealed that this particular GNGRG motif extends in a loop like structure from the core of the FN-I_5 domain into the peri-fibrillar space, were it should be easily accessible to integrins. To further examine the role of this motif as a potential αvβ3 binding site required for FN-RGE assembly, synthesised *Cys-Asn-Gly-Arg-Cys* (NGR-2C) and *Cys-*iso*Asp-Gly-Arg-Cys* (*iso*DGR-2C) peptides were applied in competitive solid-phase binding and FN *in vitro* assembly assays. As indicated in Fig. 3.15, *iso*DGR-2C strongly inhibited binding of αvβ3, but not α5β1, to FN-I_{1-9}. These data indicate that αvβ3 but not α5β1 can recognize the *iso*DGR motif. Treatment of $FN^{RGE/RGE}$ cells with NGR-2C and *iso*DGR-2C peptides resulted in effective inhibition FN-RGE fibril formation, whereas the

assembly of wild-type FN matrix was unaffected (Fig.3.16 A). The strong inhibition of FN-RGE assembly observed after treatment with NGR-2C peptides was unexpected, since GNGRG was reported to exhibit a lower binding affinity to αvβ3 integrins compared with G*iso*DGRG (Curnis, Longhi et al. 2006). NGR-2C's inhibitory effect suggested that a fraction of the peptides had rearranged into *iso*DGR-2C during 14 h of incubation in cell culture, since rearrangement of GNGRG to G*iso*DGRG or GDGRG is a well-known reaction occurring spontaneously under physiological conditions (Robinson, Robinson et al. 2004). In order to assess the kinetics of the deamidation reaction, NGR-2C peptides were incubated for 35 h at 37°C at a physiological pH of 7.2. HPLC analysis of peptide samples, taken at different time points during incubation, revealed that ~10% of purified NGR-2C had been converted to *iso*DGR-2C and DGR-2C within 16 h (Fig 3.16.B). Therefore, when testing for inhibition of FN matrix assembly, only a small amount of *iso*DGR-2C would have accumulated during 14 h of incubation. These data suggest that the observed inhibition observed was most likely due to unmodified NGR-2C interacting with αvβ3.

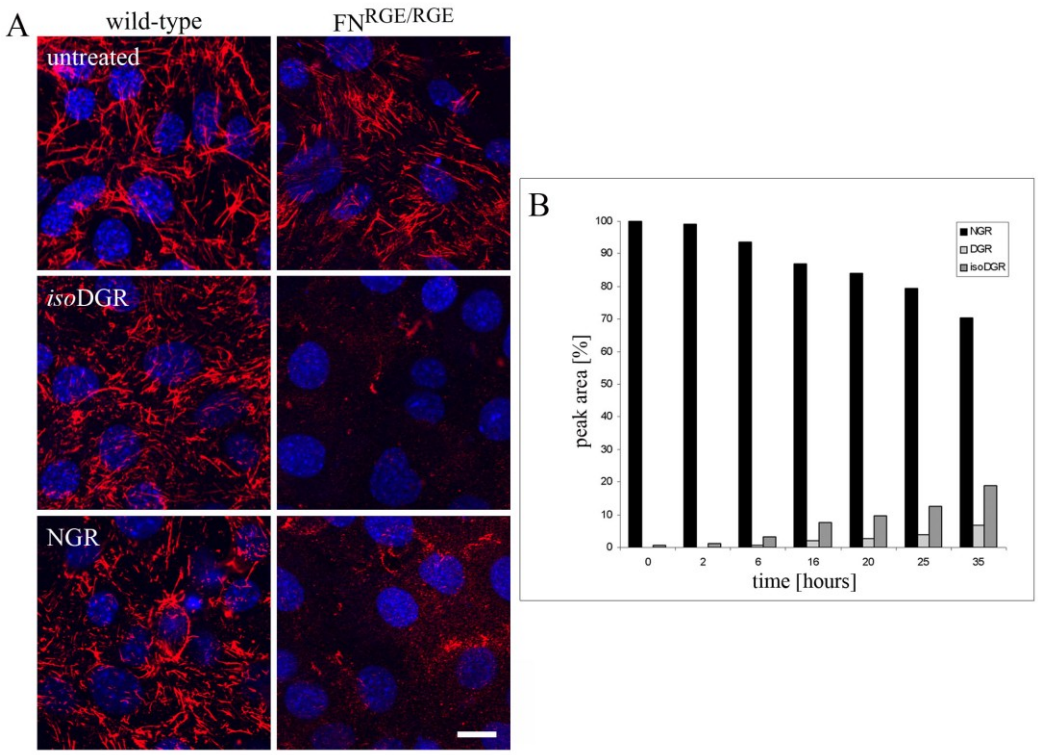

Fig. 3.16. ***Effect of NGR-2C and isoDGR-2C peptides on FN-RGE assembly****. **A**. Wild-type and FN$^{RGE/RGE}$ cells were cultured on LM111 coated dishes in serum-replacement medium for 2 h, incubated with 800 µM NGR-2C or isoDGR-2C for 14 h and stained with anti-FN antibodies. Note that both NGR-2C and isoDGR-2C peptides inhibit assembly of FN-RGE but not wild-type FN. Scale bar: 15 µm.* ***B****. Kinetics of NGR-2C deamination and rearrangement to isoDGR-2C and DGR-2C, respectively. NGR-2C peptides were incubated at 37°C and pH 7.2. Amounts of NGR-2C and the rearrangement products isoDGR-2C and DGR-2C were determined by HPLC analysis as percentage peak areas. Results were normalized against NGR-2C input. Note that*

the concentration of isoDGR-2C is steadily increasing with time, reaching ~10% of the NGR-2C input after 16 h.

Taken together, these results indicate that (1) FN-I_{1-9} contains novel αvβ3 binding / assembly sites, (2) binding sites on both integrins involve their RGD binding pocket, (3) FN-I_{1-9} contains a binding site for α5β1 that is not functional for FN matrix assembly, (4) the binding of αvβ3 to FN-I_{1-9} is of somewhat lower affinity than the RGD binding motif of wild-type FN, (5) the GNGRG motif in FN-I_5 represents a novel, selective αvβ3 binding site that can function for FN fibril assembly *in vitro* and *in vivo*.

3.2 Functional analysis of FN's dimerization motif *in vivo* and *in vitro*

The generation of the $FN^{CC>SS}$ targeting construct as well as the generation of $FN^{CC>SS/+}$ knockin ES cells was done by Drs. Fässler and Takayoshi Miyazono. Mouse-blastocyst injection of selected ES cells to obtain germ line chimeras was performed by Dr. Bösl (Max-Planck-Institute of Biochemistry, Martinsried, Germany).

3.2.1 Generation of $FN^{CC>SS/CC>SS}$ knockin mice

Fibronectin is secreted as a disulfide-bonded dimer and it is believed that the dimerization is essential for assembly of a fibrillar FN matrix (Schwarzbauer 1991). However, this acceptance is solely based on *in vitro* studies, and a confirmation for the *in vivo* situation is missing so far. To directly test the importance of FN dimerization *in vivo*, a mouse strain was generated that is incapable of expressing FN in the dimeric form. To this end, two Cysteins residues (Cys^{2458} and Cys^{2462}), located in Exon 45 at the very C-terminus of the FN-molecule, were changed to serines which should result in the abrogation of FN's capability to dimerize. The generation of mice carrying the CC>SS mutation in one of their fibronectin alleles was achieved using a gene targeting approach. Therefore, a fragment of the FN gene containing exon 45 was cloned into a pKS vector backbone. Site directed mutagensis was performed in order to change the Cys (C) encoding codons TGC to TCC, which encode for Ser (S). The resultant targeting construct $FN^{CC>SSneo}$ was used for gene targeting (Fig 3.17).

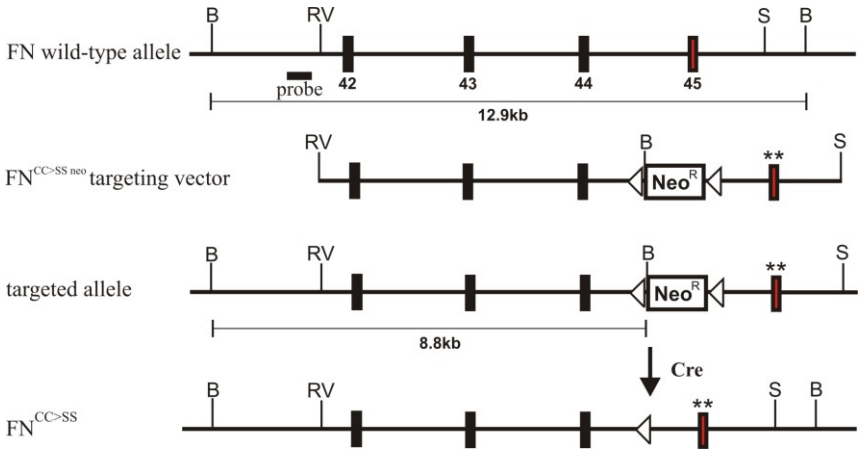

Fig 3.17. ***Schematic representation of the FN-monomer ($FN^{CC>SS}$) knockin strategy***. *A fragment of the FN wild-type allele containing exon 45 was modified with the point mutations (**). A loxP flanked neomycin resistance (Neo^R) cassette was inserted into intron 44 to allow positive selection of ES cell clones that incorporated the mutated allele by recombination. The targeting vector $FN^{CC>SSneo}$ contains the loxP flanked neomycin cassette and the mutated exon 45. Homologous recombination results in the depicted targeted allele. The removal of the neo selection cassette from the targeted allele was performed in vivo by intercrossing $FN^{CC>SS\ neo/+}$ heterozygous mice with deleter-Cre recombinase strain. Restriction sites: B, BamHI; S, SpeI; RV, EcoRV.*

The targeting construct $FN^{CC>SSneo}$ was electroporated into ES cells and the obtained transfectants were subsequently subjected to neomycin selection. Neomycin resistant ES cell clones were screened by Southern blot analysis to identify clones that had incorporated the mutant allele into their chromosomal DNA by homologous recombination. Therefore, genomic ES cell DNA was digested with BamHI restriction enzyme and hybridized with an external probe which recognized the wild-type (12.9 kbps) and the mutant allele (8.8 kbps) (Fig.3.18.A). Two positive ES cell clones carrying the $FN^{CC>SS}$ allele (Fig. 3.18.A) were identified and subjected to the same procedure as mentioned above (3.1.1) in order to obtain $FN^{CC>SS}$ heterozygous mice. Finally, the successful introduction of the mutation in mice was confirmed by Southern blot analysis of DNA derived from tail biopsies and by PCR genotyping (Fig. 3.18.B, D).

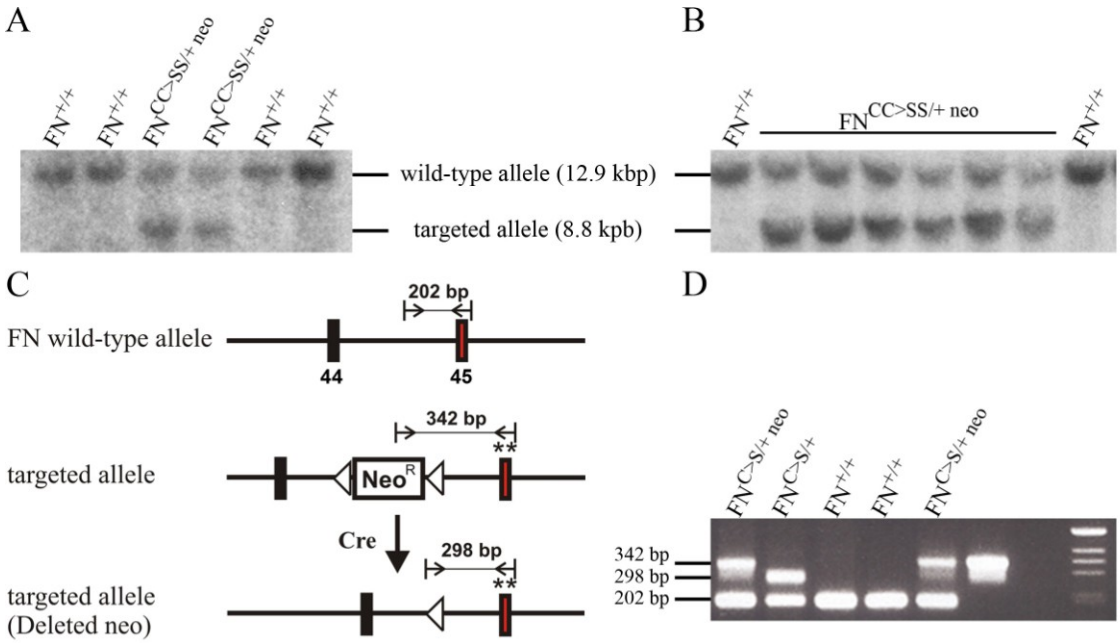

Fig 3.18. ***Confirmation of the FN$^{CC>SS}$ mutation in ES cells and mice****. **A**. Southern blot analysis of genomic ES cell DNA. DNA was hybridized with an external probe after BamHI digestion. Insertion of the targeting vector by homologous recombination changes the wild-type genomic DNA fragment of 12.9 kbp to 8.8 kbp.* ***B****. Southern analyses of genomic DNA derived from tail-tip biopsies of mice as described in A. Note that heterozygous mice exhibit the wild-type (12.9 kbp) and the targeted allele (8.8 kbp).* ***C and D****. PCR based genotyping of tail-tip DNA. Note that the targeted allele after neo deletion results in a band of 298 bp in size.*

In order to obtain homozygous mutant mice (FN$^{CC>SS/CC>SS}$), heterozygous mice (FN$^{CC>SS/+}$) were intercrossed. Genotyping of the resulting litters 3 weeks after birth (P21) revealed that no homozygous mutants were among the progeny. Out of 278 viable offspring, 49% heterozygous and 51% wild-type, but no homozygous were obtained (Fig 3.19), indicating that the FN-monomer mutation represents a recessive lethal trait. To determine the time point of lethality, embryos derived from heterozygous intercrosses were dissected at different stages of embryonic development. The genotype of each dissected embryo was determined by PCR, using DNA-extracts derived from yolk sac tissue. All embryos were alive until E11.5 and the distribution of the genotypes was according to the Mendelian law (Fig 3.19). No live FN$^{CC>SS/CC>SS}$ embryos were recovered beyond E11.5. Only a single FN$^{CC>SS/CC>SS}$ embryo had a beating heart, whereas all the mutant littermates were already dead and showed first indications of disintegration. At E12.5, all homozygous mutants were already partially absorbed.

		wild-type		$FN^{CC>SS/+}$		$FN^{CC>SS/CC>SS}$	
Stage	Total	n	%	n	%	n	%
E8.5	199	51	25.6	107	53.8	41	20.6
E9.5	307	76	24.8	148	48.2	83	27.0
E10.5	110	33	30.0	54	49.1	23	20.9
E11.5	40	12	30.0	27	67.5	1[a]	2.5
E12.5	27	11	40.7	16	59.3	0	0.0
P21	278	142	51.1	136	48.9	0	0.0

Fig 3.19. ***Genotypes of progeny derived from heterozygous ($FN^{CC>SS/+}$) intercrosses****. Homozygous mutants die around E11.5. ([a]) assigns the only homozygous mutant embryo with beating heart at E11.5.*

3.2.2 $FN^{CC>SS/CC>SS}$ embryos display growth retardation and abnormal vascular development

To investigate the reasons for the embryonic lethality of $FN^{CC>SS/CC>SS}$ embryos, embryos derived from heterozygous intercrosses were isolated at different stages of development to compare mutant with control littermates. The morphology of mutant embryos isolated at E8.5 was undistinguishable from wild-type littermates; they exhibited well developed head folds, 5 – 6 somite pairs and a properly developed neural tube (Fig 3.20 A, B). First indications of impaired development became apparent at ~E9.0. All $FN^{CC>SS/CC>SS}$ embryos at E9.5 were developmentally retarded when compared with their wild-type littermates (Fig. 3.20 E, F). They were markedly reduced in size, displayed a retarded posterior development and rarely developed beyond 20 pairs of somites. Another hallmark of mutant embryos at E9.5 was the appearance of oedema, indicated by a noticeably enlarged pericardial sac (Fig 3.20 F, H), which suggested that the FN mutation affected the development of the cardiovascular system. At E10.5, the growth arrest affecting mutant embryos became more evident and in some mutant hearts a cardiac-looping defect was observed (Fig 3.20 H).

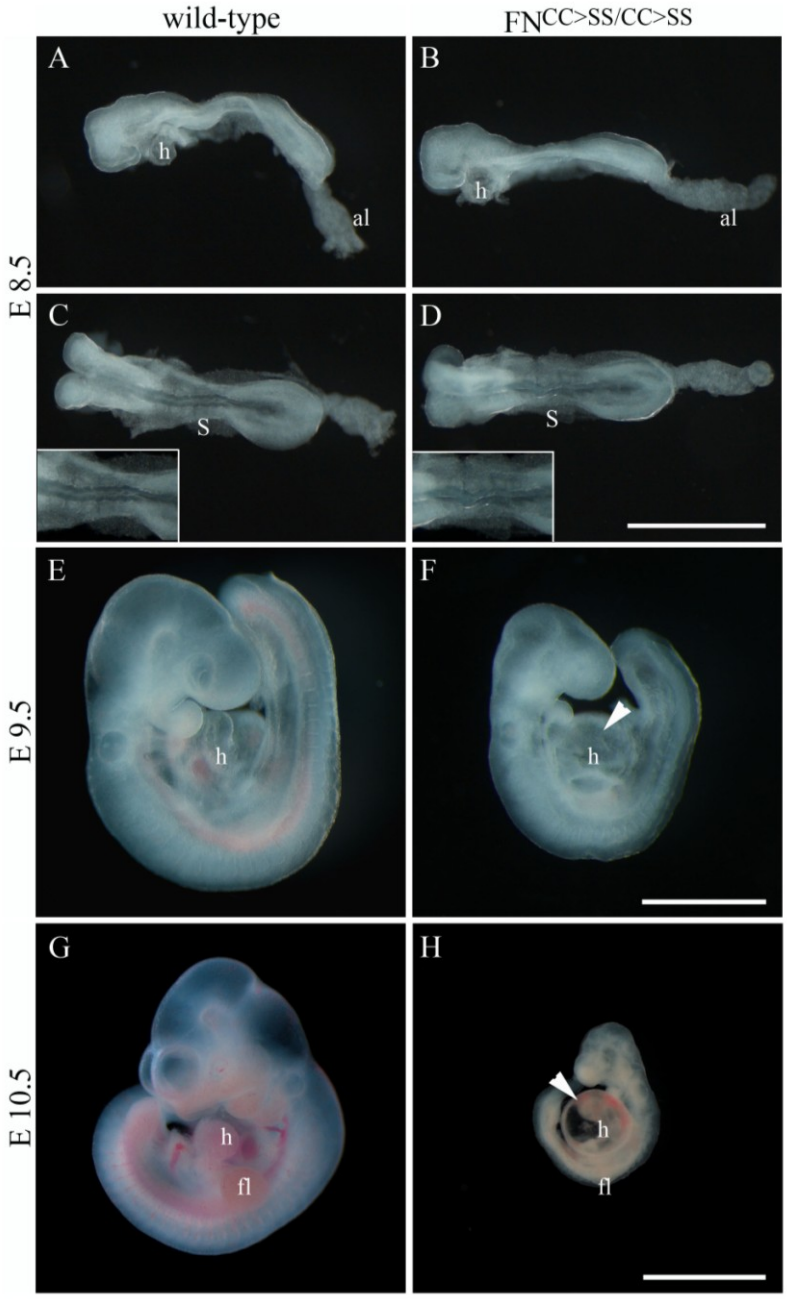

Fig 3.20. ***Whole mount images of wild-type and FN$^{CC>SS/CC>SS}$ embryos***. ***A and B***. *Side view of E8.5 embryos. Wild-type and mutant embryos are comparable in size and exhibit well developed allantoises.* ***C and D***. *Dorsal view of E8.5 embryos. Note that both, wild-type and mutant, exhibit 5 pairs of somite blocks. The insets shows properly shaped somite blocks at higher magnification.* ***E and F***. *Side view of E9.5 embryos. FN$^{CC>SS/CC>SS}$ embryos are severely growth retarded and underlie a growth arrest at the 20 - 25 somite pair stage. Note that mutants show oedema in the heart, as indicated by an enlarged pericardial sac (F and H).* ***G and H***. *Side view of E10.5 embryos. The growth arrest in FN$^{CC>SS/CC>SS}$ embryos leads to a pronounced difference in size as compared to the wild-type littermates. The arrowhead points to the markedly effused pericardial sac and the noticeable malformed heart, which is observed in most mutant embryos*

(H). al, allantois; fl, fore limb bud; h, heart; pl, placenta; s, somites; ys, yolk sac; Scale bars: (D,F) 500 µm; (H) 1 mm.

The effused pericardial sac and the growth arrest observed in $FN^{CC>SS/CC>SS}$ embryos beyond E9.0 suggested that the cardiovascular development was affected by the mutation. Clear indications of abnormal vascular development were also visible in $FN^{CC>SS/CC>SS}$ yolk sacs by E9.5. Compared to control yolk sacs, mutant yolk sacs were anemic and lacked a distinct branching network of vessels, which became even more pronounced by E10.5 (Fig 3.21.A). Some regions on the mutant yolk sac exhibited only small and disorganized vessels, whereas other regions completely lacked vessels. Furthermore, the presence of red blood cells in the mutant yolk sac cavity indicated leakiness of present small vessels, and suggested that the circulation would be impaired. To characterize these defects in more detail, the morphology of the vessel architecture in embryonic and extra-embryonic tissue was examined by means of immunohistochemistry. To this end, immunofluorescence stainings for the endothelial marker PECAM-1 (CD31) were performed on whole-mount yolk sacs. The analysis revealed that mutant yolk sacs failed to remodel their primitive vascular plexus by angiogenesis (Fig 3.21.C), which starts beyond E8.5 (Risau 1997) and results in formation of individual branched vessels through endothelial cell outgrowth and splitting of existing vessels.

The observed abnormal vascular development in the yolk sacs of $FN^{CC>SS/CC>SS}$ embryos suggested that other parts of the extra-embryonic tissue, such as the ectoplacental plate, may also be affected. To test this, paraffin sections of E10.5 placentas were stained for the endothelial marker Endomucin. At this stage of development, chorioallantoic fusion has been accomplished and fetal blood vessels derived from the extra-embryonic tissue have already invaded the maternal labyrinthine layer of the placenta in control mice. Intermingling of embryonic and maternal vessels in this layer is essential for proper exchange of gases and nutrition between the two circulations. The analysis of Endomucin stained ectoplacental plates revealed that the allantoic blood vessels of $FN^{CC>SS/CC>SS}$ mutants completely failed to invade the maternal labyrinthine layer. The mutant vessels residing in the embryonic part of the chorioallantoic plate were dilated or sometimes collapsed (Fig 3.21.F).

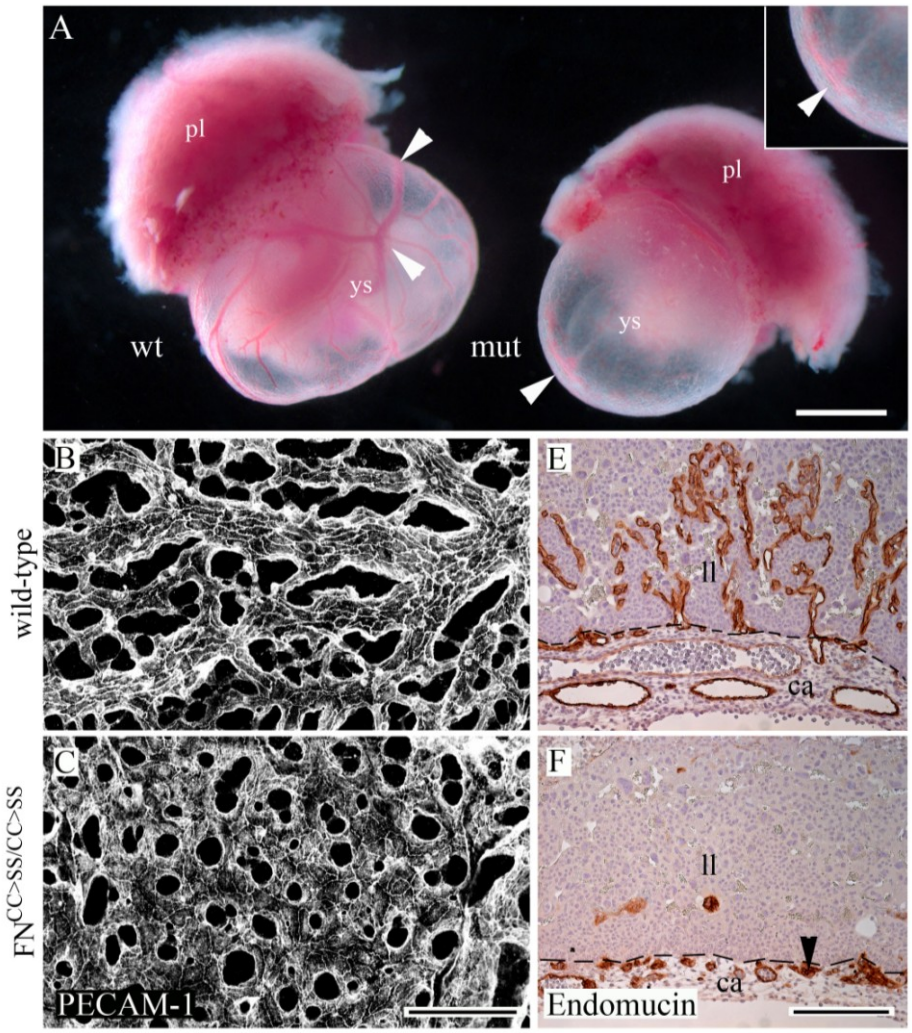

Fig 3.21. ***Abnormal vascular development in the extra-embryonic tissue of FN$^{CC>SS/CC>SS}$ mice****.* ***A****. Gross morphology of whole-mount yolk sacs of mutant embryos compared to those of wild-type littermates at E10.5. FN$^{CC>SS/CC>SS}$ yolk sacs exhibit severe defects in vascular development. Arrowheads show a defined and organized vessel structure in the wild-type yolk sac (left), whereas the mutant yolk sac exhibits severely dilated and leaky blood vessels with bleedings into the yolk sac tissue (right arrowhead and inset).* ***B and C****. Yolk sacs at E9.5, stained with an antibody against the endothelial marker PECAM-1. In contrast to the large vessels developed in wild-type yolk sacs, the primitive vascular plexus in mutant yolk sacs is not remodelled into an organized network of larger vessels (C).* ***E and F****. Paraffin sections of placentas at E10.5 stained with an antibody against the endothelial marker endomucin. Note that embryonic vessels of FN$^{CC>SS/CC>SS}$ embryos fail to invade and sprout properly into the maternal labyrinthine layer (F) The arrowhead marks a vessel of collapsed appearance. ca, chorioallantoic plate; ll, labyrinthine layer; pl, placenta; ys, yolk sac; Scale bars: (A) 1 mm; (C, F) 100 µm.*

To analyse the vessel architecture in embryonic tissue, the vascular system of whole E9.5 embryos was also stained with antibodies against endothelial markers. Similar to the observations made in extra-embryonic tissues, whole-mount staining of embryos

with endomucin antibodies revealed a markedly impaired capability of $FN^{CC>SS/CC>SS}$ embryos to develop a properly branched vascular system. In contrast to control embryos at this stage, $FN^{CC>SS/CC>SS}$ embryos exhibited dilated small vessels of fragile appearance and notably reduced lumina. Some regions of the mutant embryo - particular in the head and in intersomitic regions of the posterior trunk - showed only a weak expression of endomucin, suggesting an abnormal endothelial differentiation (Fig 3.22.A, C). Furthermore, immunofluorescence stainings with an antibody against PECAM-1 revealed that mutant vessels were irregularly shaped and showed numerous dilations. Some regions of the mutant embryo proper completely lacked a discernable organisation of vessels into a branched network (Fig 3.22.E).

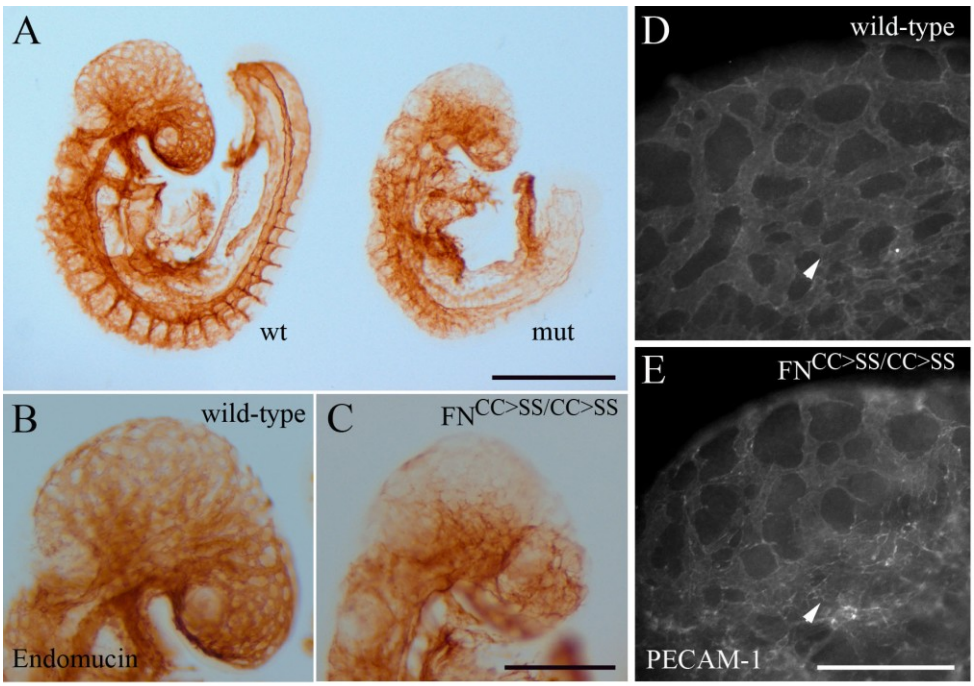

Fig 3.22. ***Abnormal vascular development in $FN^{CC>SS/CC>SS}$ embryos****. **A**. Image of whole-mount embryos at E9.5, stained with antibodies against endomucin. Mutant embryos (right) display a profoundly impaired vessel architecture as compared to control embryos (left).* ***B and C****. Higher magnification of embryo head-regions (from A). Note that $FN^{CC>SS/CC>SS}$ embryos form fragile, disoriented vessels with markedly reduced lumina (C).* ***D and E****. Immunofluorescence image of the head region of E9.5 embryos stained with antibodies against PECAM-1. Note the dilated vessels with markedly diverse diameters in $FN^{CC>SS/CC>SS}$ embryos (E), compared to control embryos (D). Arrowheads in D and E mark regions of normally developed vessels in the wild-type (D), and a severly disoriented vessel architecture in the head of a mutant embryo (E), respectively. Scale bars: (A) 500 µm; (C) 250 µm; (E) 100 µm*

Together, the expression of FN-monomers results in a growth arrest at the 20-25 somite stage with an abnormal vascular development in both embryonic and extra-embryonic tissues. Defects in vascular development may explain embryonic lethality at the time-point when the embryo starts to become dependent on placental supply. In the case of $FN^{CC>SS/CC>SS}$ embryos, however, the growth is arrested around E9.5 (Fig 3.20.F) when

the embryo is not yet dependent on placental exchange of nutrients (Cross, Werb et al. 1994).

3.2.3 $FN^{CC>SS/CC>SS}$ mice display enhanced apoptotic cell death

The early embryonic lethality of $FN^{CC>SS/CC>SS}$ mice raised the question, whether the mutation caused abnormal apoptotis and/or cell proliferation. In order to address this question, paraffin sections from E9.5 embryos were stained with antibodies for the apoptotic marker cleaved caspase-3 and for the cell proliferation marker phospho-histone-3. Whereas phospho-histone-3 staining showed no difference between wild-type and $FN^{CC>SS/CC>SS}$ embryos, stainings for cleaved caspase-3 revealed markedly elevated numbers of apoptotic cell-death in $FN^{CC>SS/CC>SS}$ embryos, particularly in the developing facial and trunk mesenchyme and in the posterior trunk region (Fig 3.23.B, C). Furthermore, cleaved caspase-3 staining of sections through the chorioallantoic region of E10.5 placentas showed that mutant allantoic blood vessels derived from extra-embryonic tissue did not only fail to invade the maternal part of the placenta (labyrinthine layer) (Fig 3.23.E, F), but also exhibited pronounced apoptotic cell-death in endothelial cells, as indicated by the strong immunofluorescence signal of cleaved caspase-3 staining (Fig 3.23.E to H). Together, these results show that the FN-monomer mutation accounts for elevated levels of apoptotic cell death events in the embryonic mesoderm and in endothelial cells of the extra-embryonic tissue.

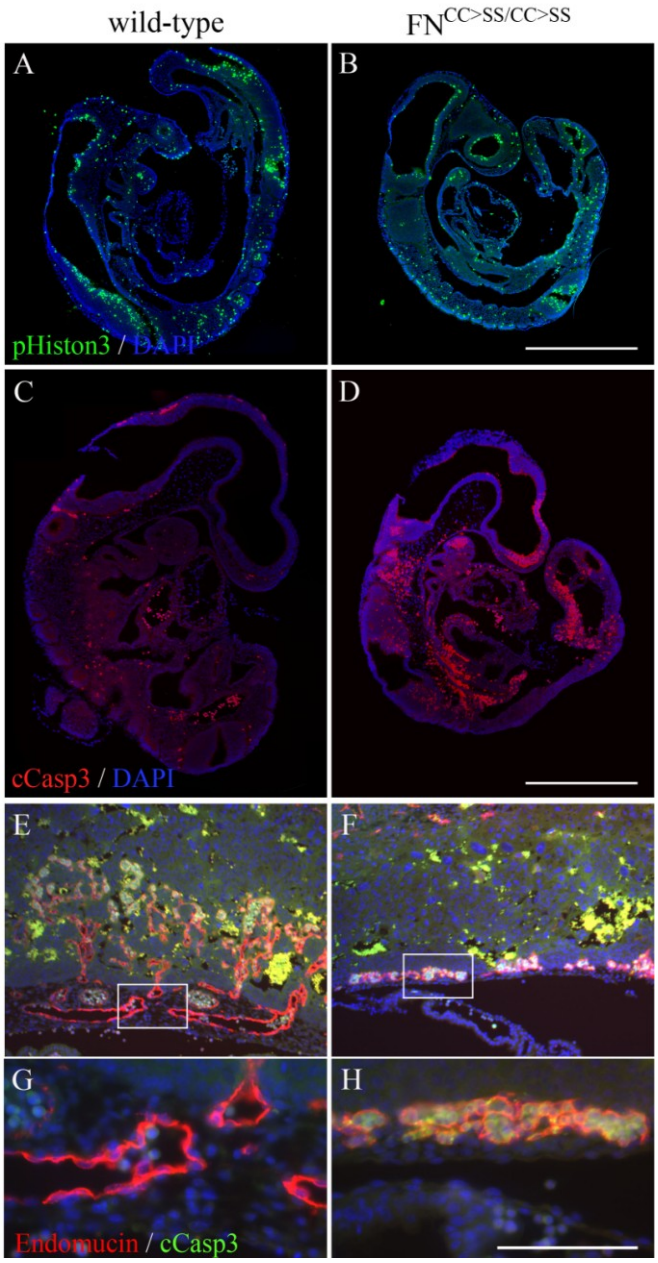

Fig 3.23. ***Analysis of cell proliferation and apoptotic cell death in E9.5 embryos***. ***A and B***. *Analysis of the cell proliferation marker phospho-histone-3 revealed no notable difference between* $FN^{CC>SS/CC>SS}$ *and wild-type embryos.* ***C and D***. *Cleaved caspase-3 staining on sections of E9.5 embryos revealed massive apoptosis in the posterior trunk region of* $FN^{CC>SS/CC>SS}$ *embryos as compared to very few apoptotic cells in the wild-type control embryo.* ***E and F***. *Analysis of apoptosis in the chorioallantoic region of E10.5 placenta sections. Note that mutant allantoic blood vessels (stained in red with the endothelial marker endomucin) derived from extra-embryonic tissue display markedly enhanced apoptotic cell-death. The boxed areas - shown with higher magnification in* ***G and H -*** *show that mutant endothelial cells (red) of the extra-embryonic tissue are in particular affected by apoptotic cell-death (green). Scale bars: (B and D) 500 µm; (H) 100 µm.*

3.2.4 Monomeric FN is expressed and assembled into a fibrillar matrix-network

According to the current model for the mechanism of FN fibrillogenesis, dimerization of FN is regarded as a prerequisite for the assembly of a fibrillar matrix (Wierzbicka-Patynowski and Schwarzbauer 2003). Therefore, disruption of the dimer was expected to result in abrogation of FN fibril assembly. However, embryos exclusively expressing monomeric FN developed further than FN knock out mice, suggesting that monomeric FN was at least partially assembled into a functional network. To test this hypothesis, histological analyses of embryo sections and Western blot analyses of whole embryo lysates were performed to detect the amount and distribution of FN. FN immunofluorescence staining of parasagittal paraffin-sections from PFA fixed E9.5 $FN^{CC>SS/CC>SS}$ embryos revealed a strong FN-monomer deposition surrounding the somite blocks, nervous tissue and the large vessels, resembling the expression pattern in control embryos (Fig 3.24.A, bottom). Similar immunosignal intensities implied comparable expression levels of FN in $FN^{CC>SS/CC>SS}$ embryos and control littermates. To confirm this data, a comparative Western blot analysis for FN of whole embryo lysates was performed which revealed similar FN levels expressed in mutant embryos and wild-type controls (Fig 3.24.B). The finding of apparently normal levels of FN-monomer deposition raised the question, whether the chemical properties in terms of intermolecular cross-linking resembled those of a dimeric FN matrix in the control embryos. To address this question, FN derived from embryo lysates was extracted with the mild detergent deoxycholate (DOC). This procedure allows the separation of the FN matrix into two fractions; a DOC-soluble fraction of recently assembled FN, which is cross-linked to a lesser extent, and a DOC-insoluble fraction, represented by the mature and highly cross-linked proportion of the FN matrix (Sechler, Takada et al. 1996). Western blot analysis of DOC-fractions derived from mutant embryos and wild-type controls showed comparable amounts of FN in both fractions. This data indicated that FN-monomer - despite the lacking disulfide bonds - becomes normally deposited and cross-linked after secretion into the extra-cellular space.

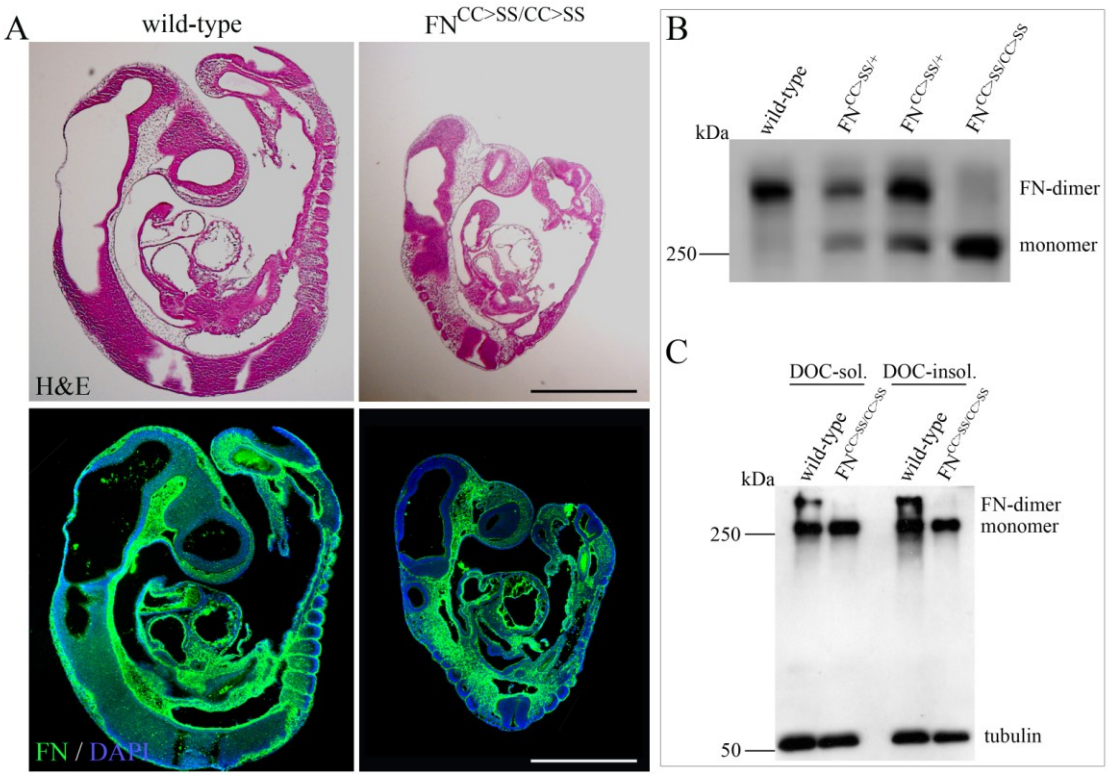

Fig 3.24. ***FN-monomer expression and deposition in FN$^{CC>SS/CC>SS}$ embryos****. **A**. Sagittal paraffin sections of E9.5 embryos stained with hematoxylin-eosin (H&E, top) and an antibody against FN (bottom). FN$^{CC>SS/CC>SS}$ embryos are notably smaller than their wild-type littermates but express and deposit comparable levels of FN. **B**. Western blot of whole E8.5 embryo lysates shows similar amounts of FN expressed in wild-type and FN$^{CC>SS/CC>SS}$ littermates. **C**. Deoxycholate fractionations of FN derived from E9.5 embryos. Comparable amounts of FN in both, DOC-soluble and DOC-insoluble fractions derived from wild-type and FN$^{CC>SS/CC>SS}$ embryos indicate that FN-monomer is normally deposited and cross-linked. Scale bars: 500 µm*

To further analyse whether assembled FN-monomer effectively formed fibrils, immunofluorescence images of embryo sections stained with antibodies against FN were taken at higher magnifications. Closer examination of deposited FN on paraffin fixed E9.5 embryo sections revealed a similar morphology of the monomeric FN matrix-network in FN$^{CC>SS/CC>SS}$ embryos as compared to FN networks in their wild-type littermates (Fig 3.25.A, B). A fine, ramified FN meshwork was visible within the developing head-mesenchyme (Fig 3.25.C, D), as well as in the heart (Fig 3.25.E, F), somites, trunk mesenchyme and tail bud mesoderm. To rule out the possibility that the observed FN-monomer fibrils represent artefacts generated by PFA mediated cross-linking during fixation, unfixed cryo-sections derived from E9.5 embryos were immunostained for FN. In line with the previous findings, this staining on native sections confirmed the presence of comparable amounts of normally distributed, delicate FN fibrils in FN$^{CC>SS/CC>SS}$ embryos (Fig 3.25.E, F).

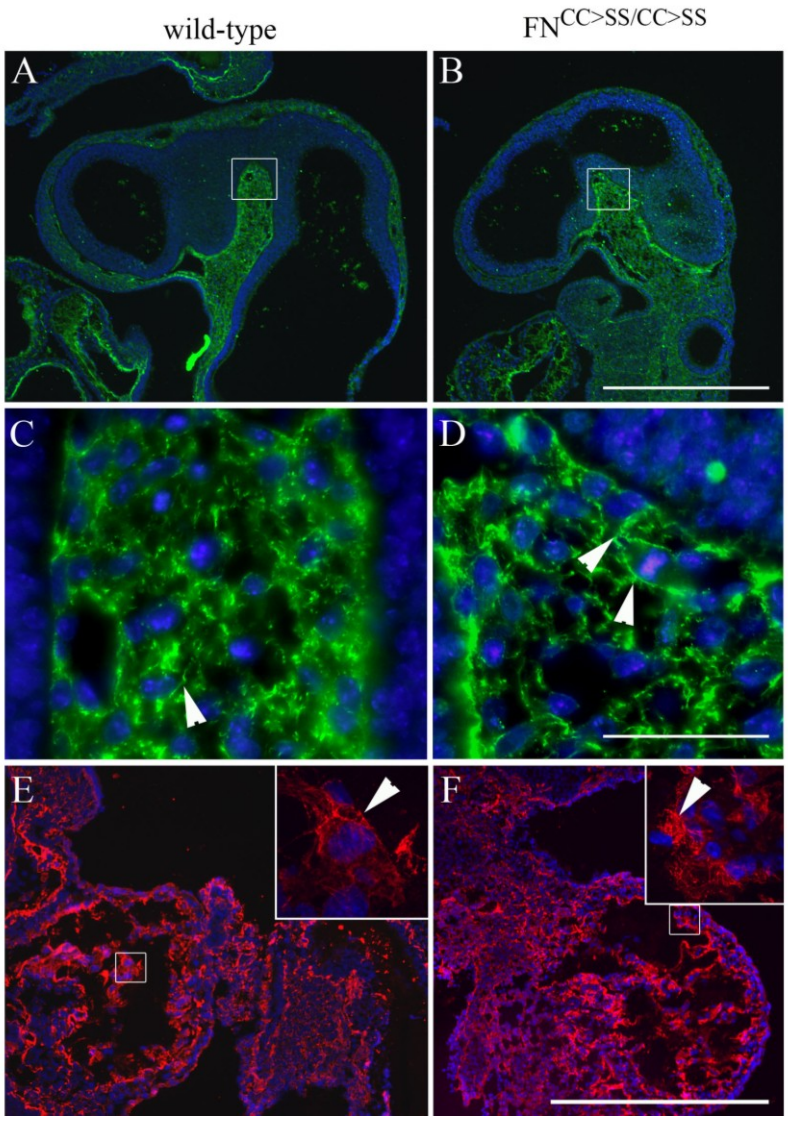

Fig 3.25. ***Fibrillar FN-monomer meshwork in FN$^{CC>SS/CC>SS}$ embryos****. **A and B**. PFA fixed paraffin sections of E9.5 embryos were stained for FN. Boxed areas in the head-mesenchyme were imaged at higher magnification.* ***C and D****. Higher magnification image of the head-mesenchyme: FN is deposited in similar density, comparable FN fibril-shape and thickness in wild-type and FN$^{CC>SS/CC>SS}$ embryos.* ***E and F****. Native cryo-sections of unfixed E9.5 embryos were stained for FN. Note that similar amounts of FN are deposited in FN$^{CC>SS/CC>SS}$ and control embryos. Higher magnification image of the heart (inset) shows similar FN fibril-thickness and ramifications in the heart ventricle of wild-type and FN$^{CC>SS/CC>SS}$ embryos. Scale bars: (B, F) 500 µm, (D) 50 µm.*

3.2.5 FN$^{CC>SS/CC>SS}$ cells assemble a morphologically distinct FN-monomer matrix *in vitro*

The data above demonstrates normal expression, assembly and chemical properties of monomeric FN in FN$^{CC>SS/CC>SS}$ embryos. Therefore, the reasons for the early embryonic lethality of FN$^{CC>SS/CC>SS}$ mice must be attributed to impaired functionality

of the FN-monomer matrix. In order to facilitate more detailed *in vitro* examinations of the FN-monomer matrix properties, fibroblast-like cell lines were established from E9.5 embryos. Clonal mutant and wild-type cell lines, which showed similar cell surface expression levels of α2, α5, α6, αv, α4, β1 and β3 integrin by FACS analysis, were chosen for further analysis (Fig 3.26.A). The chosen clones lacked α4 integrin expression in order to exclude a potential contribution of this particular integrin to FN matrix assembly *in vitro* (Fig 3.26.A). To test the functionality of FN binding integrins on the surface of $FN^{CC>SS/CC>SS}$ clones, labelled wild-type plasma FN (pFN) was added to the cells in serum replacement medium. Immunofluorescence imaging of $FN^{CC>SS/CC>SS}$ cells stained with antibodies against α5 integrin and FN revealed that the mutant cells were capable to assemble normal FN into a fibrillar network. FN aligned with α5 integrins in fibrillar adhesions, confirming that FN binding integrins on the cell surface were fully functional (Fig 3.26.B).

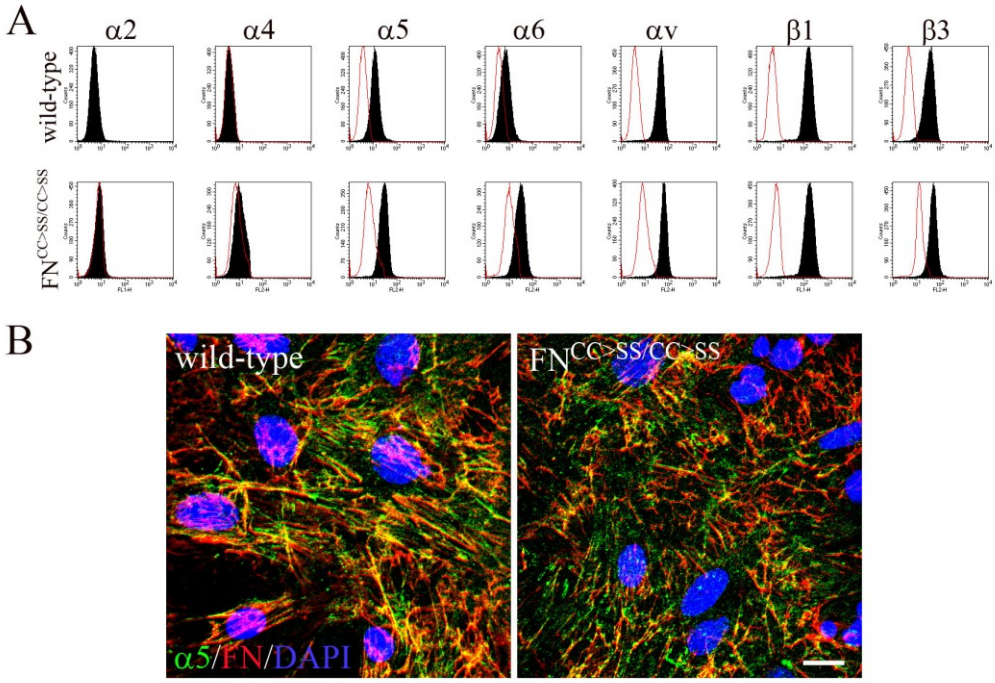

Fig 3.26. ***$FN^{CC>SS/CC>SS}$ cell surface integrin expression profile and plasma FN assembly assay***. ***A***. *Integrin expression profile of a selected wild-type and $FN^{CC>SS/CC>SS}$ clone determined by FACS. Cell lines were incubated with antibodies to α2, α4, α5, αv, α6, β1 and β3 integrin subunits (blue histogram). Note that α5, αv, β1 and β3 integrins are expressed at comparable levels, while both clones lack α4 integrins. (Isotype controls are depicted in black).* ***B***. *Wild-type and $FN^{CC>SS/CC>SS}$ cells cultured in presence of exogenous plasma FN (60 nM). Note that $FN^{CC>SS/CC>SS}$ cells are equally capable to assemble exogenous pFN as the control cells. Scale Bar: 15 μm*

In vitro FN assembly assays provide the opportunity to study the kinetics of initiation and completion of FN fibril formation. They facilitate the detection of delays and variations in early fibril formation which might affect the development of the embryo

but are impossible to observe *in vivo*. To determine (i) whether the $FN^{CC>SS/CC>SS}$ cell line was capable to assemble endogenously produced FN-monomer into fibrils; (ii) whether the kinetics of the assembly process were comparable between wild-type and mutant cells; and (iii) which sort of integrin heterodimer was required for the FN-monomer assembly, cells were seeded either on laminin 1 (LM111) or vitronectin (VN) and were cultured for indicated lengths of time in serum-replacement medium. As previously mentioned (3.1.4), cells preferentially adhere to VN via their αvβ3 integrins and to LM111 via their α6β1 integrins. Only the latter integrin does not bind to FN and thus should not affect the FN assembly process. In contrast, adhesion of cells on VN should result in depletion of FN binding αvβ3 integrins from the apical cell surface, leaving only α5β1 integrins available to participate in FN matrix assembly (Fath, Edgell et al. 1989). $FN^{CC>SS/CC>SS}$ cells were found to initiate and complete the assembly of a dense FN-monomer network equally well on both substrates, indicating that α5β1 integrin alone was sufficient to facilitate the assembly of a FN-monomer matrix. While both cell lines showed similar kinetics of fibril formation, a clear difference in matrix morphology was evident between the FN networks on control and $FN^{CC>SS/CC>SS}$ cells. In contrast to the long and ramified fibrils produced by the control cells (Fig 3.27.A, B, top), FN-monomer fibrils were more numerous, appeared to be thinner and shorter with only few ramifications (Fig 3.27.A, B, bottom) Unfortunately, it was not possible to test whether the distinct morphology of the FN-monomer matrix was caused by a time delay in fibril formation, since the postconfluent cells tended to detach during the prolonged incubation times necessary to answer this question.

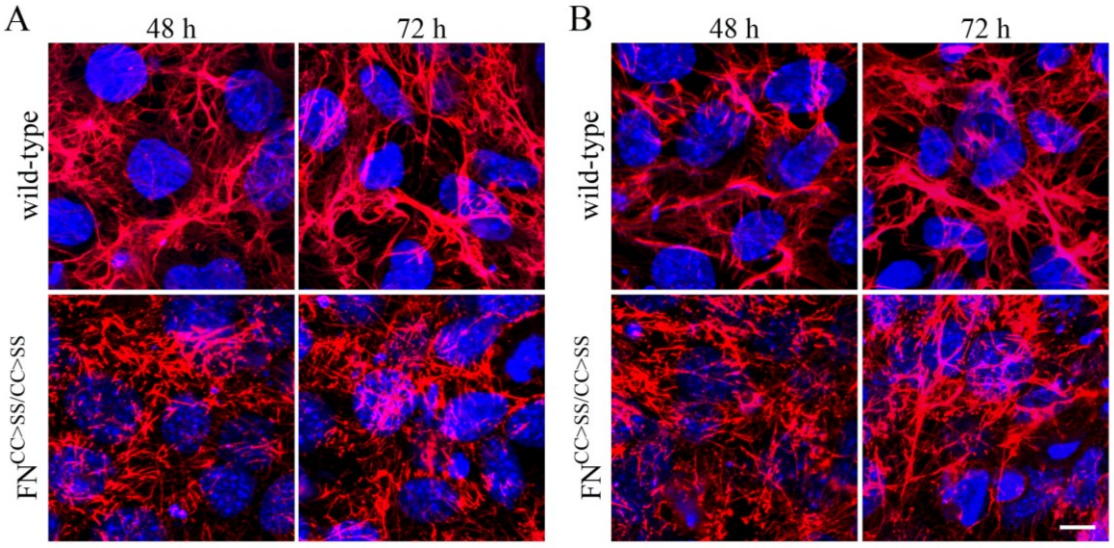

Fig 3.27. ***FN-monomer assembly kinetics on LM111 and VN. A and B****. Wild-type and* $FN^{CC>SS/CC>SS}$ *cells grown in serum replacement medium and either plated on LM111 (A) or VN (B). Cells were fixed after 48 and 72 h and stained for FN (red, DAPI stained cell-nuclei are depicted in blue). Note that* $FN^{CC>SS/CC>SS}$ *cells are capable to assemble FN-monomer on both substrates, but the fibrils appear shorter and thinner (A and B, bottom) as compared to fibrils on wild-type cells (A and B, top). Scale bar: 15 µm*

3.2.6 FN-monomer leads to altered α5β1 integrin distribution but largely unaffected "outside-in" signaling

Among all FN binding integrins, α5β1 is one of the most important cell surface receptors to initiate and complete FN fibril formation. FN aligned α5β1 integrins are trans-locating along actin stress fibers forming fibrillar adhesions (Geiger, Bershadsky et al. 2001). The movement of α5β1 integrins induces the stretching of FN fibers on the cell surface which facilitates the exposure of additional cryptic binding sites on FN. These binding sites in turn allow interactions with a variety of other ECM components. The comparably thin and short morphology of FN-monomer fibrils observed on $FN^{CC>SS/CC>SS}$ cells suggested that FN aligned α5β1 integrins might be differently clustered when assembling monomeric FN. To test whether this was the case, $FN^{CC>SS/CC>SS}$ and wild-type control cells grown on LM 111 and in serum-replacement medium were fixed and stained with antibodies against the α5 integrin subunit and FN. Fluorescently labelled phalloidin was used to facilitate the detection of cytoskeletal F-actin, along which fibrillar adhesion structures form. As demonstrated in Fig 3.28, wild-type cells showed elongated, streak-like fibrillar adhesions in which long FN fibrils were aligned with α5β1 integrins and F-actin (Fig 3.28.top). In contrast, fibrillar adhesions on $FN^{CC>SS/CC>SS}$ cells were markedly shorter with accordingly shortened FN-monomer fibrils (Fig 3.28.bottom).

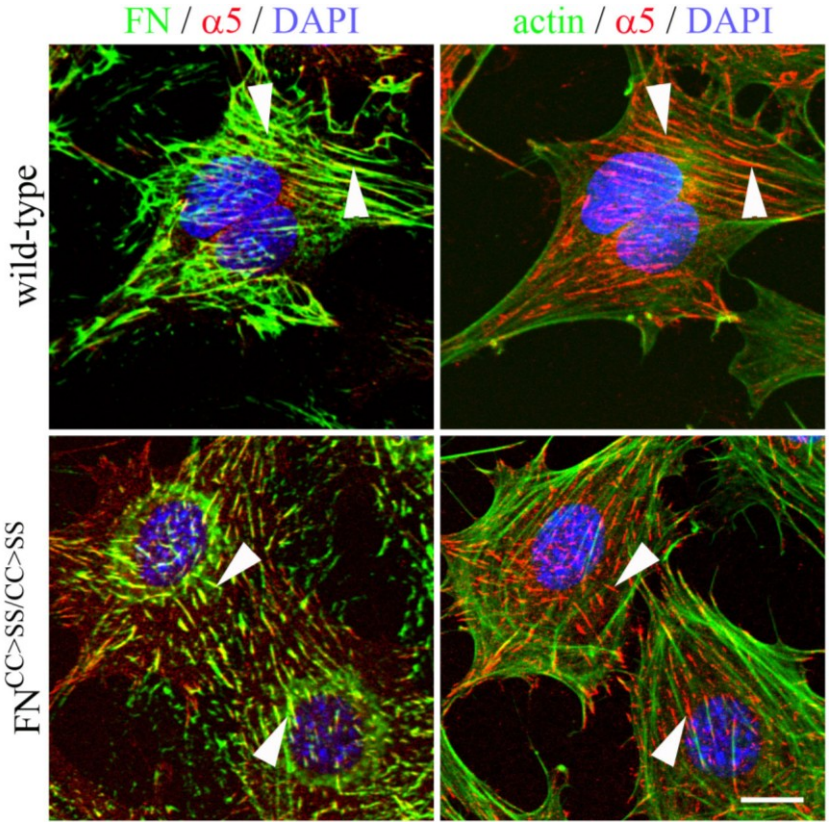

Fig 3.28. ***Altered morphology of fibrillar adhesions on $FN^{CC>SS/CC>SS}$ cells*** *. Distribution of α5 integrin, F-actin and FN fibers in wild-type and $FN^{CC>SS/CC>SS}$ cells cultured for 18 h on LM111 and in serum-replacement medium. Note that F-actin, α5β1 integrin and FN co-localize in*

elongated fibrillar adhesions of wild-type cells (white arrowheads, top), whereas fibrillar adhesions on $FN^{CC>SS/CC>SS}$ cells (white arrowheads, bottom) are reduced in length which presumably causes the shortened morphology of FN-monomer fibers. Scale bar: 15 µm.

The activated and ligand-bound integrins clustered in fibrillar adhesions are able to transmit a vast array of intracellular changes referred to as "outside-in" signaling via the recruitment of intra-cellular signaling complexes. Previous studies have shown that FN-bound active α5β1 integrin triggers "outside-in" signals required for early vasculogenesis and angiogenesis processes (Francis, Goh et al. 2002). The abnormal vascular development observed in $FN^{CC>SS/CC>SS}$ mice and the comparably short streaks of α5β1 integrins clustered in fibrillar adhesions on $FN^{CC>SS/CC>SS}$ cells suggested that α5β1 integrin mediated "outside-in" signaling may be affected in mutant mice. To test this hypothesis, a biochemical analysis of selected signaling molecules which act downstream of α5β1 integrin was performed using an *in vitro* cell culture assay. In most situations *in vivo*, however, "outside-in" signaling is triggered through integrin interactions with components of a three-dimensional (3D) extracellular matrix network. In order to mimic the 3D extracellular environment of cells *in vivo*, mutant and wild-type 3D networks were generated in cell culture (Fig 3.29.A) (2.7.4) (Mao and Schwarzbauer 2005). FN-null cells were seeded into these matrices and the levels and phosphorylation states of two important downstream effectors of α5β1 integrin, the focal adhesion kinase (FAK) and the extracellular signal related kinases 1&2 (ERK1/2), were analysed.

FAK plays a central role in cell migration and proliferation and has been shown to function as an early mediator of integrin-mediated signaling. Its activity is regulated in response to integrin engagement by phosphorylation at multiple tyrosine and serine residues (Abedi and Zachary 1997). A recent study reported that number and bond-strength of α5β1-FN interactions correlate with levels of FAK specifically phosphorylated at tyrosine residue Y397 (Shi and Boettiger 2003). Further, it was shown that increased matrix stiffness results in increased resistance to integrin mediated pulling forces generated by the cytoskeleton. The emerging tension between extracellular matrix and cytoskeleton controls the mechanical, switch-like activation of α5β1 tethered to FN, which in turn regulates the phosphorylation of FAK Y397 (Friedland, Lee et al. 2009). For this reason, semi-quantitative analysis of FAK Y397 phosphorylation levels provides information about number and strength of FN-α5β1 interactions and an indirect measure for matrix stiffness.

ERK is a member of the mitogen-activated protein kinase family and has been shown to promote cell growth and cell cycle progression. The initial ERK activation is largely dependent on growth-factor signaling, whereas elevated levels of active ERK require signals triggered by integrin mediated cell adhesion, implicating activated FAK as an intermediate effector (Hughes, Renshaw et al. 1997; Giancotti and Ruoslahti 1999; Danen and Yamada 2001). In order to perform a biochemical analysis of integrin "outside-in" signaling on 3D matrices, a FN knock out cell line was used (Sakai,

Johnson et al. 2001). This cell line offered two advantages; firstly, FN knock out cells would not deposit endogenous FN into the 3D matrix during the assay, and secondly, results obtained from assays on wild-type and FN-monomer 3D matrix could be readily compared when one and the same cell line is used. Prior to the experiment, the cells were starved in serum-free medium for several hours and subsequently incubated in suspension for an additional hour. Starving and suspension culture leads to inactivation of cell adhesion dependent kinases. Subsequently, the cells were seeded on the mutant and wild-type 3D matrices and incubated for indicated periods of time to allow integrin signaling to occur. Western blot analysis of the cell lysates probed with site-specific anti-phospho antibodies against pERK1/2 (Thr 202/Tyr 204) revealed similar activation kinetics and comparable levels of phospho-ERK in cells plated on wild-type and FN-monomer 3D matrices (Fig 3.29.B). This result indicated that the FN-monomer mutation did not affect ERK1/2. Immunoblotting with anti-pFAKY397 antibodies showed slightly reduced levels of pFAKY397 on FN-monomer 3D matrices as compared to the control fibrilar network (Fig 3.29.B). This finding suggests that the monomeric FN matrix differs from control fibrils with regard to its mechanical pliability and the number and bond-strength of α5β1-FN interactions. However, it is unclear to which extent these rather subtle changes in "outside-in" signaling contribute to the severe defects observed in $FN^{CC>SS/CC>SS}$ mice and therefore suggest that changes in other signaling pathways may be primarily responsible for the $FN^{CC>SS/CC>SS}$ phenotype.

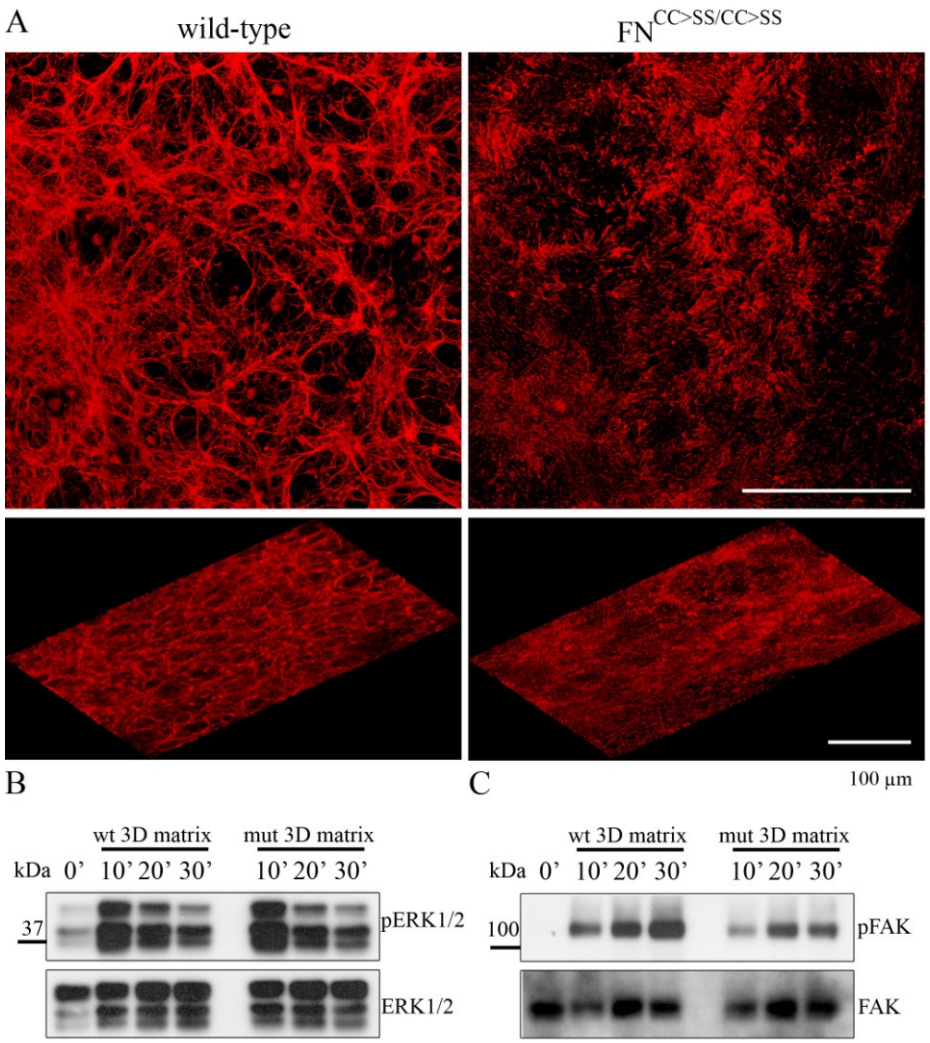

Fig 3.29. ***Biochemical analysis of "outside-in" signaling on FN 3D matrices****. (**A, top**). Confocal stack image of cell free FN 3D matrices, stained with antibodies against FN. Confluent layers of wild-type and FN$^{CC>SS/CC>SS}$ cells were grown on gelatine for 5 days in serum-replacement medium to allow endogenous FN-derived matrix assembly to occur.* ***(A, bottom)****. Subsequently, the cells were lysed and cell remnants were washed out, leaving a ~ 6 - 10 µm thick layer of 3D extracellular matrix behind. Note that the morphology of the FN-monomer matrix differs markedly from the wild-type matrix.* ***(A and B).*** *Western blot analysis of selected signaling molecules activated by integrin mediated cell adhesion.* ***B****. ERK1/2 (p44/42 MAPK) activation on 3D matrices. The immunoblot was probed with site-specific anti-phospho-ERK1/2 antibodies. Note that cells on both matrices exhibit a comparable pERK1/2 profile (B, top). Reprobing with anti-ERK1/2 antibodies revealed equal protein loading per each lane (B, bottom).* ***C****. Determinatining integrin-dependent FAK activation using anti-Y397-FAK antibodies. Cells on FN-monomer matrices exhibited a slightly reduced amount of pFAK Y397 as compared to cells on the control matrix (C, top). Reprobing with anti-FAK antibodies revealed equal protein loading per each lane (C, bottom). Scale bar: 100 µm*

3.2.7 Monomeric FN matrices fail to deposit latent TGF-β *in vitro*

An interesting feature of all $FN^{CC>SS/CC>SS}$ embryos is that the severely defective vascular development resembles the abnormalities reported in mice with compromised transforming growth factor-β (TGF-β) signaling (Dickson, Martin et al. 1995; Oshima, Oshima et al. 1996; Goumans, Zwijsen et al. 1999; Oh, Seki et al. 2000; Larsson, Goumans et al. 2001). Growth factor binding to the ECM is a major mechanism for regulation of growth factor activity and plays a crucial role in tissue morphogenesis and repair (Taipale and Keski-Oja 1997). FN has been shown to store latent TGF-β secreted by fibroblasts (Dallas, Sivakumar et al. 2005). TGF-βs are deposited as inactive complexes containing the TGF-β, its propetide, the so called latency-associated protein (LAP) and the latent TGF-β binding proteins (LTBP-1, -4). The LTBPs are playing a functional role in the integrin dependent activation of latent TGF-β, since LTBPs are tightly anchored to FN (Annes, Rifkin et al. 2002). How LTBPs are incorporated into the FN matrix is still unknown (Chen, Sivakumar et al. 2007). This raised the question, whether the monomeric FN matrix fails to assemble FN-LTBP-complexes, which in turn affects TGF-β signaling. To address this question, I first investigated how LTBP-1 is distributed in the control and mutant FN matrix. To this end, cells were grown on LM111 in serum-replacement medium for 3, 4 and 5 days. The cells were subsequently fixed and immunostained with anti-FN and anti-LTBP-1 antibodies. A distinct network of fibrilar LTBP-1 was already visible on the control cells after 3 days, which became more pronounced after 4 and 5 days, respectively (Fig 3.30.A). Shape and co-distribution of FN fibers and LTBP-1 indicated that FN served as a scaffold for initial LTBP-1 fibril formation (Koli, Hyytiainen et al. 2005). In sharp contrast, $FN^{CC>SS/CC>SS}$ cells largely failed to deposit LTBP-1. Hardly any fibrilar LTBP-1 was visible on cells after 3 days. Even after 5 days only few and short LTBP-1 fibrils were deposited on the FN-monomer matrix (Fig 3.30.A). In order to compare the total amounts of LTBP-1 secreted by $FN^{CC>SS/CC>SS}$ and control cells, a Western blot analysis of ECM derived LTBP-1 levels after plasmin-release was performed (2.7.3.2). It revealed slightly reduced amounts of LTBP-1 in the ECM of two $FN^{CC>SS/CC>SS}$ clones as compared to the control cells (Fig 3.30.B). This finding suggests that non-incorporated LTBP-1 was either degraded or released into the medium. The latter hypothesis was confirmed by immunoblotting showing increased amounts of LTBP-1 in conditioned medium of $FN^{CC>SS/CC>SS}$ cells (Fig 3.30.C). To analyse the amount of LTBP-1 cross-linked to the matrix *in vivo*, DOC-insoluble fractions derived from E9.5 embryos were plasmin digested and the amount of released LTBP-1 was determined by immunoblotting. Comparable amounts of deposited LTBP-1 in both, mutant and control embryos were detected (Fig 3.30.D).

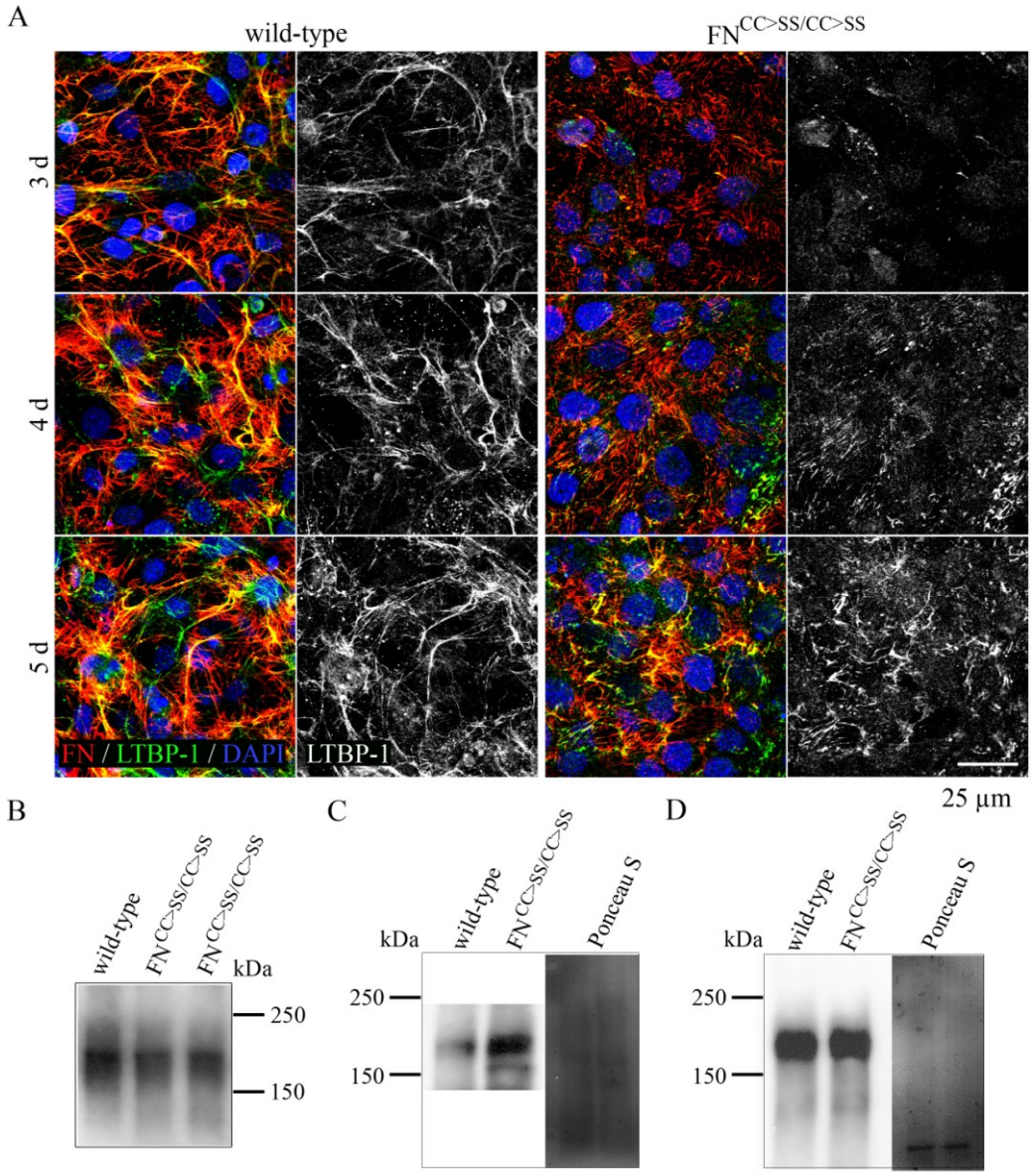

Fig 3.30. ***Impaired deposition of LTBP-1 on FN-monomer matrices****.* ***A****. Time course of FN and LTBP-1 assembly on cells plated on LM111 and cultured in serum-replacement medium. Note that* $FN^{CC>SS/CC>SS}$ *cells fail to properly assemble fibrillar LTBP-1.* ***B****. Western blot analysis of LTBP-1 levels reveals decreased amounts deposited in the ECM of* $FN^{CC>SS/CC>SS}$ *cells.* ***C****. Impaired deposition of LTBP-1 by mutant cells leads to increased amounts of unbound LTBP-1 in conditioned medium.* ***D****. Analysis of LTBP-1 deposition in the ECM of E9.5 embryos. Note that the amount of ECM-cross-linked LTBP-1 is similar in mutant and control embryos. Scale bar: 25 µm*

These *in vivo* findings are contradictory to the results *in vitro*. However, the *in vitro* assays demonstrate the kinetics of FN facilitated LTBP assembly, whereas the *in vivo* result merely represents a snap-shot. Since the development of a complex organism requires a tightly timed control of ongoing processes, it is conceivable that small delays might cause major defects. To further examine possible implications of altered TGF-β

signaling in $FN^{CC>SS/CC>SS}$ mice, analyses of TGF-β downstream effectors were performed.

3.2.8 Impaired deposition of LTBP-1 results in increased activation of TGF-β

A recent study reports that ECM displaced LTBP results in increased activation of TGF-β (Chaudhry, Cain et al. 2007). The increased amounts of latent TGF-β in the conditioned medium of $FN^{CC>SS/CC>SS}$ cells suggested that elevated levels of active TGF-β were present. To check whether this was indeed the case, the activation status of TGF-β downstream effectors was tested by means of Western blot analysis. Smad proteins transmit TGF-β signals from the cell-surface into the nucleus. Receptor-regulated (R-Smads) Smads 2 and 3 are specifically phosphorylated in response to TGF-β receptor I & II activation. Upon phosphorylation, they associate with the so called common mediator (co-Smad) Smad 4 and translocate into the nucleus to facilitate the transcriptional activation of TGF-β target genes. Immunoblotting for pSmad 2/3 in nuclear fractions of cells after 3 and 5 days in culture revealed increased levels of phosphorylated Smad 2 and 3 in the nuclei of $FN^{CC>SS/CC>SS}$ cells compared to control cells (Fig 3.31.A). This data could be confirmed by immunodetection of correspondingly enhanced nuclear translocation of Smad 4 into nuclei of mutant cells (Fig 3.31.A). To address whether this altered signaling could also be detected *in vivo*, a Western blot analysis of pSmad2/3 levels in E9.5 embryonic and extra-embryonic tissue was performed. It revealed elevated levels of pSmad 2/3 in yolk sacs (Fig. 3.31.B) and $FN^{CC>SS/CC>SS}$ embryo proper (Fig. 3.31.C), confirming that the mutation increased TGF-β signaling both *in vitro* and *in vivo*. The previous *in vitro* experiments corroborated the notion that impaired deposition of LTBP-1 by $FN^{CC>SS/CC>SS}$ cells resulted in enhanced levels of active TGF-β in conditioned medium. To test the significance of this finding, an active TGF-β reporter assay was performed to exactly measure the amount of active TGF-β present in conditioned medium of $FN^{CC>SS/CC>SS}$ and control cells. To this end, conditioned medium from control and $FN^{CC>SS/CC>SS}$ cells was collected after indicated days in culture and added on top of Mink lung epithelial cells (MLECs) stably transfected with an expression construct containing a TGF-β sensitive promotor fused to the firefly luciferase reporter gene. Levels of active TGF-β were found to be significantly higher in conditioned medium of $FN^{CC>SS/CC>SS}$ cells compared to medium from control cells (Fig 3.31.D). In agreement with the results of previous studies, a decrease of active TGF-β amounts in conditioned medium during extended culture (3, 4 and 5 days) was observed (Koli, Hyytiainen et al. 2005) in both cell lines. To test the specificity of the assay, a control experiment utilizing the specific TGF-β receptor I inhibitor SB 431542 was performed in parallel, which resulted in the expected inhibition of TGF-β induced luciferase expression (Fig 3.31.E).

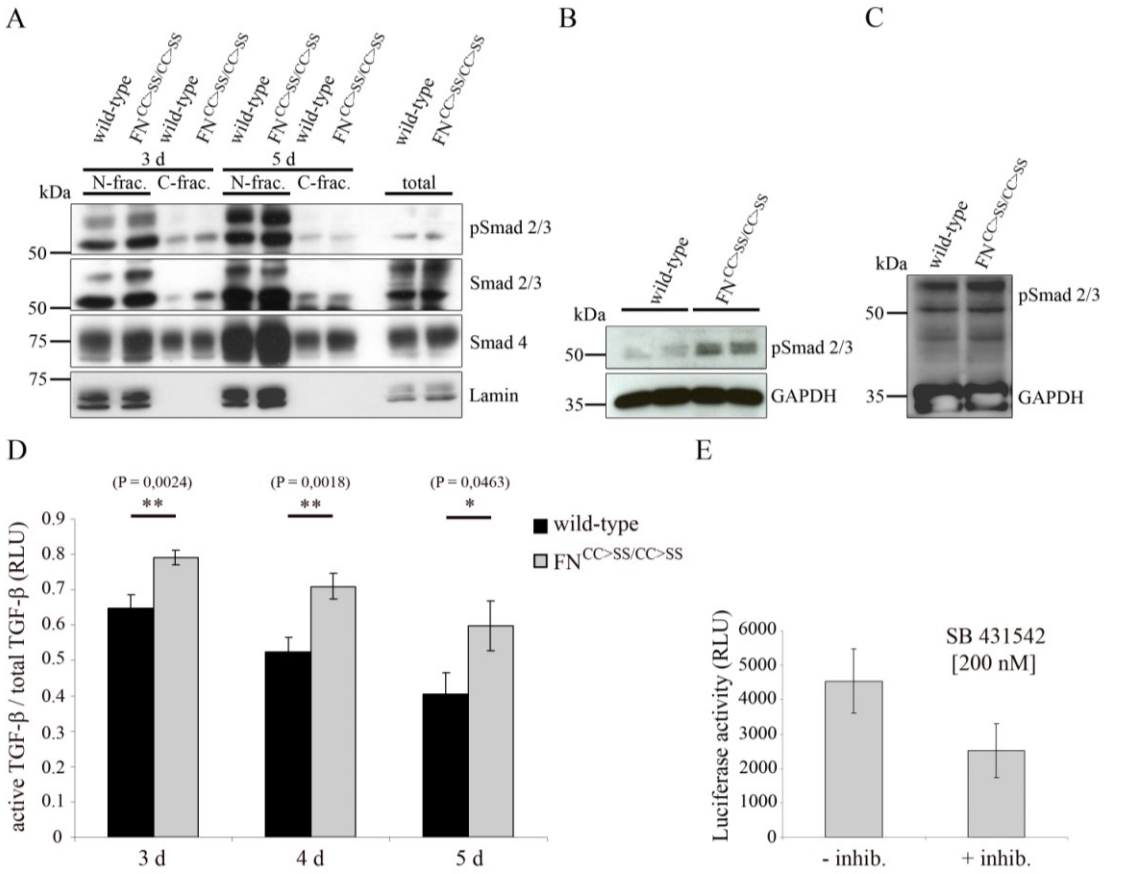

Fig 3.31. ***Analysis of TGF-β signaling in vitro and in vivo****.* ***A****. Nuclear fractions of* $FN^{CC>SS/CC>SS}$ *and control cells after 3 and 5 days in culture.* ***A****. Immunoblot analysis for nuclear translocation of pSmad 2/3 and Smad 4. (A, top) The immunoblot was probed with anti-phospho Smad 2/3 and anti-Smad 4 antibodies. Note that mutant cells exhibit an increased amount of pSmad 2/3 in the nuclei as compared to wild-type cells. (A, bottom) Enhanced levels of Smad 4 detected in the nuclei of* $FN^{CC>SS/CC>SS}$ *cells correspond with increased pSmad 2/3 levels. Reprobing with anti-Smad 2/3 and anti-Lamin A antibodies revealed equal protein loading per each lane. Equal expression of Smad protein levels in both cell lines was confirmed by immunoblotting of total cell lysates.* ***B****. TGF-β signaling in vivo. Levels of pSmad 2/3 in* $FN^{CC>SS/CC>SS}$ *yolk sacs are increased as compared to control yolk sacs.* ***C****. Comparison of pSmad 2/3 levels in whole embryo lysates at E9.5. Note the increased amounts of pSmad 2/3 in mutant embryos. (B and C) Reprobing with anti-GAPDH antibodies revealed equal protein loading per each lane.* ***D****. Luciferase based active TGF-β reporter assay. Conditioned medium of cells cultured for 3, 4 and 5 days was added to the reporter cell line and incubated for further 24 h prior to detection of TGF-β induced luciferase expression. Shown are ratios of active TGF-β in conditioned medium versus total ECM-bound TGF-β after its release into the medium by a 10 min heat-step at 80°C. Note that* $FN^{CC>SS/CC>SS}$ *cells fail to deposit latent TGF-β in their ECM, resulting in a significantly higher ratio of active versus total ECM-bound TGF-β.* ***E****. Specificity test to validate the reporter assay. Addition of the TGF-β receptor I inhibitor SB 431542 at 200 nM markedly reduced the TGF-β induced luciferase expression.*

The *in vivo* role of altered TGF-β signaling during development of $FN^{CC>SS/CC>SS}$ mice requires more detailed analyses in future. This tests should include *in utero* TGF-β inhibitor assays in $FN^{CC>SS/CC>SS}$ embryos. Through application of endothelial cells derived from mutant embryos in 3D gels, the effect of altered TGF-β signaling on angiogenesis will be tested. Furthermore, the mechanical activation of integrin dependent signaling in cells on FN 3D matrices and the phosphorylation levels of α5β1 integrin downstream effectors should be analysed in more depth.

4 Discussion

4.1 Mutational analysis of the RGD motif in FN

4.1.1 The RGD motif in FN is dispensable for fibril formation

The RGD binding motif in FN is thought to play a central role in FN matrix assembly and RGD-mediated integrin signaling. In the first part of the present study, this role was assessed by creating a non-functional RGE site in the FN gene of mice. The phenotype of the $FN^{RGE/RGE}$ mice is identical in type and quality to the defects reported for α5β1 integrin-deficient mice (Yang, Rayburn et al. 1993), but much less severe than the phenotype of FN-null or α5/αv integrin double-null mice (George, Georges-Labouesse et al. 1993; Yang, Bader et al. 1999). This finding allows drawing several important conclusions. First, the mesodermal defects caused by absent α5β1 expression are solely based on disruption of α5β1 integrin binding to the RGD motif of FN and do not involve binding to other α5β1 ligands (Collagen XVIII, ADAMs, etc.). Second, the development of a less severe phenotype in $FN^{RGE/RGE}$ mice than in α5/αv double-null mice indicates that αv integrin-FN interactions are either not required for early development or occur in an RGD-independent manner. Third, the direct observation of FN matrix in $FN^{RGE/RGE}$ mice shows that the RGD motif must be dispensable for the formation of a fibrillar FN network.

4.1.2 FN-RGE can assemble into a fibrillar network

A large number of integrins can bind FN (Pankov and Yamada 2002; Leiss, Beckmann et al. 2008). Although FN fibrillogenesis can still proceed in mice carrying single gene deletions of FN binding integrins, double deficiencies for α5 and αv integrin dramatically reduce the amount of FN matrix, suggesting that the two integrins bind, activate, and assemble FN fibrils independently of each other (Yang, Bader et al. 1999). Based on this mouse work and previous assembly studies performed *in vitro*, one would have predicted that a non-functional RGD motif in FN would abrogate binding to both α5β1 and αv integrins and hence render fibrillogenesis equally impossible as in α5/αv double-null mice. However, this was not the case. Neither quantitative nor qualitative differences in the FN network of $FN^{RGE/RGE}$ mice were found, irrespective of whether the embryo sections were treated with fixative or examined in native cryo-sections.

One reason for this unexpected finding could have been that the D>E mutation was too conservative and hence would still permit binding to integrins. Such a possibility, however, was ruled out experimentally: the assembly of FN-RGE by $FN^{RGE/RGE}$ cells grown on LM111 was inhibited by the addition of neither linear RGE peptides nor recombinant FN-$III_{7\text{-}10}$ fragments, in which the RGD was converted into an RGE.

Moreover, the same recombinant FN-III$_{7\text{-}10}$RGE fragment was unable to bind integrins in a highly sensitive solid-phase binding assay.

4.1.3 FN-RGE is assembled by αv integrins

FN assembly via the RGD motif can occur through either α5β1 or αv integrins. The αv integrin-mediated assembly, however, leads to a less dense network with shorter and thicker fibrils *in vitro* (Wennerberg, Lohikangas et al. 1996), which is thought to be due to the different subcellular localization and associated shape of αv versus α5β1 integrin clusters (α5β1 form thin fibrillar adhesions and αv arrowhead-like focal adhesions) and/or to the differential activation of small Rho GTPases such as RhoA, which occurs through FN binding to α5β1 but not to αv integrins (Danen, Sonneveld et al. 2000).

The FN-RGE fibrils of FN$^{RGE/RGE}$ cells displayed appearance and behaviour typical of αv-mediated fibrils: they were short and thick, whereas fibrils of wild-type cells were thin, long and ramified. Furthermore, the assembly of FN-RGE could be efficiently inhibited by *cyc*RGD, which was shown to bind with higher affinity to αvβ3 than to α5β1 integrin (Pfaff, Tangemann et al. 1994). The interpretation that αv integrins mediate FN-RGE assembly was further supported by siRNA-mediated depletion of the αv integrin protein in FN$^{RGE/RGE}$ cells, which showed that αv integrin-depleted cells were unable to form a fibrillar FN-RGE network. The role of αv integrins was further confirmed by direct binding assays, with recombinant fragments spanning almost the entire FN molecule, which revealed a novel high-affinity binding interaction for αvβ3 integrin and the N-terminal FN-I$_{1\text{-}9}$ fragment. Moreover, the assembly of FN-RGE by FN$^{RGE/RGE}$ cells was efficiently inhibited by FN-I$_{1\text{-}9}$ and synthetic peptides comprising the novel αvβ3 integrin binding site.

RGD-independent mechanisms for FN assembly have been observed with different cell culture systems. One report showed that binding of Mn^{2+} activated α4β1 integrin to the v-region can induce FN assembly *in vitro* (Sechler, Cumiskey et al. 2000). It is not clear, however, whether the α4β1-mediated mechanism also operates *in vivo* and, if so, whether its role is substantial during embryogenesis. In the E9.5 control and FN$^{RGE/RGE}$ embryos, we observed a very restricted expression of α4β1 in the cranial region and the developing epicard. Thus, the abundant FN-RGE fibrils in sites without α4β1 expressing cells must have been assembled using an α4β1-independent mechanism. This conclusion was further confirmed with FN$^{RGE/RGE}$ cell lines that lacked α4 integrin but still efficiently assembled FN-RGE fibrils.

A second RGD-independent FN assembly mechanism has been described for cells isolated from α5 integrin deficient mice (Sottile, Hocking et al. 2000). Incubation of FN-null cells grown in serum-replacement medium and on VN with recombinant FN lacking the RGD motif (FNΔRGD) assembled short stitch-like aggregates on the cell surface. A potential explanation for the development of the dot-like FNΔRGD aggregates could be that a view αvβ3 integrins failed to bind to the VN substrate and were available to recruit FNΔRGD to the cell surface by binding to the site in FN-I$_{1\text{-}9}$.

Alternatively, the recruitment and aggregation of FNΔRGD may have been accomplished by syndecans, which also bind FN. Potential syndecan-FNΔRGD interaction would also explain why heparin treatment inhibited the formation of the stitch-like aggregates on the surface of FN-null cells. The potential involvement of such interactions with FN-RGE was also tested in this study by treatment of $FN^{RGE/RGE}$ cells with heparin. Interestingly, heparin had no considerable effect on the assembly of FN-RGE fibrils, indicating that in the $FN^{RGE/RGE}$ system, proteoglycan binding to FN-RGE is not essential for FN fibril development.

4.1.4 The GNGRG motif in FN-I_5 is a novel αvβ3 binding site that can function for FN matrix assembly

The FN-I_{1-9} fragment (also called 70 kDa N-terminal fragment) inhibits FN assembly with efficiencies similar to RGD containing peptides. It is generally believed that the inhibitory effect of FN-I_{1-9} is caused by high-affinity binding sites for FN, which block the FN-FN interactions required to align and cross-link FNs into fibrils (McKeown-Longo and Mosher 1984; McDonald, Quade et al. 1987; Schwarzbauer 1991; Aguirre, McCormick et al. 1994; Hocking, Sottile et al. 1994; Sechler, Corbett et al. 1998). The fact that FN-RGE assembly could be inhibited with FN-I_{1-9} pointed to the possibility that FN-I_{1-9} may, in addition to its FN binding activity, contain a αv integrin binding site. This was confirmed in direct binding assays which revealed that FN-I_{1-9} bound αvβ3 integrin. Curnis et al. (2006) reported that the Asn-Gly-Arg (NGR) sequence of FN-I_5 could be converted to a high-affinity binding site for αvβ3 integrin through the deamidation and rearrangement of the asparagine residue and the creation of an *iso*DGR sequence. Isoaspartate formation is a well-known, non-enzymatic process that can occur during ageing of ECM proteins (David, Orpiszewski et al. 1998; Lanthier and Desrosiers 2004) and during isolation and storage of proteins (Paranandi, Guzzetta et al. 1994). The properties of the novel αvβ3 integrin binding sites in FN agreed with direct binding assay results, which showed that FN-I_{1-9} bound αvβ3 and offered a potential explanation for the αv integrin-dependent and FN-I_{1-9}-sensitive assembly of FN-RGE. Indeed, an *iso*DGR peptide was found to efficiently inhibit the binding of αvβ3 to FN-I_{1-9} in a direct binding assay, and it blocked the assembly of FN-RGE by $FN^{RGE/RGE}$ cells.

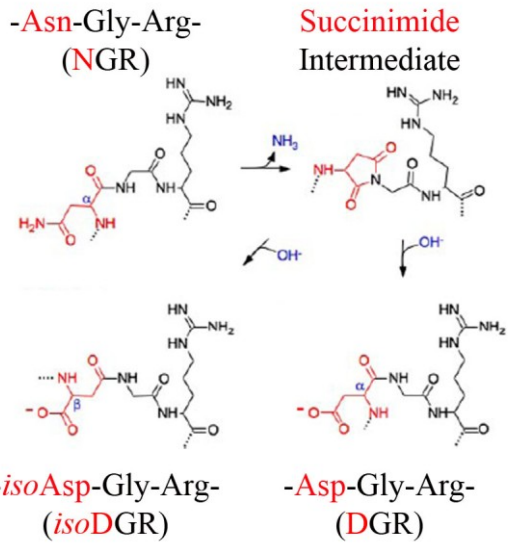

Fig 4.1. ***Schematic representation of the NGR deamidation reaction****. Asparagine deamidation occurs via hydrolysis of a succinimide intermediate, leading to formation of DGR and the biological active isoDGR (Modified from Curnis et al., 2006).*

Interestingly, the assembly of the FN-RGE matrix was equally inhibited by both, NGR-2C and *iso*DGR-2C peptides. This suggests that the native NGR sequence itself may already be able to bind αvβ3 and function for FN-RGE matrix assembly. It is more likely, however, that the NGR motif was sufficiently modified to *iso*DGR in culture to inhibit FN-RGE assembly. Supporting this hypothesis is the fact that NGR peptides failed to block αvβ3 integrin binding to the FN-I_5 module (Curnis, Longhi et al. 2006). Moreover, assembly of the FN-RGE matrix in both embryos and cell culture requires only a small fraction of *iso*DGR-modified FN molecules to bind cell surface integrins, whereas the remaining fractions becomes integrated into fibrils via FN-FN interactions, which proceeds independent of the *iso*DGR modification.

Interestingly, α5β1 integrin also bound the FN-$I_{1\text{-}9}$ fragment, but the *iso*DGR-2C peptide failed to inhibit this binding or assembly of wild-type FN. A likely explanation is that the interaction of α5β1 with FN-$I_{1\text{-}9}$ is weaker than the interaction of αvβ3 with the *iso*DGR motif in FN-I_5 and fails to provide a necessary binding strength to allow assembly of FN-RGE fibrils. Conversely, the findings in this study indicate that FN-$I_{1\text{-}9}$ inhibits FN assembly not only by affecting the FN-FN but also FN-αvβ3 integrin interactions, which has profound consequences for assembly of FN-RGE. Collectively, these results revealed, that the GNGRG loop (see Fig 4.1) in FN-I_5 represents a novel and functional αvβ3 integrin binding and FN assembly site. Future experiments will be necessary to test whether additional motifs in FN-$I_{1\text{-}9}$ can also provide functional integrin binding and FN assembly sites (Shpiro, Ellis et al. 2005).

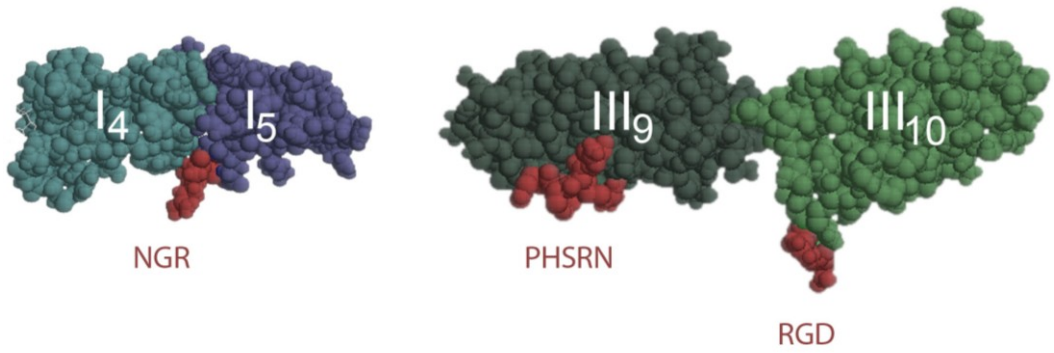

Fig 4.2. ***Schematic depiction of selected FN-domain structures****. Depicted in blue and cyan are the type I modules 4-5 and the NGR motif (shown in red). The type III modules 9-10 (coloured in green) harbouring the synergy site (PHSRN) and the RGD motif (both shown in red). Note that the proposed integrin binding GNGRG motif forms a exposed loop-like structure - comparable to the RGD loop in domain III_{10} - which is likely accessible to water and receptors (Modified from Leiss et al., 2008).*

4.1.5 The integrity of FN's RGD motif is essential for development

The $FN^{RGE/RGE}$ mice survive substantially longer than FN-null mice, indicating that FN-RGE fibrils are biologically active. $FN^{RGE/RGE}$ embryos display defects that are strikingly similar to those observed in α5-null mice (Yang, Rayburn et al. 1993), suggesting that high-affinity interactions of α5β1 with FN triggers unique functions during early development that can not be compensated by αv integrin-RGD, αv integrin-NGR or α5β1-FN-$I_{1\text{-}9}$ interactions. In both mouse mutants, the posterior trunk is shortened, underdeveloped and lacks somites. TUNEL assays and immunostaining for activated caspase-3 revealed diminished survival of posterior trunk mesoderm in $FN^{RGE/RGE}$ mice, suggesting that RGD triggered α5β1 integrin signals inhibit caspase-3 activation and anoikis.

A consistent feature of all $FN^{RGE/RGE}$ embryos analysed between E9.5 and E10.5 was that their somite number was limited to 12-13 somites. A plausible explanation for this finding could be that somites 12-13 represent the transition from the gastrulation- to tail-bud derived mesoderm (Wilson and Beddington 1996). This would indicate that the integrin-triggered survival signals are mainly required for the posterior trunk- and tail bud-derived mesoderm. Such a α5β1 integrin independency of the anterior, streak-derived mesoderm could be explained by expression and compensation of αv integrins. Unfortunately, it could not be tested in this study whether αv is high in the anterior and low or absent in the posterior mesoderm, because all available anti-αv antibodies produced only background staining.

Zebrafish also require α5 integrin for somite development along the body axis. In contrast to the mouse, *α5 integrin* mutant zebrafish display anterior somite defects, suggesting that α5 integrin is indispensable for anterior somitogenesis, whereas the

posterior somites developed normally (Julich, Geisler et al. 2005; Koshida, Kishimoto et al. 2005). Interestingly, knockdown of *fibronectin1* in *α5 integrin* mutant zebrafish, as well as knock down of *fibronectin1* and *fibronectin3*, led to a more severe phenotype, suggesting that the restriction of defects in zebrafish to the anterior somites is probably due to functional redundancy (Julich, Geisler et al. 2005; Koshida, Kishimoto et al. 2005). A further difference from the findings presented in this study is the absence of apoptosis in the anterior somites of α5 integrin-deficient zebrafish. It was even shown that the anterior somites develop perfectly well, but their boundaries can not be maintained because of the loss of FN fibrils that would normally surround somite boundaries. In about half of the $FN^{RGE/RGE}$ mouse embryos, normal amounts of FN-RGE fibrils were observed at the boundaries of the anterior somites, whereas in the remaining half, the levels were reduced (unpublished data).

In conclusion, this part of the thesis shows that FN-RGE can be assembled into fibrils *in vivo* and *in vitro* via αvβ3 binding to the *iso*DGR motif in FN-I_5. The *iso*DGR site in FN-I_5 is generated by NGR deamidation and, as previously demonstrated, can be readily reverted by the enzymatic action of the protein L-isoaspartyl methyl-transferase (Reissner and Aswad 2003; Lanthier and Desrosiers 2004). The ability of tissues to swiftly activate and deactivate binding of αvβ3 and likely other αv integrins to FN may represent a novel strategy to spatially and temporally trigger FN-mediated αv integrin signaling during development and disease.

4.2 Functional in vivo analysis of the dimerization motif in FN

It is widely accepted that the dimeric structure of FN is essential for the *de novo* formation of FN fibrils *in vitro* (Schwarzbauer 1991). However, it remained an open question whether this condition also applies to the *in vivo* situation. In the second part of this study, the role of the dimerization domain for FN fibrillogenesis and FN functions was tested *in vivo*. To this end, a mouse strain was generated that is exclusively expressing a monomeric form of FN. The mutation resulted in recessive embryonic lethality at around E11.0. The phenotype of $FN^{CC>SS/CC>SS}$ mice, however, was much less severe than the phenotype observed in FN-null mice which die at E8.5. Furthermore, unlike in FN-null and α5 integrin-null mice (George, Georges-Labouesse et al. 1993; Yang, Rayburn et al. 1993), $FN^{CC>SS/CC>SS}$ mice exhibit comparably mild defects in mesoderm-derived structures of the embryo proper. Surprisingly, the analysis of $FN^{CC>SS/CC>SS}$ mice further revealed, that FN-monomer was normally expressed and assembled into a fibrillar matrix. Several conclusions can be drawn from these observations. First, in contrast to the current model, the dimerization of FN is not required for FN fibril formation. Second, the moderate severity of defects observed in the embryonic mesoderm of $FN^{CC>SS/CC>SS}$ mice suggests that integrins interacting with the FN-monomer matrix are capable to trigger signals required for mesoderm development (e.g. somitogenesis in the posterior trunk region). Third, the embryonic lethality of $FN^{CC>SS/CC>SS}$ mice indicates that the FN-monomer matrix lacks functions

required for normal development. The impairment is likely compromising the scaffold function of FN necessary for assembling other ECM components.

4.2.1 FN-monomer can assemble into a fibrillar FN network *in vivo*

Almost two decades ago it was demonstrated in *in vitro* studies that the carboxy-terminal interchain bonds of FN, together with the N-terminal region (FN-I_{1-5}), are indispensable for FN fibrillogenesis and its incorporation into the ECM (Schwarzbauer 1991; Ichihara-Tanaka, Maeda et al. 1992). These observations led to the widely accepted concept that these two domains represent the minimal requirements for FN fibrillogenesis to occur. According to this concept, $FN^{CC>SS/CC>SS}$ mice should not be capable of assembling a FN matrix network, and consequently should display a similar phenotype as FN-null mice. However, this was not the case. Although the FN-monomer mutation resulted in early embryonic lethality, $FN^{CC>SS/CC>SS}$ mice developed beyond the stage at which FN-null embryos die, and their comparably moderate phenotype suggested that FN-monomer was assembled into an at least partially functional matrix network. Closer examination of native and fixed tissue sections of $FN^{CC>SS/CC>SS}$ embryos revealed that FN-monomer was assembled into a morphological normal matrix. Furthermore, no difference in terms of FN quantity or cross-linking biochemistry was detectable between mutants and control embryos. These findings showed that the FN-monomer mutation allows normal secretion of the protein, although FN monomers are disulfide-bonded into dimers in the lumen of the endoplasmic reticulum shortly after synthesis (Choi and Hynes 1979), and hence FN-monomer is passing the protein quality control system of the cell before secretion. The apparently normal FN-monomer fibril morphology observed *in vivo* in turn was clearly in disagreement with the dogma that FN's dimeric structure is essential for FN-fibrillogenesis (Schwarzbauer 1991). These findings further show that the N-terminal region (FN-I_{1-5}) of FN is the only fragment essential for FN fibril formation.

4.2.2 FN-monomer fibrils align with abnormal adhesive structures

The *de novo* generation of FN fibrils starts shortly after FN has bound integrins at sites of nascent focal adhesions. Acto-myosin contractile forces drive the translocation of FN-bound α5β1 integrins from the cell periphery towards the cell center. This movement applies tension to FN which promotes fibril formation through exposure of cryptic FN-self binding sites, and concurrently leads to formation of a new type of cell-matrix adhesion in which FN, α5β1 integrin and F-actin filaments co-align with multiple signaling molecules. This adhesive structure, called fibrillar adhesion, is characterized by a typical streak-like appearance. Finally, when cells interact with a 3D extracellular matrix, they form a more complex adhesion structure called 3D-adhesion. Both adhesive structures are implicated in ECM remodelling processes and multiple integrin-mediated signaling events (Pankov, Cukierman et al. 2000; Zamir, Katz et al. 2000; Ohashi, Kiehart et al. 2002). Cell interactions with a FN-rich 3D-matrix are

mediated primarily by α5β1 integrin and depend on matrix pliability, which results in FAK signaling and ERK activation (Yamada, Pankov et al. 2003).

Immunocytochemical analysis of the FN matrices in cell culture revealed a markedly different FN fibril morphology between FN-monomer and wild-type control fibrils. While the latter contained an elaborated and ramified network of elongated fibrils, FN-monomer fibrills were of short and thin appearance with only few ramifications. Furthermore, also α5β1 integrin and F-actin of $FN^{CC>SS/CC>SS}$ cells displayed markedly altered structures of fibrillar adhesions, suggesting that α5 integrin signaling might have been modified in response to FN-monomer binding. This notion could be confirmed experimentally. Western blot analysis revealed slightly decreased levels of p397FAK in cells adhering to $FN^{CC>SS/CC>SS}$ matrices. FAK activation at tyrosine residue Y397 is regulated by acto-myosin contractility, integrin-mediated adhesion and matrix stiffness in a mechano-responsive manner (Tilghman and Parsons 2008). It is therefore conceivable that the FN-monomer matrix exhibits a differential mechanical pliability and rigidity when compared to the wild-type matrix, which leads to altered integrin signaling and to the defects observed in $FN^{CC>SS/CC>SS}$ mice.

Targeted inactivation of the FAK gene in mice results in a strikingly similar phenotype compared to FN-null mice. FAK-null mice display a severely defective development of mesoderm-derived structures, including the inability to form somites, and fail to develop an organized vascular system (Furuta, Ilic et al. 1995; Ilic, Furuta et al. 1995). The importance of FAK in vascular development is evident because of its abundant expression in the vasculature at the time of critical vascular development (Polte, Naftilan et al. 1994; Braren, Hu et al. 2006). However, the unaffected somite formation in $FN^{CC>SS/CC>SS}$ mice suggests that the mesoderm is less sensitive to changes in FAK signaling than endothelial cells.

Future experiments will be necessary to test to which extent the diminished FAK activation caused by the altered composition and mechanical properties of the FN-monomer matrix is contributing to the severe vascular defects observed in the extraembryonic tissues of $FN^{CC>SS/CC>SS}$ mice.

4.2.3 FN dimers are essential for normal vascular development

Targeted inactivation of the FN gene in mice has leads to impaired development of mesoderm-derived structures including somites, notochord, heart and embryonic vessels. $FN^{CC>SS/CC>SS}$ mice develop posterior somites, although their posterior trunk region appears smaller.

A hallmark of $FN^{CC>SS/CC>SS}$ embryos was their anemic yolk sac, which completely lacked a distinct branching network of vessels. Areas of accumulated red blood cells in the yolk sac indicated leaky vessels and an impaired blood circulation. These circulation defects might lead to elevated intracardial pressure which could explain the enlarged pericardial sac observed in the hearts of $FN^{CC>SS/CC>SS}$ embryos. Immunohistochemical analysis of the mutant yolk sacs revealed, that the formation of the primary capillary

plexus occurred (vasculogenesis; (Risau 1997)), but that remodelling (pruning) into a ramified network of vessels did not take place, indicating a defect in angiogenesis (Risau 1997). Similarly, in the embryo proper of E9.5 mutants, only fragile, disorganized and enlarged vessel-like structures were formed, probably exacerbating the circulation defect that possibly causes the growth arrest affecting $FN^{CC>SS/CC>SS}$ embryos. This growth arrest commenced at 20-25 somite stage, which corresponds to E9.0 - E9.5 of embryonic development. Sections through the placenta indicated further defects of the mutant vascular system, which were characterized by the inability of embryonic vessels to properly sprout into the maternal labyrinthine layer, and by the pronounced apoptotic cell death in $FN^{CC>SS/CC>SS}$ endothelial cells at E10.5.

The vascular defects of $FN^{CC>SS/CC>SS}$ mice are similar to those observed in mice with compromised TGF-β signaling. The cytokine TGF-β is an inhibitor of endothelial proliferation and migration (Muller, Behrens et al. 1987; Merwin, Newman et al. 1991), and can also induce growth arrest in a variety of other cell types including epithelial, hematopoietic, neural and certain types of mesenchymal cells (Massague and Gomis 2006). Furthermore, TGF-β has also been shown to induce a number of pro-apoptotic responses (Siegel and Massague 2003). Targeted inactivation of the genes for the TGF-β1 ligand, as well as for the TGF-β receptors ALK5, TGF-βRII, endoglin and the endothelial specific ALK1 result in severe angiogenesis defects that lead to embryonic growth arrest and early embryonic lethality around E10-11 (Dickson, Martin et al. 1995; Oshima, Oshima et al. 1996; Li, Sorensen et al. 1999; Oh, Seki et al. 2000; Larsson, Goumans et al. 2001). A major difference between the ALK1-null phenotype and the other TGF-β knock out phenotypes is identified by the vascular morphogenesis in the embryo proper around E9.5, which is only defective in ALK1-null mice. This difference is likely attributed to the fact that mutations of other TGF-β components disrupt both ALK1 and ALK5 pathways, whereas mutation of ALK1 disrupts only the endothelial specific ALK1 pathway (which signals through R-Smads 1/5) (Attisano, Carcamo et al. 1993), leading to a dominance of the ubiquitous ALK5 mediated R-Smad2/3 signaling in the endothelial tissue (Oh, Seki et al. 2000). This finding indicates that ALK1 signaling can inhibit ALK5 mediated functions in endothelial cells, and suggests that a balance between ALK1 and ALK5 signaling is an essential prerequisite for angiogenesis. In summary, the results of these studies suggest that the defects in $FN^{CC>SS/CC>SS}$ embryos, which closely resemble the defects observed in ALK1-null mice, may be attributed to impaired endothelial functions in response to altered TGF-β signaling.

Western blot analysis of lysates derived from $FN^{CC>SS/CC>SS}$ embryos and yolk sacs for phospho-Smad2/3 levels confirmed increased levels of active TGF-β *in vivo*, suggesting that most parts of the defects observed in $FN^{CC>SS/CC>SS}$ mice could be attributed to elevated levels of active TGF-β. This notion is supported by the study of Agah et al., which demonstrated that vasculature-specific over-expression of TGF-β in mice results in a phenotype that shares striking similarity with the phenotype observed in $FN^{CC>SS/CC>SS}$ mice (Agah, Prasad et al. 2000). Moreover, it was reported that elevated

levels of active TGF-β can inhibit angiogenesis processes (Pepper 1997) and that overexpression of the type II TGF-β receptor (TGF-βRII) in murine extraembryonic mesoderm leads to impaired yolk sac vasculogenesis (Goumans, Zwijsen et al. 1999). In summary, these findings indicate that increased levels of active TGF-β in highly responsive tissue undergoing rapid morphogenesis, such as the developing yolk sac vasculature, is poorly tolerated.

4.2.4 Enhanced levels of active TGF-β do not result in increased ECM production in $FN^{CC>SS/CC>SS}$ mice

Numerous studies have demonstrated that TGF-β is one of the most potent cytokines to induce ECM production *in vivo* (Taipale, Saharinen et al. 1996); reviewed in (Rahimi and Leof 2007). Furthermore, TGF-β is thought to be a master-regulator of FN production in the extraembryonic mesoderm (Goumans, Zwijsen et al. 1999). Surprisingly, no evidence for increased extracellular matrix deposition in response to increased levels of active TGF-β was observed in mice overexpressing TGF-β in the vasculature (Agah, Prasad et al. 2000) or in $FN^{CC>SS/CC>SS}$ mice. Although R-Smads are clearly critical for increased ECM deposition induced by TGF-β, it remains unclear, whether they are differentially regulated in distinct cell types.

4.2.5 The FN-monomer matrix fails to deposit latent TGF-β causing increased levels of active TGF-β

The detection of increased levels of active TGF-β in FN-monomer mutants suggested that FN and TGF-β crosstalk with each other. Studies from Dallas et al. indicated that FN regulates the deposition of latent TGF-β into the matrix (Dallas, Sivakumar et al. 2005) by controlling the assembly of the latent TGF-β binding proteins (LTBPs). LTBPs constitute a fibrillar component of the ECM and have been well established as major regulators of TGF-β functions (reviewed in (Hyytiainen, Penttinen et al. 2004)). Interestingly, initiation and sustained LTBP assembly into the ECM has been demonstrated to be critically dependent on a fibrillar FN matrix acting as a scaffold. There is conflicting data whether the FN-LTBP interaction is direct or indirect (Chen, Sivakumar et al. 2007; Kantola, Keski-Oja et al. 2008). However, studies with FN-null fibroblasts indicated that an absent FN matrix leads to a loss of LTBP-mediated TGF-β targeting to the ECM. As a result, soluble LTBPs accumulated, the levels of phospho Smad2/3 increased, suggesting that impaired deposition of LTBP leads to enhanced bioavailability of active TGF-β (Chaudhry, Cain et al. 2007; Kantola, Keski-Oja et al. 2008).

Unfortunately, it was not possible to analyse the fibrillar properties of LTBP deposits in embryo sections by immunohistochemistry. Therefore, it was sought to prove the hypothesis of impaired LTBP assembly on FN-monomer matrices in cell culture.

In all $FN^{CC>SS/CC>SS}$ clones tested, the FN-monomer matrix failed to properly assemble LTBP-1, a prototypic LTBP associated to TGF-β1. Western blot analysis of LTBP-1

released from cell derived matrices revealed that the absence of LTBPs on mutant cells was not due to lower expression levels, but that LTBPs rather accumulated in the medium. These data clearly indicate that FN-monomer fails to target LTBP-1 to the ECM. However, it still remains unanswered whether the impaired capability of FN-monomer to deposit LTBPs into the ECM indeed resulted in increased levels of active TGF-β. To address this question experimentally, a luciferase-based TGF-β reporter system was used (Abe, Harpel et al. 1994) to comparatively analyse the levels of active TGF-β in conditioned medium of $FN^{CC>SS/CC>SS}$ and control cells. The assays revealed significantly increased levels of active TGF-β accumulated in the medium of $FN^{CC>SS/CC>SS}$ cells, demonstrating that the FN-monomer matrix is not capable of regulating the bioavailability of TGF-β.

In line with the previously mentioned studies, these data indicate that increased levels of active TGF-β may be responsible for the vascular defects observed in $FN^{CC>SS/CC>SS}$ mice. However, it can not be ruled out completely, that modified integrin signaling events additionally contribute to defects observed particularly in the extraembryonic tissues of $FN^{CC>SS/CC>SS}$ mice. Future *in vivo* experiments applying TGF-β inhibitors *in vivo* should help to discriminate between these two defects and should demonstrate how diminished TGF-β signaling affects the development of $FN^{CC>SS/CC>SS}$ embryos *in utero*.

It is tempting to speculate that FN-monomer probably does not completely fail to assemble ECM components such as LTBP-1, but rather delays FN dependent ECM assembly processes. This notion is substantiated by the observation of marked morphological differences between the FN-monomer matrix *in vivo* and *in vitro*. Further studies will be necessary to examine FN-monomers capabilities to assemble ECM components whose deposition into the ECM has been shown to be critically dependent on a fully functional FN matrix.

In conclusion, the second part of the thesis shows that monomeric FN can be assembled into a matrix network *in vivo* and *in vitro*, but fails to deposit ECM components critical for the regulation of the growth factor TGF-β. The present mouse model exemplifies that the structural integrity of FN is of critical importance to properly fulfil its role as a master-organizer for ECM formation during development and tissue homeostasis.

5 References

Abe, M., J. G. Harpel, et al. (1994). "An assay for transforming growth factor-beta using cells transfected with a plasminogen activator inhibitor-1 promoter-luciferase construct." Anal Biochem **216**(2): 276-84.

Abedi, H. and I. Zachary (1997). "Vascular endothelial growth factor stimulates tyrosine phosphorylation and recruitment to new focal adhesions of focal adhesion kinase and paxillin in endothelial cells." J Biol Chem **272**(24): 15442-51.

Agah, R., K. S. Prasad, et al. (2000). "Cardiovascular overexpression of transforming growth factor-beta(1) causes abnormal yolk sac vasculogenesis and early embryonic death." Circ Res **86**(10): 1024-30.

Aguirre, K. M., R. J. McCormick, et al. (1994). "Fibronectin self-association is mediated by complementary sites within the amino-terminal one-third of the molecule." J Biol Chem **269**(45): 27863-8.

Annes, J. P., D. B. Rifkin, et al. (2002). "The integrin alphaVbeta6 binds and activates latent TGFbeta3." FEBS Lett **511**(1-3): 65-8.

Aota, S. and K. M. Yamada (1997). "Integrin functions and signal transduction." Adv Exp Med Biol **400B**: 669-82.

Armant, D. R., H. A. Kaplan, et al. (1986). "Fibronectin and laminin promote in vitro attachment and outgrowth of mouse blastocysts." Dev Biol **116**(2): 519-23.

Arnaout, M. A., B. Mahalingam, et al. (2005). "Integrin structure, allostery, and bidirectional signaling." Annu Rev Cell Dev Biol **21**: 381-410.

Astrof, S., D. Crowley, et al. (2007). "Multiple cardiovascular defects caused by the absence of alternatively spliced segments of fibronectin." Dev Biol **311**(1): 11-24.

Attisano, L., J. Carcamo, et al. (1993). "Identification of human activin and TGF beta type I receptors that form heteromeric kinase complexes with type II receptors." Cell **75**(4): 671-80.

Aulehla, A. and O. Pourquie (2008). "Oscillating signaling pathways during embryonic development." Curr Opin Cell Biol **20**(6): 632-7.

Aumailley, M. and T. Krieg (1996). "Laminins: a family of diverse multifunctional molecules of basement membranes." J Invest Dermatol **106**(2): 209-214.

Baron, M., A. L. Main, et al. (1992). "1H NMR assignment and secondary structure of the cell adhesion type III module of fibronectin." Biochemistry **31**(7): 2068-73.

Baron, M., D. Norman, et al. (1990). "Structure of the fibronectin type 1 module." Nature **345**(6276): 642-6.

Bennett, J. S. (2005). "Structure and function of the platelet integrin alphaIIbbeta3." J Clin Invest **115**(12): 3363-9.

Bowditch, R. D., M. Hariharan, et al. (1994). "Identification of a novel integrin binding site in fibronectin. Differential utilization by beta 3 integrins." J Biol Chem **269**(14): 10856-63.

Braren, R., H. Hu, et al. (2006). "Endothelial FAK is essential for vascular network stability, cell survival, and lamellipodial formation." J Cell Biol **172**(1): 151-62.

Brown, M., M. McCormack, et al. (1986). "A recombinant murine retrovirus for simian virus 40 large T cDNA transforms mouse fibroblasts to anchorage-independent growth." J Virol **60**(1): 290-3.

Brummelkamp, T. R., R. Bernards, et al. (2002). "A system for stable expression of short interfering RNAs in mammalian cells." Science **296**(5567): 550-3.

Bultmann, H., A. J. Santas, et al. (1998). "Fibronectin fibrillogenesis involves the heparin II binding domain of fibronectin." J Biol Chem **273**(5): 2601-9.

Calderwood, D. A. (2004). "Integrin activation." J Cell Sci **117**(Pt 5): 657-66.

Carman, C. V. and T. A. Springer (2003). "Integrin avidity regulation: are changes in affinity and conformation underemphasized?" Curr Opin Cell Biol **15**(5): 547-56.

Chada, D., T. Mather, et al. (2006). "The synergy site of fibronectin is required for strong interaction with the platelet integrin alphaIIbbeta3." Ann Biomed Eng **34**(10): 1542-52.

Chaudhry, S. S., S. A. Cain, et al. (2007). "Fibrillin-1 regulates the bioavailability of TGFbeta1." J Cell Biol **176**(3): 355-67.

Chen, Q., P. Sivakumar, et al. (2007). "Potential role for heparan sulfate proteoglycans in regulation of transforming growth factor-beta (TGF-beta) by modulating assembly of latent TGF-beta-binding protein-1." J Biol Chem **282**(36): 26418-30.

Cho, J. and D. F. Mosher (2006). "Role of fibronectin assembly in platelet thrombus formation." J Thromb Haemost **4**(7): 1461-9.

Chodniewicz, D. and R. L. Klemke (2004). "Guiding cell migration through directed extension and stabilization of pseudopodia." Exp Cell Res **301**(1): 31-7.

Choi, C. K., M. Vicente-Manzanares, et al. (2008). "Actin and alpha-actinin orchestrate the assembly and maturation of nascent adhesions in a myosin II motor-independent manner." Nat Cell Biol **10**(9): 1039-50.

Choi, M. G. and R. O. Hynes (1979). "Biosynthesis and processing of fibronectin in NIL.8 hamster cells." J Biol Chem **254**(23): 12050-5.

Chong, S. W. and Y. J. Jiang (2005). "Off limits--integrins holding boundaries in somitogenesis." Trends Cell Biol **15**(9): 453-7.

Constantine, K. L., S. A. Brew, et al. (1992). "1H-n.m.r. studies of the fibronectin 13 kDa collagen-binding fragment. Evidence for autonomous conserved type I and type II domain folds." Biochem J **283 (Pt 1)**: 247-54.

Cross, J. C., Z. Werb, et al. (1994). "Implantation and the placenta: key pieces of the development puzzle." Science **266**(5190): 1508-18.

Cukierman, E., R. Pankov, et al. (2001). "Taking cell-matrix adhesions to the third dimension." Science **294**(5547): 1708-12.

Curnis, F., R. Longhi, et al. (2006). "Spontaneous formation of L-isoaspartate and gain of function in fibronectin." J Biol Chem **281**(47): 36466-76.

Dallas, S. L., Q. Chen, et al. (2006). "Dynamics of assembly and reorganization of extracellular matrix proteins." Curr Top Dev Biol **75**: 1-24.

Dallas, S. L., K. Miyazono, et al. (1995). "Dual role for the latent transforming growth factor-beta binding protein in storage of latent TGF-beta in the extracellular matrix and as a structural matrix protein." J Cell Biol **131**(2): 539-49.

Dallas, S. L., P. Sivakumar, et al. (2005). "Fibronectin regulates latent transforming growth factor-beta (TGF beta) by controlling matrix assembly of latent TGF beta-binding protein-1." J Biol Chem **280**(19): 18871-80.

Danen, E. H., P. Sonneveld, et al. (2000). "Dual stimulation of Ras/mitogen-activated protein kinase and RhoA by cell adhesion to fibronectin supports growth factor-stimulated cell cycle progression." J Cell Biol **151**(7): 1413-22.

Danen, E. H. and K. M. Yamada (2001). "Fibronectin, integrins, and growth control." J Cell Physiol **189**(1): 1-13.

David, C. L., J. Orpiszewski, et al. (1998). "Isoaspartate in chrondroitin sulfate proteoglycans of mammalian brain." J Biol Chem **273**(48): 32063-70.

Di Matteo, P., F. Curnis, et al. (2006). "Immunogenic and structural properties of the Asn-Gly-Arg (NGR) tumor neovasculature-homing motif." Mol Immunol **43**(10): 1509-18.

Dickinson, C. D., B. Veerapandian, et al. (1994). "Crystal structure of the tenth type III cell adhesion module of human fibronectin." J Mol Biol **236**(4): 1079-92.

Dickson, M. C., J. S. Martin, et al. (1995). "Defective haematopoiesis and vasculogenesis in transforming growth factor-beta 1 knock out mice." Development **121**(6): 1845-54.

Fath, K. R., C. J. Edgell, et al. (1989). "The distribution of distinct integrins in focal contacts is determined by the substratum composition." J Cell Sci **92 (Pt 1)**: 67-75.

Ffrench-Constant, C. and R. O. Hynes (1988). "Patterns of fibronectin gene expression and splicing during cell migration in chicken embryos." Development **104**(3): 369-82.

Flamme, I., T. Frolich, et al. (1997). "Molecular mechanisms of vasculogenesis and embryonic angiogenesis." J Cell Physiol **173**(2): 206-10.

Flaumenhaft, R. and D. B. Rifkin (1992). "Cell density dependent effects of TGF-beta demonstrated by a plasminogen activator-based assay for TGF-beta." J Cell Physiol **152**(1): 48-55.

Fontana, L., Y. Chen, et al. (2005). "Fibronectin is required for integrin alphavbeta6-mediated activation of latent TGF-beta complexes containing LTBP-1." Faseb J **19**(13): 1798-808.

Francis, S. E., K. L. Goh, et al. (2002). "Central roles of alpha5beta1 integrin and fibronectin in vascular development in mouse embryos and embryoid bodies." Arterioscler Thromb Vasc Biol **22**(6): 927-33.

Friedland, J. C., M. H. Lee, et al. (2009). "Mechanically activated integrin switch controls alpha5beta1 function." Science **323**(5914): 642-4.

Fukuda, T., N. Yoshida, et al. (2002). "Mice lacking the EDB segment of fibronectin develop normally but exhibit reduced cell growth and fibronectin matrix assembly in vitro." Cancer Res **62**(19): 5603-10.

Furuta, Y., D. Ilic, et al. (1995). "Mesodermal defect in late phase of gastrulation by a targeted mutation of focal adhesion kinase, FAK." Oncogene **11**(10): 1989-95.

Gallant, N. D., K. E. Michael, et al. (2005). "Cell adhesion strengthening: contributions of adhesive area, integrin binding, and focal adhesion assembly." Mol Biol Cell **16**(9): 4329-40.

Geiger, B., A. Bershadsky, et al. (2001). "Transmembrane crosstalk between the extracellular matrix--cytoskeleton crosstalk." Nat Rev Mol Cell Biol **2**(11): 793-805.

George, E. L., E. N. Georges-Labouesse, et al. (1993). "Defects in mesoderm, neural tube and vascular development in mouse embryos lacking fibronectin." Development **119**(4): 1079-91.

Georges-Labouesse, E. N., E. L. George, et al. (1996). "Mesodermal development in mouse embryos mutant for fibronectin." Dev Dyn **207**(2): 145-56.

Giancotti, F. G. and E. Ruoslahti (1999). "Integrin signaling." Science **285**(5430): 1028-32.

Giancotti, F. G. and G. Tarone (2003). "Positional control of cell fate through joint integrin/receptor protein kinase signaling." Annu Rev Cell Dev Biol **19**: 173-206.

Godyna, S., D. M. Mann, et al. (1995). "A quantitative analysis of the incorporation of fibulin-1 into extracellular matrix indicates that fibronectin assembly is required." Matrix Biol **14**(6): 467-77.

Goumans, M. J., Z. Liu, et al. (2009). "TGF-beta signaling in vascular biology and dysfunction." Cell Res **19**(1): 116-27.

Goumans, M. J., A. Zwijsen, et al. (1999). "Transforming growth factor-beta signalling in extraembryonic mesoderm is required for yolk sac vasculogenesis in mice." Development **126**(16): 3473-83.

Gregory, K. E., R. N. Ono, et al. (2005). "The prodomain of BMP-7 targets the BMP-7 complex to the extracellular matrix." J Biol Chem **280**(30): 27970-80.

Gridley, T. (2006). "The long and short of it: somite formation in mice." Dev Dyn **235**(9): 2330-6.

Guan, J. L. and R. O. Hynes (1990). "Lymphoid cells recognize an alternatively spliced segment of fibronectin via the integrin receptor alpha 4 beta 1." Cell **60**(1): 53-61.

Guo, W. and F. G. Giancotti (2004). "Integrin signalling during tumour progression." Nat Rev Mol Cell Biol **5**(10): 816-26.

Hocking, D. C., J. Sottile, et al. (1994). "Fibronectin's III-1 module contains a conformation-dependent binding site for the amino-terminal region of fibronectin." J Biol Chem **269**(29): 19183-7.

Hoefen, R. J. and B. C. Berk (2006). "The multifunctional GIT family of proteins." J Cell Sci **119**(Pt 8): 1469-75.

Hughes, P. E., M. W. Renshaw, et al. (1997). "Suppression of integrin activation: a novel function of a Ras/Raf-initiated MAP kinase pathway." Cell **88**(4): 521-30.

Humphries, J. D., A. Byron, et al. (2006). "Integrin ligands at a glance." J Cell Sci **119**(Pt 19): 3901-3.

Humphries, J. D., P. Wang, et al. (2007). "Vinculin controls focal adhesion formation by direct interactions with talin and actin." J Cell Biol **179**(5): 1043-57.

Humphries, M. J., M. A. Travis, et al. (2004). "Mechanisms of integration of cells and extracellular matrices by integrins." Biochem Soc Trans **32**(Pt 5): 822-5.

Hynes, R. O. (2002). "Integrins: bidirectional, allosteric signaling machines." Cell **110**(6): 673-87.

Hynes, R. O. and A. Destree (1977). "Extensive disulfide bonding at the mammalian cell surface." Proc Natl Acad Sci U S A **74**(7): 2855-9.

Hyytiainen, M., C. Penttinen, et al. (2004). "Latent TGF-beta binding proteins: extracellular matrix association and roles in TGF-beta activation." Crit Rev Clin Lab Sci **41**(3): 233-64.

Icardo, J. M., A. Nakamura, et al. (1992). "Effects of injecting fibronectin and antifibronectin antibodies on cushion mesenchyme formation in the chick. An in vivo study." Anat Embryol (Berl) **185**(3): 239-47.

Ichihara-Tanaka, K., T. Maeda, et al. (1992). "Matrix assembly of recombinant fibronectin polypeptide consisting of amino-terminal 70 kDa and carboxyl-terminal 37 kDa regions." FEBS Lett **299**(2): 155-8.

Ilic, D., Y. Furuta, et al. (1995). "Reduced cell motility and enhanced focal adhesion contact formation in cells from FAK-deficient mice." Nature **377**(6549): 539-44.

Iozzo, R. V. (1998). "Matrix proteoglycans: from molecular design to cellular function." Annu Rev Biochem **67**: 609-52.

Julich, D., R. Geisler, et al. (2005). "Integrinalpha5 and delta/notch signaling have complementary spatiotemporal requirements during zebrafish somitogenesis." Dev Cell **8**(4): 575-86.

Kadler, K. E., A. Hill, et al. (2008). "Collagen fibrillogenesis: fibronectin, integrins, and minor collagens as organizers and nucleators." Curr Opin Cell Biol **20**(5): 495-501.

Kantola, A. K., J. Keski-Oja, et al. (2008). "Fibronectin and heparin binding domains of latent TGF-beta binding protein (LTBP)-4 mediate matrix targeting and cell adhesion." Exp Cell Res **314**(13): 2488-500.

Keski-Oja, J., D. F. Mosher, et al. (1977). "Dimeric character of fibronectin, a major cell surface-associated glycoprotein." Biochem Biophys Res Commun **74**(2): 699-706.

Kielty, C. M., M. J. Sherratt, et al. (2005). "Fibrillin microfibrils." Adv Protein Chem **70**: 405-36.

Kinsey, R., M. R. Williamson, et al. (2008). "Fibrillin-1 microfibril deposition is dependent on fibronectin assembly." J Cell Sci **121**(Pt 16): 2696-704.

Klass, C. M., J. R. Couchman, et al. (2000). "Control of extracellular matrix assembly by syndecan-2 proteoglycan." J Cell Sci **113 (Pt 3)**: 493-506.

Koli, K., M. Hyytiainen, et al. (2005). "Sequential deposition of latent TGF-beta binding proteins (LTBPs) during formation of the extracellular matrix in human lung fibroblasts." Exp Cell Res **310**(2): 370-82.

Kornblihtt, A. R., C. G. Pesce, et al. (1996). "The fibronectin gene as a model for splicing and transcription studies." Faseb J **10**(2): 248-57.

Koshida, S., Y. Kishimoto, et al. (2005). "Integrinalpha5-dependent fibronectin accumulation for maintenance of somite boundaries in zebrafish embryos." Dev Cell **8**(4): 587-98.

Lallier, T., M. Artinger, et al. (1990). "Distribution and biochemical characterization of the INO antigen during chick neural crest cell migration." Neurosci Res Suppl **13**: S126-40.

Lanthier, J. and R. R. Desrosiers (2004). "Protein L-isoaspartyl methyltransferase repairs abnormal aspartyl residues accumulated in vivo in type-I collagen and restores cell migration." Exp Cell Res **293**(1): 96-105.

Larsen, M., V. V. Artym, et al. (2006). "The matrix reorganized: extracellular matrix remodeling and integrin signaling." Curr Opin Cell Biol **18**(5): 463-71.

Larsson, J., M. J. Goumans, et al. (2001). "Abnormal angiogenesis but intact hematopoietic potential in TGF-beta type I receptor-deficient mice." Embo J **20**(7): 1663-73.

Laurent, T. C. and J. R. Fraser (1992). "Hyaluronan." Faseb J **6**(7): 2397-404.

Lee, J. W. and R. Juliano (2004). "Mitogenic signal transduction by integrin- and growth factor receptor-mediated pathways." Mol Cells **17**(2): 188-202.

Legate, K. R. and R. Fassler (2009). "Mechanisms that regulate adaptor binding to beta-integrin cytoplasmic tails." J Cell Sci **122**(Pt 2): 187-98.

Legate, K. R., S. A. Wickstrom, et al. (2009). "Genetic and cell biological analysis of integrin outside-in signaling." Genes Dev **23**(4): 397-418.

Leiss, M., K. Beckmann, et al. (2008). "The role of integrin binding sites in fibronectin matrix assembly in vivo." Curr Opin Cell Biol **20**(5): 502-7.

Li, D. Y., L. K. Sorensen, et al. (1999). "Defective angiogenesis in mice lacking endoglin." Science **284**(5419): 1534-7.

Li, S., C. Van Den Diepstraten, et al. (2003). "Vascular smooth muscle cells orchestrate the assembly of type I collagen via alpha2beta1 integrin, RhoA, and fibronectin polymerization." Am J Pathol **163**(3): 1045-56.

Liao, Y. F., P. J. Gotwals, et al. (2002). "The EIIIA segment of fibronectin is a ligand for integrins alpha 9beta 1 and alpha 4beta 1 providing a novel mechanism for regulating cell adhesion by alternative splicing." J Biol Chem **277**(17): 14467-74.

Linask, K. K. and J. W. Lash (1986). "Precardiac cell migration: fibronectin localization at mesoderm-endoderm interface during directional movement." Dev Biol **114**(1): 87-101.

Liu, S., D. A. Calderwood, et al. (2000). "Integrin cytoplasmic domain-binding proteins." J Cell Sci **113 (Pt 20)**: 3563-71.

Lo, S. H., E. Weisberg, et al. (1994). "Tensin: a potential link between the cytoskeleton and signal transduction." Bioessays **16**(11): 817-23.

Luo, B. H., C. V. Carman, et al. (2007). "Structural basis of integrin regulation and signaling." Annu Rev Immunol **25**: 619-47.

Mao, Y. and J. E. Schwarzbauer (2005). "Fibronectin fibrillogenesis, a cell-mediated matrix assembly process." Matrix Biol **24**(6): 389-99.

Massague, J. and R. R. Gomis (2006). "The logic of TGFbeta signaling." FEBS Lett **580**(12): 2811-20.

McDonald, J. A., D. G. Kelley, et al. (1982). "Role of fibronectin in collagen deposition: Fab' to the gelatin-binding domain of fibronectin inhibits both fibronectin and collagen organization in fibroblast extracellular matrix." J Cell Biol **92**(2): 485-92.

McDonald, J. A., B. J. Quade, et al. (1987). "Fibronectin's cell-adhesive domain and an amino-terminal matrix assembly domain participate in its assembly into fibroblast pericellular matrix." J Biol Chem **262**(7): 2957-67.

McKeown-Longo, P. J. and D. F. Mosher (1984). "Mechanism of formation of disulfide-bonded multimers of plasma fibronectin in cell layers of cultured human fibroblasts." J Biol Chem **259**(19): 12210-5.

Merwin, J. R., W. Newman, et al. (1991). "Vascular cells respond differentially to transforming growth factors beta 1 and beta 2 in vitro." Am J Pathol **138**(1): 37-51.

Miner, J. H. and P. D. Yurchenco (2004). "Laminin functions in tissue morphogenesis." Annu Rev Cell Dev Biol **20**: 255-84.

Miranti, C. K. and J. S. Brugge (2002). "Sensing the environment: a historical perspective on integrin signal transduction." Nat Cell Biol **4**(4): E83-90.

Miyamoto, S., H. Teramoto, et al. (1996). "Integrins can collaborate with growth factors for phosphorylation of receptor tyrosine kinases and MAP kinase activation: roles of integrin aggregation and occupancy of receptors." J Cell Biol **135**(6 Pt 1): 1633-42.

Moretti, F. A., A. K. Chauhan, et al. (2007). "A major fraction of fibronectin present in the extracellular matrix of tissues is plasma-derived." J Biol Chem **282**(38): 28057-62.

Morgan, M. R., M. J. Humphries, et al. (2007). "Synergistic control of cell adhesion by integrins and syndecans." Nat Rev Mol Cell Biol **8**(12): 957-69.

Moro, L., M. Venturino, et al. (1998). "Integrins induce activation of EGF receptor: role in MAP kinase induction and adhesion-dependent cell survival." Embo J **17**(22): 6622-32.

Moser, M., K. R. Legate, et al. (2009). "The tail of integrins, talin, and kindlins." Science **324**(5929): 895-9.

Moser, M., B. Nieswandt, et al. (2008). "Kindlin-3 is essential for integrin activation and platelet aggregation." Nat Med **14**(3): 325-30.

Muller, G., J. Behrens, et al. (1987). "Inhibitory action of transforming growth factor beta on endothelial cells." Proc Natl Acad Sci U S A **84**(16): 5600-4.

Muro, A. F., A. K. Chauhan, et al. (2003). "Regulated splicing of the fibronectin EDA exon is essential for proper skin wound healing and normal lifespan." J Cell Biol **162**(1): 149-60.

Nagai, T., N. Yamakawa, et al. (1991). "Monoclonal antibody characterization of two distant sites required for function of the central cell-binding domain of fibronectin in cell adhesion, cell migration, and matrix assembly." J Cell Biol **114**(6): 1295-305.

Naito, Y., T. Yamada, et al. (2004). "siDirect: highly effective, target-specific siRNA design software for mammalian RNA interference." Nucleic Acids Res **32**(Web Server issue): W124-9.

Ni, H., P. S. Yuen, et al. (2003). "Plasma fibronectin promotes thrombus growth and stability in injured arterioles." Proc Natl Acad Sci U S A **100**(5): 2415-9.

O'Reilly, D. R. (1986). "p53 and transformation by SV40." Biol Cell **57**(3): 187-96.

Oh, S. P., T. Seki, et al. (2000). "Activin receptor-like kinase 1 modulates transforming growth factor-beta 1 signaling in the regulation of angiogenesis." Proc Natl Acad Sci U S A **97**(6): 2626-31.

Ohashi, T., D. P. Kiehart, et al. (2002). "Dual labeling of the fibronectin matrix and actin cytoskeleton with green fluorescent protein variants." J Cell Sci **115**(Pt 6): 1221-9.

Oshima, M., H. Oshima, et al. (1996). "TGF-beta receptor type II deficiency results in defects of yolk sac hematopoiesis and vasculogenesis." Dev Biol **179**(1): 297-302.

Pankov, R., E. Cukierman, et al. (2000). "Integrin dynamics and matrix assembly: tensin-dependent translocation of alpha(5)beta(1) integrins promotes early fibronectin fibrillogenesis." J Cell Biol **148**(5): 1075-90.

Pankov, R. and K. M. Yamada (2002). "Fibronectin at a glance." J Cell Sci **115**(Pt 20): 3861-3.

Paranandi, M. V., A. W. Guzzetta, et al. (1994). "Deamidation and isoaspartate formation during in vitro aging of recombinant tissue plasminogen activator." J Biol Chem **269**(1): 243-53.

Pepper, M. S. (1997). "Transforming growth factor-beta: vasculogenesis, angiogenesis, and vessel wall integrity." Cytokine Growth Factor Rev **8**(1): 21-43.

Pereira, M., B. J. Rybarczyk, et al. (2002). "The incorporation of fibrinogen into extracellular matrix is dependent on active assembly of a fibronectin matrix." J Cell Sci **115**(Pt 3): 609-17.

Pfaff, M., K. Tangemann, et al. (1994). "Selective recognition of cyclic RGD peptides of NMR defined conformation by alpha IIb beta 3, alpha V beta 3, and alpha 5 beta 1 integrins." J Biol Chem **269**(32): 20233-8.

Pierschbacher, M. D. and E. Ruoslahti (1984). "Cell attachment activity of fibronectin can be duplicated by small synthetic fragments of the molecule." Nature **309**(5963): 30-3.

Plopper, G. E., H. P. McNamee, et al. (1995). "Convergence of integrin and growth factor receptor signaling pathways within the focal adhesion complex." Mol Biol Cell **6**(10): 1349-65.

Polte, T. R., A. J. Naftilan, et al. (1994). "Focal adhesion kinase is abundant in developing blood vessels and elevation of its phosphotyrosine content in vascular smooth muscle cells is a rapid response to angiotensin II." J Cell Biochem **55**(1): 106-19.

Pourquie, O. (2001). "Vertebrate somitogenesis." Annu Rev Cell Dev Biol **17**: 311-50.

Price, L. S., J. Leng, et al. (1998). "Activation of Rac and Cdc42 by integrins mediates cell spreading." Mol Biol Cell **9**(7): 1863-71.

Rahimi, R. A. and E. B. Leof (2007). "TGF-beta signaling: a tale of two responses." J Cell Biochem **102**(3): 593-608.

Reissner, K. J. and D. W. Aswad (2003). "Deamidation and isoaspartate formation in proteins: unwanted alterations or surreptitious signals?" Cell Mol Life Sci **60**(7): 1281-95.

Ren, X. D., W. B. Kiosses, et al. (1999). "Regulation of the small GTP-binding protein Rho by cell adhesion and the cytoskeleton." Embo J **18**(3): 578-85.

Risau, W. (1991). "Embryonic angiogenesis factors." Pharmacol Ther **51**(3): 371-6.

Risau, W. (1997). "Mechanisms of angiogenesis." Nature **386**(6626): 671-4.

Robinson, N. E., Z. W. Robinson, et al. (2004). "Structure-dependent nonenzymatic deamidation of glutaminyl and asparaginyl pentapeptides." J Pept Res **63**(5): 426-36.

Sabatier, L., D. Chen, et al. (2009). "Fibrillin assembly requires fibronectin." Mol Biol Cell **20**(3): 846-58.

Sakai, T., K. J. Johnson, et al. (2001). "Plasma fibronectin supports neuronal survival and reduces brain injury following transient focal cerebral ischemia but is not essential for skin-wound healing and hemostasis." Nat Med **7**(3): 324-30.

Sakai, T., M. Larsen, et al. (2003). "Fibronectin requirement in branching morphogenesis." Nature **423**(6942): 876-81.

Saoncella, S., F. Echtermeyer, et al. (1999). "Syndecan-4 signals cooperatively with integrins in a Rho-dependent manner in the assembly of focal adhesions and actin stress fibers." Proc Natl Acad Sci U S A **96**(6): 2805-10.

Schaller, M. D. (2001). "Biochemical signals and biological responses elicited by the focal adhesion kinase." Biochim Biophys Acta **1540**(1): 1-21.

Schlaepfer, D. D. and T. Hunter (1996). "Evidence for in vivo phosphorylation of the Grb2 SH2-domain binding site on focal adhesion kinase by Src-family protein-tyrosine kinases." Mol Cell Biol **16**(10): 5623-33.

Schwartz, M. A. and M. H. Ginsberg (2002). "Networks and crosstalk: integrin signalling spreads." Nat Cell Biol **4**(4): E65-8.

Schwarzbauer, J. E. (1991). "Alternative splicing of fibronectin: three variants, three functions." Bioessays **13**(10): 527-33.

Schwarzbauer, J. E. (1991). "Fibronectin: from gene to protein." Curr Opin Cell Biol **3**(5): 786-91.

Schwarzbauer, J. E. (1991). "Identification of the fibronectin sequences required for assembly of a fibrillar matrix." J Cell Biol **113**(6): 1463-73.

Schwarzbauer, J. E. and J. L. Sechler (1999). "Fibronectin fibrillogenesis: a paradigm for extracellular matrix assembly." Curr Opin Cell Biol **11**(5): 622-7.

Schwarzbauer, J. E., C. S. Spencer, et al. (1989). "Selective secretion of alternatively spliced fibronectin variants." J Cell Biol **109**(6 Pt 2): 3445-53.

Sechler, J. L., S. A. Corbett, et al. (1997). "Modulatory roles for integrin activation and the synergy site of fibronectin during matrix assembly." Mol Biol Cell **8**(12): 2563-73.

Sechler, J. L., S. A. Corbett, et al. (1998). "Modulation of cell-extracellular matrix interactions." Ann N Y Acad Sci **857**: 143-54.

Sechler, J. L., A. M. Cumiskey, et al. (2000). "A novel RGD-independent fibronectin assembly pathway initiated by alpha4beta1 integrin binding to the alternatively spliced V region." J Cell Sci **113 (Pt 8)**: 1491-8.

Sechler, J. L., Y. Takada, et al. (1996). "Altered rate of fibronectin matrix assembly by deletion of the first type III repeats." J Cell Biol **134**(2): 573-83.

Sheppard, D. (2000). "In vivo functions of integrins: lessons from null mutations in mice." Matrix Biol **19**(3): 203-9.

Shi, Q. and D. Boettiger (2003). "A novel mode for integrin-mediated signaling: tethering is required for phosphorylation of FAK Y397." Mol Biol Cell **14**(10): 4306-15.

Shinde, A. V., C. Bystroff, et al. (2008). "Identification of the peptide sequences within the EIIIA (EDA) segment of fibronectin that mediate integrin alpha9beta1-dependent cellular activities." J Biol Chem **283**(5): 2858-70.

Shpiro, N., I. R. Ellis, et al. (2005). "Synthesis of an IGD peptidomimetic with motogenic activity." Mol Biosyst **1**(4): 318-20.

Sieg, D. J., C. R. Hauck, et al. (2000). "FAK integrates growth-factor and integrin signals to promote cell migration." Nat Cell Biol **2**(5): 249-56.

Siegel, P. M. and J. Massague (2003). "Cytostatic and apoptotic actions of TGF-beta in homeostasis and cancer." Nat Rev Cancer **3**(11): 807-21.

Smith, J. C., K. Symes, et al. (1990). "Mesoderm induction and the control of gastrulation in Xenopus laevis: the roles of fibronectin and integrins." Development **108**(2): 229-38.

Soldi, R., S. Mitola, et al. (1999). "Role of alphavbeta3 integrin in the activation of vascular endothelial growth factor receptor-2." Embo J **18**(4): 882-92.

Sottile, J. and D. C. Hocking (2002). "Fibronectin polymerization regulates the composition and stability of extracellular matrix fibrils and cell-matrix adhesions." Mol Biol Cell **13**(10): 3546-59.

Sottile, J., D. C. Hocking, et al. (2000). "Fibronectin polymerization stimulates cell growth by RGD-dependent and -independent mechanisms." J Cell Sci **113 Pt 23**: 4287-99.

Stromblad, S. and D. A. Cheresh (1996). "Integrins, angiogenesis and vascular cell survival." Chem Biol **3**(11): 881-5.

Sundberg, C. and K. Rubin (1996). "Stimulation of beta1 integrins on fibroblasts induces PDGF independent tyrosine phosphorylation of PDGF beta-receptors." J Cell Biol **132**(4): 741-52.

Taipale, J. and J. Keski-Oja (1997). "Growth factors in the extracellular matrix." Faseb J **11**(1): 51-9.

Taipale, J., J. Saharinen, et al. (1996). "Latent transforming growth factor-beta 1 and its binding protein are components of extracellular matrix microfibrils." J Histochem Cytochem **44**(8): 875-89.

Takagi, J., B. M. Petre, et al. (2002). "Global conformational rearrangements in integrin extracellular domains in outside-in and inside-out signaling." Cell **110**(5): 599-11.

Takagi, J., K. Strokovich, et al. (2003). "Structure of integrin alpha5beta1 in complex with fibronectin." Embo J **22**(18): 4607-15.

Tanentzapf, G., M. D. Martin-Bermudo, et al. (2006). "Multiple factors contribute to integrin-talin interactions in vivo." J Cell Sci **119**(Pt 8): 1632-44.

ten Dijke, P. and H. M. Arthur (2007). "Extracellular control of TGFbeta signalling in vascular development and disease." Nat Rev Mol Cell Biol **8**(11): 857-69.

Tilghman, R. W. and J. T. Parsons (2008). "Focal adhesion kinase as a regulator of cell tension in the progression of cancer." Semin Cancer Biol **18**(1): 45-52.

Timpl, R. (1993). "Proteoglycans of basement membranes." Experientia **49**(5): 417-28.

Travis, M. A., J. D. Humphries, et al. (2003). "An unraveling tale of how integrins are activated from within." Trends Pharmacol Sci **24**(4): 192-7.

Ui-Tei, K., Y. Naito, et al. (2004). "Guidelines for the selection of highly effective siRNA sequences for mammalian and chick RNA interference." Nucleic Acids Res **32**(3): 936-48.

Vakonakis, I. and I. D. Campbell (2007). "Extracellular matrix: from atomic resolution to ultrastructure." Curr Opin Cell Biol **19**(5): 578-83.

van der Flier, A. and A. Sonnenberg (2001). "Function and interactions of integrins." Cell Tissue Res **305**(3): 285-98.

Velling, T., J. Risteli, et al. (2002). "Polymerization of type I and III collagens is dependent on fibronectin and enhanced by integrins alpha 11beta 1 and alpha 2beta 1." J Biol Chem **277**(40): 37377-81.

Vinogradova, O., A. Velyvis, et al. (2002). "A structural mechanism of integrin alpha(IIb)beta(3) "inside-out" activation as regulated by its cytoplasmic face." Cell **110**(5): 587-97.

Wayner, E. A., A. Garcia-Pardo, et al. (1989). "Identification and characterization of the T lymphocyte adhesion receptor for an alternative cell attachment domain (CS-1) in plasma fibronectin." J Cell Biol **109**(3): 1321-30.

Wegener, K. L. and I. D. Campbell (2008). "Transmembrane and cytoplasmic domains in integrin activation and protein-protein interactions (review)." Mol Membr Biol **25**(5): 376-87.

Wegener, K. L., A. W. Partridge, et al. (2007). "Structural basis of integrin activation by talin." Cell **128**(1): 171-82.

Wennerberg, K., L. Lohikangas, et al. (1996). "Beta 1 integrin-dependent and -independent polymerization of fibronectin." J Cell Biol **132**(1-2): 227-38.

Wierzbicka-Patynowski, I., Y. Mao, et al. (2004). "Analysis of fibronectin matrix assembly." Curr Protoc Cell Biol **Chapter 10**: Unit 10 12.

Wierzbicka-Patynowski, I. and J. E. Schwarzbauer (2003). "The ins and outs of fibronectin matrix assembly." J Cell Sci **116**(Pt 16): 3269-76.

Wilson, V. and R. S. Beddington (1996). "Cell fate and morphogenetic movement in the late mouse primitive streak." Mech Dev **55**(1): 79-89.

Woods, A., R. L. Longley, et al. (2000). "Syndecan-4 binding to the high affinity heparin-binding domain of fibronectin drives focal adhesion formation in fibroblasts." Arch Biochem Biophys **374**(1): 66-72.

Wu, C., P. E. Hughes, et al. (1996). "Identification of a new biological function for the integrin alpha v beta 3: initiation of fibronectin matrix assembly." Cell Adhes Commun **4**(3): 149-58.

Wu, C., V. M. Keivens, et al. (1995). "Integrin activation and cytoskeletal interaction are essential for the assembly of a fibronectin matrix." Cell **83**(5): 715-24.

Xiong, J. P., T. Stehle, et al. (2001). "Crystal structure of the extracellular segment of integrin alpha Vbeta3." Science **294**(5541): 339-45.

Xu, J., E. Bae, et al. (2009). "Display of cell surface sites for fibronectin assembly is modulated by cell adherence to (1)F3 and C-terminal modules of fibronectin." PLoS ONE **4**(1): e4113.

Yamada, K. M., R. Pankov, et al. (2003). "Dimensions and dynamics in integrin function." Braz J Med Biol Res **36**(8): 959-66.

Yang, J. T., B. L. Bader, et al. (1999). "Overlapping and independent functions of fibronectin receptor integrins in early mesodermal development." Dev Biol **215**(2): 264-77.

Yang, J. T., H. Rayburn, et al. (1993). "Embryonic mesodermal defects in alpha 5 integrin-deficient mice." Development **119**(4): 1093-105.

Zaidel-Bar, R., S. Itzkovitz, et al. (2007). "Functional atlas of the integrin adhesome." Nat Cell Biol **9**(8): 858-67.

Zamir, E. and B. Geiger (2001). "Molecular complexity and dynamics of cell-matrix adhesions." J Cell Sci **114**(Pt 20): 3583-90.

Zamir, E., M. Katz, et al. (2000). "Dynamics and segregation of cell-matrix adhesions in cultured fibroblasts." Nat Cell Biol **2**(4): 191-6.

Zhang, X., G. Jiang, et al. (2008). "Talin depletion reveals independence of initial cell spreading from integrin activation and traction." Nat Cell Biol **10**(9): 1062-8.

Zhou, X., R. G. Rowe, et al. (2008). "Fibronectin fibrillogenesis regulates three-dimensional neovessel formation." Genes Dev **22**(9): 1231-43.

Zhu, J., B. H. Luo, et al. (2008). "Structure of a complete integrin ectodomain in a physiologic resting state and activation and deactivation by applied forces." Mol Cell **32**(6): 849-61.

6 Publications

Salmenpera, P., E. Kankuri, J. Bizik, V. Siren, I. Virtanen, S. Takahashi, **M. Leiss**, R. Fässler, A. Vaheri (2008). „Formation and activation of fibroblast spheroids depend on fibronectin-integrin interaction." Exp Cell Res **314**(19): 3444-52

Leiss, M.*, K. Beckmann*, A. Giros, C. Costell, R. Fässler (2008). „The role of integrin binding sites in fibronectin matrix assembly in vivo." Curr Opin Cell Biol **20**(5): 502-7

Takahashi, S.*, **M. Leiss***, M. Moser, T. Ohashi, T. Kitao, D. Heckmann, A. Pfeiffer, H. Kessler, J. Takagi, HP. Erickson, R. Fässler (2007). „The RGD motif in fibronectin is essential for development but dispensable for fibril assembly." J Cell Biol **178**(1): 167-78.

*: equal contribution

7 Acknowledgement

I would like to express my sincere gratitude to:

Prof. Dr. Reinhard Fässler, my supervisor, for giving me the possibility to work on this exciting project and for the opportunity to perform my study under such excellent conditions. He always left his door open for stimulating discussions, honest criticisms and constructive suggestions. I would like to thank him for his outstanding support throughout my PhD study.

Prof. Dr. Rainer Deutzmann, my official "Doktorvater", for assuming this responsibility. I would like to thank him for his excellent support during all these years, and for reviewing my thesis.

Prof. Dr. Tamm, the third referee of my thesis, as well as **Prof. Dr. Sterner** and **Prof. Dr. Warth**, the members of my thesis committee, for agreeing to evaluate my work.

Dr. Seiichiro Takahashi for our excellent cooperation on the „FN-RGE"-project and for valuable lessons in cross-cultural teamwork.

Dr. Eloi Montañez Miralles for his expert advice and numerous constructive discussions in the lab, in Barcelona or in the beergarden.

Dr. Karsten Beckmann for years of great cooperation in a team and for revising my manuscript.

Amparo Girós for creating a friendly work environment and for the great time we had together.

Dr. Markus Moser, for his diligent introduction into histological techniques.

Prof. Dr. Erickson, **Prof. Dr. Takagi**, **Prof. Dr. Kessler** and **Dr. Dominik Heckmann** for very fruitful cooperations.

Dr. Walther Göring for solving all my equipment-related problems.

Simone Bach for her kind practical help in the histology-lab.

Carmen Schmitz for her tireless assistance in all organizational matters.

All **members of the Department** of Molecular Medicine for their kind support, for creation of a nice work environment and the great time we had together.

My girlfriend Kerstin and my parents, who gave me the tireless, outstanding backing that was necessary to succeed in this work.

8 Erklärung

Ich erkläre hiermit an Eides statt, dass ich die vorliegende Arbeit ohne unzulässige Hilfe Dritter und ohne Benutzung anderer als der angegebenen Quellen und Hilfsmittel angefertigt habe.

Michael Leiß